

**Biophysical and Proteomic Characterization of the Voltage-Dependent
Anion-Selective Channel of *Neurospora crassa***

by

Fraser G. Ferens

A Thesis Submitted to the Faculty of Graduate Studies of
The University of Manitoba
in partial fulfilment of the requirements of the degree of

DOCTOR OF PHILOSOPHY

Department of Microbiology
University of Manitoba
Winnipeg

Copyright © 2019 by Fraser G. Ferens

Thesis Abstract

The oligomeric state of the voltage-dependent anion-selective channel (VDAC) and the stability of the VDAC-hexokinase complex play integral roles in mitochondrially mediated apoptotic signaling. Various small to large assemblies of VDAC have been observed in mitochondrial outer membranes but they do not predominate in detergent-solubilized VDAC samples. In this work, a cholesterol analogue, cholesteryl-hemisuccinate (CHS), was shown induce the formation of *Neurospora crassa* VDAC multimers in detergent solution. The oligomeric states of VDAC in the absence and presence of CHS were deciphered through an integrated biophysics approach using microscale thermophoresis, analytical ultracentrifugation and size exclusion chromatography-small angle X-ray scattering. It was determined that CHS stabilizes the interaction between VDAC and hexokinase (K_d of $27 \pm 6 \mu\text{M}$). Thus, sterols such as cholesterol in higher eukaryotes or ergosterol in fungi may regulate the VDAC oligomeric state and may provide a potential target for the modulation of apoptotic signaling by effecting VDAC-VDAC and VDAC-hexokinase interactions. In a separate study, the physiological effects of a small 5 amino-acid deletion in the *Neurospora crassa* VDAC sequence (238porin) were examined using proteomic and biochemical analysis of a strain expressing only this variant. 238porin was determined to be assembled in the mitochondrial outer membrane by a protease resistance assay; however, the level of expression of 238porin was only 3% of that of the wild-type protein. 238Por displayed respiratory defects; however, it exhibited an almost wild-type linear growth rate. Analysis of mitochondrial proteomes from a VDAC wild-type strain, a strain lacking VDAC ($\Delta\text{Por-1}$) and 238Por revealed that the expression of 238poin partially compensates for

respiratory defects caused by VDAC knockout. The deletion (Δ Por-1) or depletion (238Por) of VDAC was found to increase the expression of a Rubredoxin-NAD⁺ reductase, a homologue of the higher eukaryotic apoptosis inducing factor. The studies in this work examined the behavior of isolated VDAC *in vitro* and the effects of VDAC dysfunction *in vivo* and provide a better understanding of VDAC behaviors involved in apoptotic signaling and in addition, the integrated biophysical approach described provides a powerful platform for the study of membrane protein complexes solubilized in detergent solutions.

Acknowledgements

I would like to thank the funding agencies that made this work possible. The presented work was funded by the Natural Science and Engineering Council of Canada through NSERC Discovery grants awarded to Deborah Court and Jörg Stetefeld. In addition Fraser Ferens was partially supported by the Faculty of Science (Faculty of Science Graduate Student Award) and the Faculty of Graduate Studies (Manitoba Graduate Enhancement of Tri-Council Stipends) at the University of Manitoba.

The SEC-SAXS data were collected at Diamond Light Source at beamline B21 under the proposal SM16028. I would like to thank the staff of beamline B21 for their assistance with SAXS data collection and advice. I would also like to thank Dr. Jason Treberg and Mr. Andre Dufresne, Department of Biological Sciences, University of Manitoba, for assistance with alternative oxidase measurements, and fluorescence microscopy, respectively.

This work could not have been possible without the support of my supervisor Deb, without her ability to listen and thoughtfully respond to every one of my endless questions I would have been lost, thank you. I thank Jörg for the opportunity to work in his lab and with his group, I could not have asked for a better collaboration. I would also like to thank the remainder of my advisory committee, Dr. Joe O'Neil and Dr. Ivan Oresnik for their thoughtful discussions throughout my project. Thank you to lab colleagues Dr. Matt McDougall, Dr. George Orriss, Dr. Markus Meier, Dr. Trushar Patel, Dr. Natalie Krahn and Dr. Sabbir Rahman Shuvo for advice, technical expertise and excellent discussions.

Table of Contents

Thesis Abstract.....	II
Acknowledgements	IV
Table of Contents	V
List of Tables	VII
List of Figures.....	VIII
List of Copyrighted Material for Which Permission has Been Granted	X
List of Abbreviations	XI
Chapter 1: Literature Review.....	14
1.1 Introduction.....	14
1.2 IMP-Protein Interactions	16
1.3 Molecular Mass Analysis of IMP and IMP-Containing Complexes	20
1.4 Modelling of IMP-Detergent Complexes from Small-Angle Scattering Data.....	30
1.5 Combined Biophysics Approach	35
1.6 Voltage-Dependent Anion-Selective Channels.....	36
1.7 Thesis Objectives.....	38
Chapter 2: A Cholesterol Analogue Induces an Oligomeric Reorganization of VDAC	40
2.1 Publication Details and Author Contributions	40
2.2 Abstract.....	40
2.3 Introduction.....	41
2.4 Materials and Methods.....	43
2.4.1 Plasmids, Strains and Reagents	43
2.4.2 VDAC ^N Purification.....	43
2.4.3 VDAC ^R Overexpression, Purification and Refolding.....	44
2.4.4 Circular Dichroism Spectropolarimetry (CD)	45

2.4.5 Analytical Ultracentrifugation (AUC)	46
2.4.6 Small-Angle X-ray Scattering (SAXS)	48
2.4.7 Microscale Thermophoresis (MST).....	49
2.5 Results	52
2.5.1 Evaluation of Recombinant <i>Neurospora crassa</i> VDAC	52
2.5.2 CHS Alters the Oligomeric State and Secondary Structure of VDAC ^R	56
2.5.3 SEC-SAXS Modelling Supports Previously Proposed VDAC Multimer Arrangements	63
2.5.4 CHS Allows for a Stable VDAC-Hexokinase Interaction	72
2.6 Discussion.....	75
Chapter 3: A Deletion Variant Partially Complements a Porin-Less Strain of <i>Neurospora crassa</i>.....	82
3.1 Publication Details and Author Contributions	82
3.2 Abstract.....	83
3.3 Introduction.....	83
3.4 Materials and Methods.....	87
3.4.1 Strains and Growth Conditions.....	87
3.4.2 Analysis of Mitochondria	89
3.4.3 Proteomic Analysis of Mitochondria.....	90
3.5 Results and Discussion.....	92
3.5.1 1-Dimensional LC MS/MS analysis of the mitochondrial proteomes ...	96
3.5.2 Electron Transport Chain.....	97
3.5.3 Oxidative Stress.....	106
3.5.4 Mitochondrial Biogenesis	108
3.6 Conclusions.....	115
4.1 Conclusions.....	116
4.2 Future Directions	118
5. Appendix 1: Supporting Information for Chapter 2	121
6. Appendix 2: Supporting Information for Chapter 3	130
7. References	170

List of Tables

Table 2.1 VDAC Secondary Structure Contributions Obtained from Deconvolution of CD Data.....	55
Table 2.2 Parameters of VDAC-Detergent Species Determined from Sedimentation Velocity Experiments.....	60
Table 2.3 Parameters of Best Fitting VDAC-Detergent Complex Models.....	71
Table 3.1 <i>Neurospora crassa</i> Strains Utilized and their Respective Genotypes.....	88
Table 3.2 Linear Growth Rates and Cyanide-Resistant Respiration of <i>Neurospora crassa</i> Strains on Vogel’s Minimal Medium.....	94
Table 3.3 Protein Identification by LC-MS/MS.....	98
Table 3.4 Proteins Detected in Altered Levels in ΔPor-1 Mitochondria.....	100
Table 3.5 Proteins Detected in Altered Levels in 238por Mitochondria.....	104
Table 5.1 Raw Data Obtained from AUC c(s) Distributions.....	121
Table 6.1 Primer sequences.....	130
Table 6.2 Levels of predicted mitochondrial proteins in ΔPor-1 relative to wild-type.....	131
Table 6.3 Levels of predicted mitochondrial proteins in 238Por relative to wild-type.....	144
Table 6.4. Levels of predicted mitochondrial proteins in ΔPor-1 relative to 238Por.....	157

List of Figures

Figure 1.1 Microscale Thermophoresis Workflow.....	18
Figure 1.2 Sedimentation Velocity Data Analysis.....	22
Figure 1.3 Comparison of $c(s)$ and $c(s, f/f_0)$ Analyses.....	28
Figure 1.4 SEC-SAXS Analysis of Detergent Solubilized IMPs.....	33
Figure 1.5 Summary of the Biophysics Pipeline for the <i>In vitro</i> Characterization of IMPs.....	37
Figure 2.1 VDAC ^R Retains Structural Integrity and Functionality Relative to VDAC ^N	53
Figure 2.2 CHS Alters the Oligomeric State and Secondary Structure of VDAC ^R	58
Figure 2.3 Microscale Thermophoresis Screening and Controls.....	61
Figure 2.4 SEC-SAXS Model of Monomeric VDAC ^R Fits Experimental Scattering Data.....	65
Figure 2.5 SEC-SAXS model of dimeric VDAC ^R +CHS fits experimental scattering data.....	67
Figure 2.6 Hexameric VDAC SAXS Model.....	69
Figure 2.7 CHS Allows for the Formation of a Stable VDAC-Hexokinase Complex.....	73
Figure 3.1 Porin Variant Used in this Study.....	85
Figure 3.2 Western Blot Analysis of Wild-type (Por-WT) and 238por-Containing Mitochondria.....	93
Figure 3.3 The Reduced Minus Oxidized Difference Spectra Obtained from Wild-Type (Por-WT), 238por, and Δ Por-1 Mitochondria.....	95
Figure 3.4 Red-Native PAGE of DDM-Solubilized Mitochondrial Membrane Complexes.....	99
Figure 3.5 Western Blot Detection of the Translocase of the Outer Membrane (TOM) Complex from Red-Native PAGE of DDM-Solubilized Mitochondrial Membrane Complexes.....	110

Figure 3.6 Fluorescence Microscopy of *N. crassa* Mitochondria.....111

**Figure 3.7 Connections Among Proteins Present in Different Relative Amounts
in 238por and Δ Por-1 Mitochondria.....113**

**Figure 5.1 Representative Sedimentation Velocity Experimental Data and Fitted
Curves Used to Calculate $c(s)$ or $c(s, f/f_0)$ Distributions.....122**

Figure 5.2 Guinier analyses of VDAC species examined in this study.....124

Figure 5.3 Full Regions of Interest of SDS-PAGE Gels.....126

Figure 5.4 SEC-SAXS Elution profiles of VDAC-detergent complexes.....128

List of Copyrighted Material for Which Permission has Been Granted

Ferens F.G., Spicer V., Krokhin O.V., Motnenko A., Summers W.A.T., Court D.A. 2017. A deletion variant partially complements a porin-less strain of *Neurospora crassa*. *Biochemistry and Cell Biology*, 95(2): 318-327 with permission from the authors as per NRC Research Press regulations:

“Under the terms of the license to publish granted to NRC Research Press, authors retain the following rights:

To post a copy of their submitted manuscript (pre-print) on their own website, an institutional repository, a preprint server, or their funding body's designated archive (no embargo period). Publication on a preprint server prior to submitting to an NRC Research Press journal does not constitute “prior publication”.

To post a copy of their accepted manuscript (post-print) on their own website, an institutional repository, a preprint server, or their funding body's designated archive (no embargo period). Authors who archive or self-archive accepted articles are asked to provide a hyperlink from the manuscript to the Journal's website.

Authors, and any academic institution where they work at the time, may reproduce their manuscript for the purpose of course teaching.

Authors may reuse all or part of their manuscript in other works created by them non-commercial purposes, provided the original publication in an NRC Research Press journal is acknowledged through a note or citation.”

<http://www.nrcresearchpress.com/page/authors/information/rights>)

Ferens F.G., Patel T.R., Oriss G., Court D.A., Stetefeld J. 2019. A Cholesterol Analog Induces an Oligomeric Reorganization of VDAC. *Biophysical Journal*, 116(5):847-859, DOI: 10.1016/j.bpj.2019.01.031

“Authors retain the right to use their articles in full or in part in a thesis or dissertation (provided that it is not to be published commercially)”

<https://www.elsevier.com/about/policies/copyright#Author-rights>

List of Abbreviations

238Por	<i>Neurospora crassa</i> strain expressing 238porin
238porin	<i>Neurospora crassa</i> VDAC mutant lacking amino acid residues 238-242
AEBSF	4-(2-aminoethyl)benzenesulfonyl fluoride hydrochloride
AIF	Apoptosis inducing factor
ALAS	5-aminolevulinate synthase
AOD	Alternative Oxidase
ATP	Adenine tri-phosphate
AUC	Analytical ultracentrifugation
CD	Circular dichroism spectrapolarimetry
CHS	Cholesteryl-hemisuccinate
DDM	n-dodecyl- β -d-maltopyranoside
DM	n-decyl- β -d-maltopyranoside
D_{\max}	Maximum particle dimension
$E_{0.1\%}$	Protein extinction coefficient by mass at 280 nm
f/f_0	Frictional ratio
GPCR	G-protein coupled receptors
HK-I	<i>Saccharomyces cerevisiae</i> hexokinase I
HK-II	<i>Saccharomyces cerevisiae</i> hexokinase II
hVDAC1	Human VDAC isoform 1
hVDAC2	Human VDAC isoform 2
IMP	Integral membrane protein
K_d	Dissociation constant
KGD	α -ketoglutarate dehydrogenase
LAS	Lipoic acid synthetase
LC	Liquid Chromatography

MALS	Multiple angle light scattering
MitOS	Mitochondrial organizing structure
MOM	Mitochondrial outer membrane
MRE	Mean residue ellipticity
MS/MS	Tandem mass spectroscopy
MST	Microscale thermophoresis
MW	Molecular weight
NAD ⁺ (H)	Nicotinamide adenine dinucleotide
NADP ⁺ (H)	Nicotinamide adenine dinucleotide phosphate
PDB	Protein data bank
PDC	Pyruvate dehydrogenase complex
PDK	Pyruvate dehydrogenase kinase
Por-WT	<i>Neurospora crassa</i> VDAC wild-type strain
R _g	Radius of gyration
RI	Refractive index
R _s	Hydrodynamic radius (Stokes radius)
S	Sedimentation coefficient
SANS	Small angle neutron scattering
SAS	Small angle scattering
SAXS	Small angle X-ray scattering
SEC	Size exclusion chromatography
SEC-MALS	Size exclusion chromatography with in line MALS
SEC-SAXS	SEC with inline SAXS
SEC-UV-MALS-RI	SEC-MALS with additional UV absorbance and RI detectors
TCA	Tri-carboxylic acid
TMLD	Trimethyllysine dioxygenase
TOB	Topogenesis of mitochondrial outer membrane β -barrels complex
TOM	Translocase of the outer mitochondrial membrane

UV	Ultraviolet light
VDAC	Voltage-dependent anion-selective channel
VDAC ^N	Recombinant VDAC isolated from native membranes
VDAC ^R	Recombinant refolded VDAC
VMM	Vogel's minimal medium
Δ Por-1	<i>Neurospora crassa</i> VDAC knockout strain

Chapter 1: Literature Review

Biophysical characterization of detergent-solubilized integral membrane proteins

1.1 Introduction

The study of integral membrane proteins (IMPs) is essential to the understanding of physiology and disease. Notably, membrane proteins play a key role in human disease, as is evident by the number of membrane proteins targeted by the mode of action of the current generation of pharmaceutical products (1). Even though the importance of IMPs proteins is clear the understanding of the structure-function relationship of IMPs is poor in comparison to that of water-soluble proteins (2). This gap in understanding in part results from the difficulty in deciphering structural information pertaining to IMPs and IMP complexes due to their physical properties. The gap in structural knowledge can be clearly seen in the number of high-resolution IMP protein structures deposited into the protein data bank (www.rcsb.org) compared to the number of soluble protein structures (3). This chapter will describe the background to a three-method biophysics pipeline, discuss some of the currently available biophysical techniques for studying proteins in solution, how they have been adapted to the study of IMPs and what each technique adds to a larger understanding of integral membrane protein structure and function.

IMPs are inserted into the lipid bilayers that separate the interior and exterior of cells, or separate cellular compartments (4). IMPs are responsible for the trafficking of molecules across the lipid membranes (5); as well, sensory information collected by cells on the cell surface is translated across the membrane to the interior of cells by IMPs (6). These two general functions of IMPs as a group largely explain their importance in physiology and disease (7-9), although many other types of functions can be attributed to different IMPs. The general structural characteristics of membrane proteins are quite different from soluble proteins; transmembrane

domains have outwardly facing hydrophobic amino acid side chains whereas soluble proteins generally have buried hydrophobic amino acid side chains (10). From known high resolution membrane protein structures there are two main types of transmembrane domains: α -helices or α -helical bundles and β -barrels (11, 12). These two architectures allow for the positioning of hydrophobic amino acids towards the interior of the lipid bilayer and hydrophilic amino acids towards the interior of the structure where hydrogen and ionic bonds hold the structure together or face an internal aqueous channel (13). The structures and therefore properties of membrane proteins stand in stark contrast to those of water-soluble proteins.

Many *in vitro* techniques used for the analysis of proteins require the proteins to be free in solution (14, 15). The use of detergents to remove IMPs from lipid bilayers and coat them in an amphipathic detergent layer is a common solution to this problem (15). Once solubilized by detergent, the solution can be considered a polydisperse mixture of IMP-detergent complexes and empty detergent micelles (14). The same is true of protein complexes where one or more of the components is an IMP; in some cases, it is possible to identify detergents that allow for the solubilization of large intact protein complexes (16, 17). The addition of detergent to protein solutions can cause issues that complicate the data interpretation of many methods; however, many of these issues can now be overcome with careful experimental design and new methods. Here we will discuss a biophysics pipeline for the characterization of detergent solubilized IMPs using microscale thermophoresis to screen for protein-protein interactions and determine binding affinities, analytical ultracentrifugation to determine the oligomeric state of IMPs or IMP protein complex composition and small angle x-ray scattering to data to model IMP detergent complexes.

1.2 IMP-Protein Interactions

The analysis of IMP-IMP or IMP-soluble-protein binding affinities can provide a greater understanding of the behavior of protein complexes. The binding affinity of the proteins lends information on the conditions in which (for example, concentration range) and depending on the system, can aid in the understanding of the mechanisms controlled by complex formation or disassociation (complex forms an active enzyme, disassociation triggers a signaling event, etc.) (18). The ability to measure these binding affinities is paramount in the understanding of the function of these protein complexes. The study of IMP complexes is complicated by the fact that at least one component of the complex is imbedded into a lipid bilayer (11, 12, 14, 15). The immobilization of the complex is the key issue that makes studying the binding affinities of the complex components difficult as most techniques require the proteins to be free in solution (19, 20). This can be solved using standard membrane mimetic methodologies such as solubilizing the membrane-embedded components of the complex in detergent solutions, thereby removing the proteins from lipid bilayers and suspending them in solution. In the detergent-solubilized state, a powerful method, microscale thermophoresis (MST) is an ideal choice for the analysis of IMP binding affinity.

Microscale thermophoresis (MST) is a technique that relies on changes in the movement of macromolecules in solution due to interactions of the macromolecule with ligands (21). MST is very sensitive to changes in protein motion enabling the detection of macromolecule, small molecule and ion binding (21). MST utilizes an IR laser to induce the movement of proteins away from a localized area of a capillary tube (21). The relative concentration of a protein of interest is monitored using a fluorescent tag; in this way the movement of the protein molecules can be monitored through changes to localized fluorescence intensity (20, 21). The binding of

ligands or proteins to the tagged protein of interest can be observed and quantified through monitoring changes to the motion of the protein of interest in the absence and presence of the binding partner (22) (Fig. 1.1B). A disassociation constant (K_d) for the interaction can be determined by titrating the binding partner against a constant concentration of the tagged protein of interest (Fig. 1.1B)(20):

$$K_d = \frac{[A] \times [B^*]}{[AB^*]} \quad (1.1)$$

where K_d is the disassociation constant, $[A]$ is the concentration of the titrated binding partner, $[B^*]$ is the concentration of the fluorescently tagged protein and $[AB^*]$ is the concentration of the complex. Software such as Palmist allows for the analysis of MST experiments and fitting of K_d values from experimental data (20).

The use of MST in the determination of the K_d of IMP-binding partner dissociation, offers several advantages over other techniques. The most notable advantage that MST provides over other binding analysis techniques such as isothermal calorimetry is that the binding of soluble proteins to an IMP can be monitored while the IMP is imbedded in a lipid bilayer (21). This is accomplished through reconstituting the IMP in lipid vesicles and titrating the vesicles against a fluorescently labeled soluble binding partner. In membrane mimetic systems such as detergent micelles, MST has an advantage over isothermal calorimetry as the sample preparation does not require dialysis to ensure exact buffer matching (19), which can be impossible if the detergent used forms large micelles.

For use in a combined biophysics approach to examining IMP complexes, MST can provide important information on complexes or oligomerization (23) and MST can be used to screen potential binding partners for complex formation. A simple procedure is employed; the thermophoresis profiles in the absence of the binding partner and in the presence of high

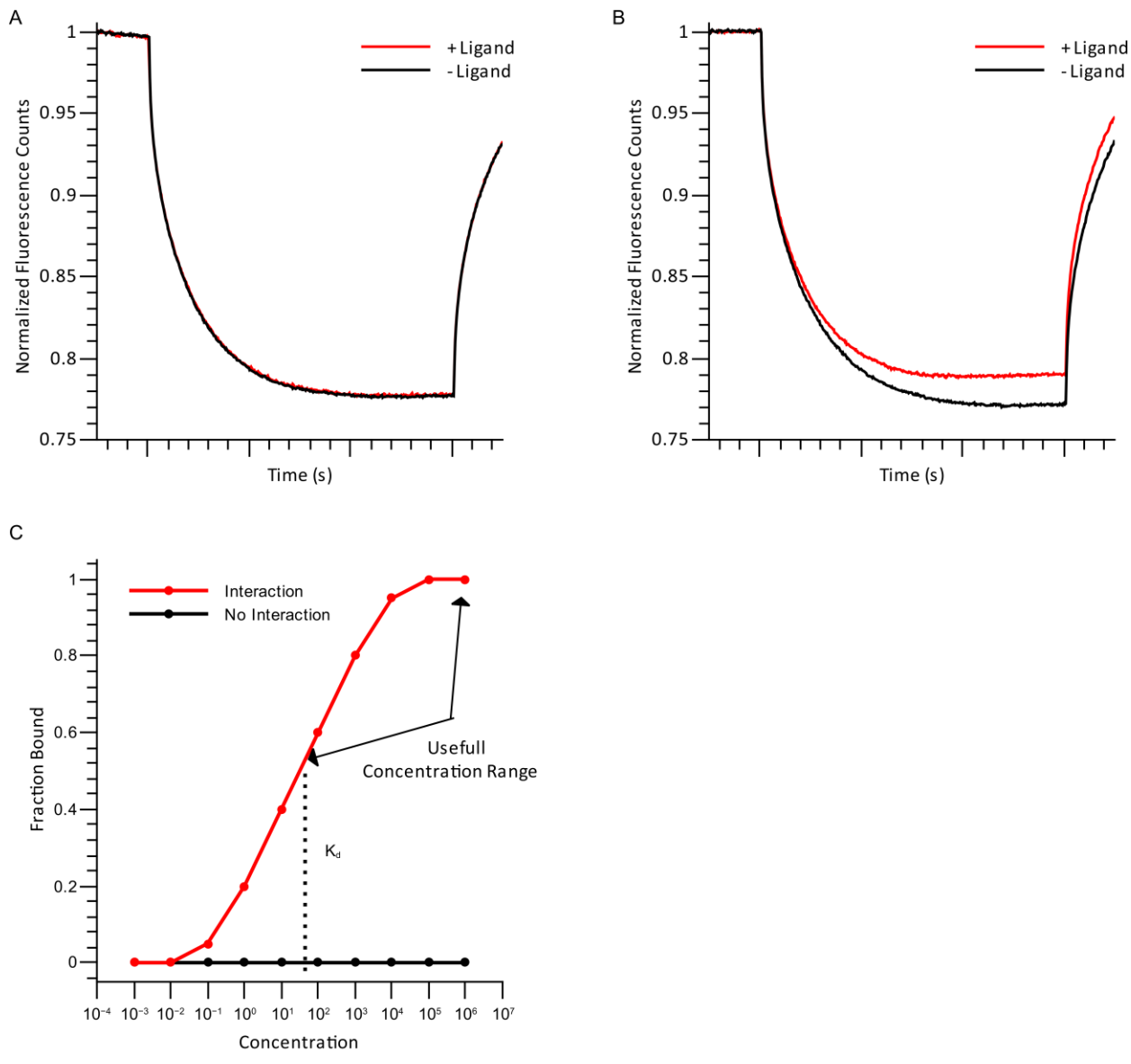


Figure 1.1 Microscale thermophoresis work flow

Figure 1.1 Microscale thermophoresis work flow. A) Thermophoresis traces of *Neurospora* VDAC in the absence (black) and presence (red) of *Saccharomyces* hexokinase II. There is no change between the two traces indicating no binding (Chapter 2). B) Thermophoresis traces of *Neurospora* VDAC in the absence (black) and presence of *Saccharomyces* hexokinase I. There is a clear shift in the MST trace due to the presence of hexokinase I indicating binding (Chapter 2). C) Example titrations of a protein that does not interact with the target protein (black) and a protein that does interact with the target protein (red).

concentrations of binding partners can provide the evidence of interaction (Chapter 2) (Fig. 1.1A & B). Once binding partners are identified, the K_d of the interaction can be determined via titration of the binding partner (20, 21) (Fig. 1.1C). With the K_d of the interaction known, the working concentrations of proteins in the complex for further experimentation should be above this value (Fig. 1.1C). For example, this simple test revealed an isoform specificity in complex formation, that hexokinase I binds VDAC (Fig. 1.1B) and hexokinase II does not (Fig. 1.1A) (see Chapter 2).

1.3 Molecular Mass Analysis of IMP and IMP-Containing Complexes

Analytical ultracentrifugation (AUC) is a method that can provide information about the size and shape of biological macromolecules or complexes. AUC sedimentation velocity experiments can allow for the examination of the size, shape and mass of macromolecules or macromolecular complexes, and as well sedimentation equilibrium experiments allow for the study of protein-protein interactions (24). For the purposes of this workflow we will discuss sedimentation velocity methodology. In general, protein sedimentation under high centrifugal force is related to the molecular weight via the equation:

$$M = \frac{6\pi s N_A \eta R_s}{1 - \rho \bar{v}} \quad (1.2)$$

Where M is the molecular weight, s is the sedimentation coefficient, N_A is Avogadro's number, η is the solvent viscosity, R_s is the Stokes radius, ρ is the solvent density and \bar{v} is the macromolecule's partial specific volume (24). The sedimentation coefficient, s , is determined from the sedimentation of the macromolecule monitored during a sedimentation velocity experiment. The sedimentation of proteins can be described by the Lamm equation:

$$\left(\frac{dc}{dt}\right)_r = -\frac{1}{r} \left(\frac{d}{dr}\right) \left[r \left(cs\omega^2 r - D \left(\frac{dt}{dr}\right)_t \right) \right]_t \quad (1.3)$$

Where c is the concentration of solute at the radial position r , t is the time of sedimentation at angular velocity ω and D is the diffusion coefficient (25). This allows for the fitting of s and D using methods such as the $c(s)$ distribution analysis in the software Sedfit (26) allowing for the determination of molecular weights from the sedimentation coefficient using equation 1.2. In the case of IMPs the protein cannot be analyzed in isolation, but rather a protein detergent complex composed of the protein and detergent bound to the IMP during the solubilization process must be analyzed. In this case equation 1.2 can be re-written:

$$M_{PD} = \frac{6\pi s N_A \eta R_s}{1 - \rho \bar{v}_{PD}} \quad (1.4)$$

Where M_{PD} is the molecular weight of the combined protein and detergent components of the protein-detergent complex and \bar{v}_{PD} is the partial specific volume of the protein detergent complex. R_s can be measured via size exclusion chromatography (SEC) elution volume relative to a calibration curve of proteins with known R_s values (27). The \bar{v}_{PD} is unknown; however, it can be determined by from the ratio of detergent to protein in the complex:

$$\bar{v}_{PD} = \frac{\bar{v}_P + \delta_D \bar{v}_D}{1 + \delta_D} \quad (1.5)$$

Where \bar{v}_P is the partial specific volume of the protein component, δ_D is the mass/mass ratio of detergent to protein complex and \bar{v}_D is the partial specific volume of the detergent micelles (27).

\bar{v}_P can be calculated from amino acid sequence using the program Sednterp

(<http://www.jphilo.mailway.com/download.htm#SEDNTERP>) which uses standardized values of

\bar{v} for each amino acid to determine a weighted average \bar{v} for the protein sequence. \bar{v}_D can be

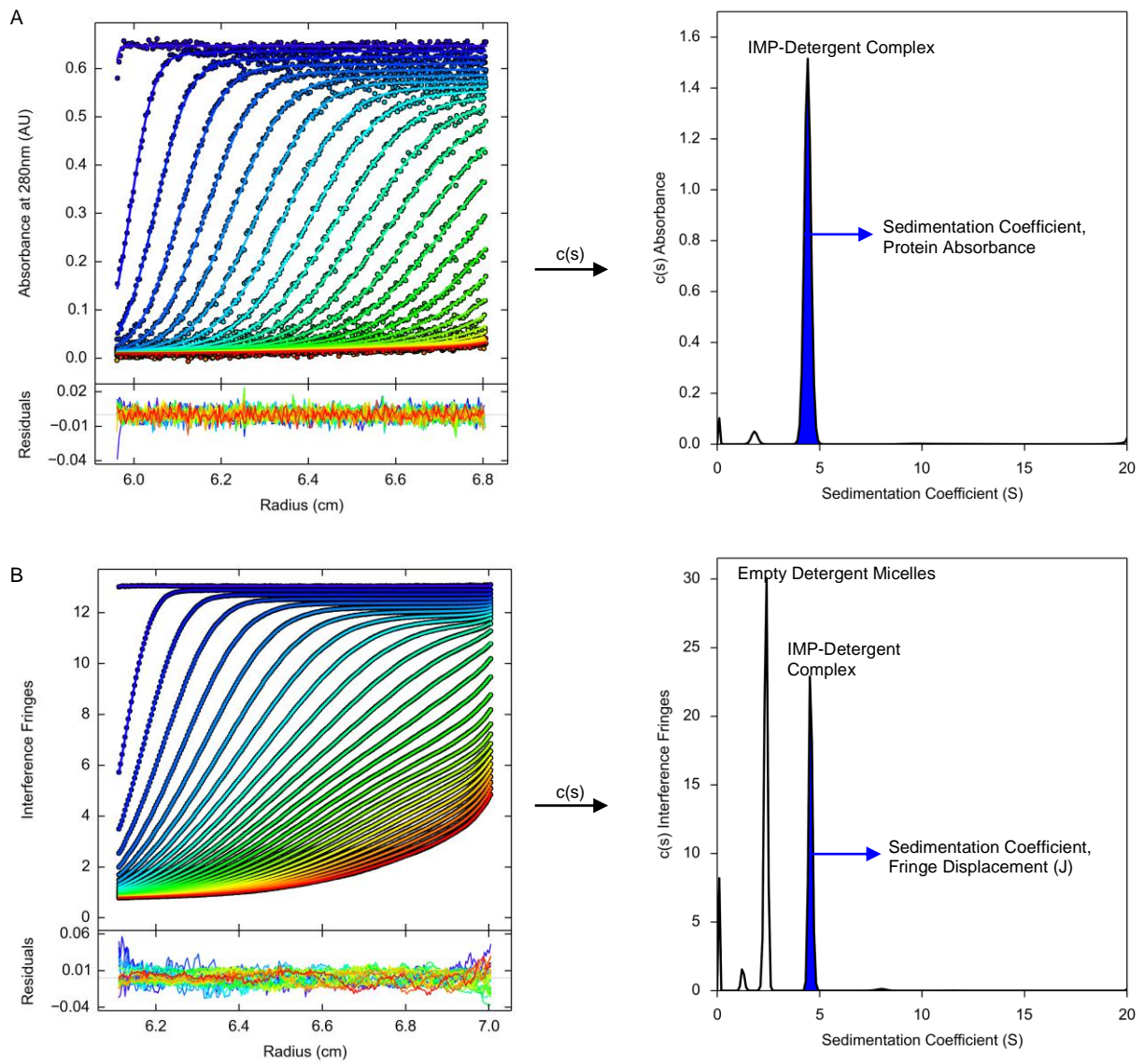


Figure 1.2 Sedimentation velocity data analysis.

Figure 1.2 Sedimentation velocity data analysis. A) The left panel depicts the raw absorbance data points (circles) and Lamm equation solutions (lines) with each scan colored from earliest (blue) to latest (red) of a detergent-solubilized VDAC sample (data from Chapter 2). The right panel depicts a $c(s)$ absorbance distribution determined using sedfit (26). The peak corresponding to the VDAC-detergent complex is indicated and the integrated area used to determine the absorbance of the sample is colored in blue. B) The left panel depicts the interference data points (circles) and Lamm equation solutions (lines) with each scan colored from earliest (blue) to latest (red) of a detergent solubilized VDAC sample (data from Chapter 2). The right panel depicts a $c(s)$ interference distribution determined using sedfit (26). The peaks corresponding to the VDAC-detergent complex and free detergent micelles are indicated and the integrated area used to determine the interference fringe displacement (J) of the sample is colored in blue.

determined by global sedimentation velocity analysis of detergent micelles in at least two different solvent densities (for example 100% H₂O and 100% D₂O; however changes to M_w due to deuterium exchange must be accounted for). In this case \bar{v}_D can be treated as a fitted parameter (28), which can be analyzed using the software Sedphat (24, 26). The δ_D value for the protein detergent complex can be determined from the dn/dc (change in refractive index relative to the protein concentration) of the protein-detergent complex:

$$\left(\frac{dn}{dc_P}\right)_{PD} = \left(\frac{dn}{dc_P}\right)_P + \left(\frac{dn}{dc_D}\right)_D \delta_D \quad (1.6)$$

Where $(dn/dc_P)_{PD}$ is the dn/dc of the protein-detergent complex relative to the protein concentration, $(dn/dc_P)_P$ is the dn/dc of the protein relative to protein concentration and $(dn/dc_D)_D$ is the dn/dc of the detergent relative to the detergent concentration (27). Proteins have a relatively narrow distribution of dn/dc values and as such a standard value of 0.185 ml/g (with light at wavelength 675 nm) can be used as the value for $(dn/dc_P)_P$ (29). $(dn/dc_D)_D$ can be determined experimentally by measuring the change in refractive index due to known concentrations of detergent. $(dn/dc_P)_{PD}$ can be determined directly from calculated sedimentation velocity $c(s)$ distributions using a two detector setup (Interference and Absorbance at 280 nm) :

$$\left(\frac{dn}{dc_P}\right)_{PD} = \frac{J\lambda}{cKl} \quad (1.7)$$

Where J is the interference fringe displacement due to the sedimenting protein-detergent complex, λ is the wavelength (cm) of light (usually 675 nm for interference detection methods), c is the concentration of protein (in g/ml) in the sedimenting IMP species, K is the magnification and l is the pathlength (cm). J can be obtained by integrating the area under the peak in the $c(s)$ Interference distribution corresponding to the protein-detergent complex (Fig. 1.2B) and similarly c can be determined by integrating the area under the peak corresponding to the protein-detergent complex in the $c(s)$ absorbance distribution and dividing by the extinction

coefficient of that protein or complex (calculated from protein sequence) to determine the protein concentration. From interference and absorbance data sets of the same sample and using equations 1.4 – 1.7 the molar mass of the protein-detergent complex can be determined. With the total mass of the protein-detergent complex known the mass of the protein component can be determined easily using the equation:

$$M_P = \frac{M_{PD}}{1 + \delta_D} \quad (1.8)$$

Where M_P is the mass of the protein component (27). In the case of a simple protein-detergent complex comprised of only one type of protein the oligomeric state of the protein can be determined by dividing the M_P by the molecular weight of the monomeric protein as determined from the amino acid sequence, which should yield a near integer value for a monodisperse species. In the case of a more complicated protein complex comprised of multiple different proteins more information will be required to determine the composition of the complex.

The composition of a protein complex can be determined in a similar manner as described above by including a third detection method, fluorescence, or simply by using tags with differing absorbance maxima. Individual components of the complex are labeled with small molecule tags or conjugated to fluorescent proteins and the relative absorbance of the tags can be related to the concentrations of each protein within the complex:

$$c_n = \left(\frac{A}{\epsilon \times l} \right) \times \frac{1}{d_n} \quad (1.9)$$

Where c_n is the concentration of component n, A is the measured absorbance of the tag linked to n, ϵ is the molar extinction coefficient of the tag, l is path length and d_n is the degree of labelling (number of tags per protein molecule) (30). Once the concentration of each component in the protein complex is determined from equation 1.9, the values can be used to determine total protein concentration (in mg/ml) and the molar mass of the protein-detergent complex can be

determined as above with equations 1.4 – 1.8. Once the molar mass of the total protein component of the protein detergent complex is determined the molar mass of each component can be determined from the ratios of the concentrations of each component in the complex.

A second method that can provide complimentary information to AUC is multiple angle light scattering (MALS). MALS relies on the visible light scattering properties of proteins to determine their size (31). MALS is commonly used in conjunction with a separation technique such as size exclusion chromatography (SEC-MALS) to allow for the analysis of individual species in polydisperse solutions (31). MALS requires the determination of the concentration of material being examined (usually through refractive index or absorbance at 280 nm in the case of proteins, SEC-UV-MALS-RI) to deconvolute the influence of concentration from the scattered light intensities (31, 32). For IMP proteins, the molar mass determined is of the protein-detergent complex and from there one can determine the mass of the protein component using two detection methods (refractive index and absorbance at 280 nm) (31).

AUC and SEC-MALS provide similar information about the molar mass of an IMP-detergent complex: the molar mass of the protein component and mass of the detergent bound to the protein; however, AUC sedimentation velocity experiments can provide additional information. The Lamm equation (Equation 1.3) describes the sedimentation of macromolecules in solution. The two terms describing the sedimentation include the variables s (sedimentation coefficient) and D (the diffusion coefficient). The diffusion coefficient term can be related to the frictional ratio, f/f_0 , which describes the friction experienced by the sedimenting species relative to the friction experienced by a sphere of the same mass:

$$D = \frac{\sqrt{2}}{18\pi} kTs^{-\frac{1}{2}} \left(\eta \left(\frac{f}{f_0} \right) \right)^{-\frac{2}{3}} \left(\frac{(1-\bar{v}\rho)}{\bar{v}} \right)^{\frac{1}{2}} \quad (1.10)$$

Where k is the Boltzmann constant and T is temperature. f/f_0 can therefore be summarized as a value that describes how spherical the sedimenting species is. An assumption is made in a $c(s)$ analysis of AUC data described above: all species in the solution have the same f/f_0 value (26). The software Sedfit (26) offers an alternative, more computationally demanding analysis, and determines $c(s, f/f_0)$, which allows for the consideration of a range of f/f_0 values producing a 2-dimensional (2D) distribution (s and f/f_0) sufficient for the deconvolution of species with similar s values but differing f/f_0 ratios (Fig. 1.3) (33).

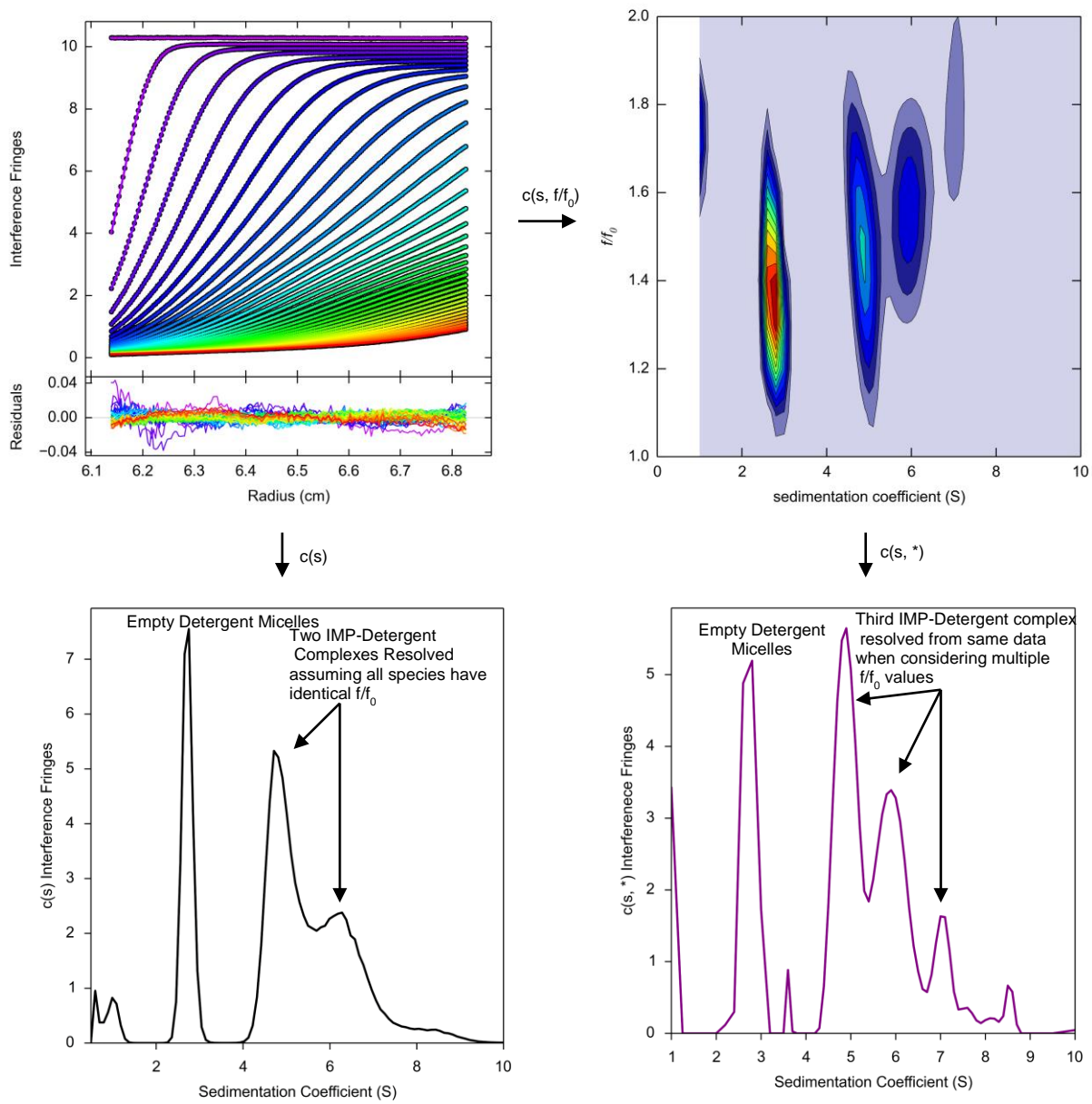


Figure 1.3 Comparison of $c(s)$ and $c(s, f/f_0)$ analyses.

Figure 1.3 Comparison of $c(s)$ and $c(s, f/f_0)$ analyses. The top left panel depicts AUC sedimentation velocity data corresponding to *Neurospora* VDAC in the presence of a cholesterol analogue (Chapter 2). The data points (circles) and Lamm equation solutions (lines) are shown. The bottom right panel depicts a $c(s)$ interference distribution determined from the sedimentation velocity data and clearly shows two VDAC species. The top right panel depicts a $c(s, f/f_0)$ interference distribution of the same data which shows three distinct VDAC species. The bottom right panel depicts a $c(s, *)$ distribution of the same data ($c(s, f/f_0)$ compressed back to a 1D distribution), which clearly shows the three VDAC species.

1.4 Modelling of IMP-Detergent Complexes from Small-Angle Scattering Data

Small angle scattering techniques have been complimentary methods to high resolution structural characterization of proteins for many years (34). Small angle scattering methods (SAS) can provide low resolution structural information about proteins or protein complexes without the need for crystallization (34, 35). More recently there have been improvements in the analysis of IMP SAS data, which have allowed for the low-resolution modelling of IMP-detergent complexes (36). Two main methods are used for the analysis of proteins by SAS, small-angle x-ray scattering (SAXS), which provides information on the electron density and small-angle neutron scattering (SANS), which provides information on the nuclei in the protein molecule. SAS techniques have several advantages over high resolution methods regarding IMPs, with the main disadvantage being the lower resolution of data produced. The main advantages are that the IMPs do not have to be crystallized, which has proven to be a major bottleneck in the high-resolution characterization of IMPs by protein crystallography and that concentrations of proteins required are not as high as those required for NMR (37, 38). The complications of using SAS techniques to study IMPs are the need for the protein to be in solution, requiring the use of detergents (36). The presence of other large components in the solution such as detergents causes two issues, the free detergent micelles will contribute to the measured scattering intensities and the detergent bound to the protein creates a layer around the protein that must be accounted for in the modelling (36).

SAXS and SANS each have benefits and disadvantages to the analysis of IMPs. SANS and SAXS both suffer from the scattering by free detergent micelles in solubilized IMP solutions. The solutions to this problem are different for each technique. To account for free detergent micelle scattering in SAXS experiments the SAXS measurements are coupled to a

separation technique such as size exclusion chromatography (SEC-SAXS) (39). In SEC-SAXS measurements a scattering curve is recorded every few seconds as the sample elutes from a SEC column; this allows for the determination of the free micelle scattering contribution of the running buffer from the scattering data obtained during the elution of the void volume of the column, which can be subtracted from the scattering curves obtained during the elution of the IMP-detergent complex (36, 39). This process is made possible using very brilliant X-ray sources such as those at synchrotrons, which allow for the rapid acquisition of scattering curves (40). Coupling to SEC is not possible for the acquisition of SANS data as the intensity of neutron sources precludes the short acquisition times required (41). The most common method to account for free-detergent micelle scattering in SANS experiments is to match the scattering-length density of the solvent to the scattering length density of the detergent micelles (41, 42). This can be accomplished using D₂O to match the scattering length density of the solvent to the scattering length density of the detergent. This methodology works well as the scattering length density of many common detergents lies within the range of H₂O and D₂O (43). This provides another benefit as the matching of the solvent to the detergent micelles will also match the scattering-length density of the detergent bound to the IMP essentially making the bound detergent appear invisible (43). This method does not work well for SAXS as the differences in electron densities between detergents and water can be quite large and as a result the quantity of solutes that would be required to alter the electron density of the solvent can be impossible to achieve (44, 45). This can be further complicated by the differing electron densities of detergent head groups and tails; therefore the entirety of the detergent contribution cannot be matched by a single solute concentration (45).

SAXS is a powerful platform for the low-resolution modeling of IMPs; even though the resulting data can be more complicated to interpret the benefit of coupling the measurements to SEC allows for the analysis of poly-disperse solutions such as the separation of oligomers or complexes from component proteins that would influence scattering data (Chapter 2). The separation by size and shape that SEC provides is important in the separation of IMP-detergent complexes from excess empty detergent micelles in the sample (Fig. 1.4A) (Chapter 2). This mismatch in the free detergent micelle concentration between the sample and reference solution can be caused by concentrating the sample before taking measurements (Fig. 1.4A). Currently, prior information about the protein component of an IMP-detergent complex such as a crystal structure or predicted structure describing the protein component of the complex is required for proper interpretation of the data (36). These models can be validated using experimental scattering intensities of a IMP-detergent complex using the software memprot (36). Memprot iteratively determines the dimensions of an ellipsoidal detergent layer (See Figure 2.4 for a visual description of the parameters describing the detergent layer) surrounding an input protein structure and outputs the model that most closely fits the experimentally measured scattering curve (36) (Fig. 1.4B). This could allow for the use of SAXS data to validate known crystal structures (determine if there are crystal packing artifacts), NMR structure (determine if the structure is similar at lower concentrations) and predicted structures or computational models. SEC-SAXS data has in fact been used as a constraint in the modelling of at least one IMP-detergent complex (46). The main limitations of memprot are the fact that only ellipsoidal geometries are considered for the detergent layer and the reliance on previous structural information pertaining to the protein. A recent development in the analysis of SAXS data allows for the direct calculation of electron density maps of macromolecules in solution (47). This is an

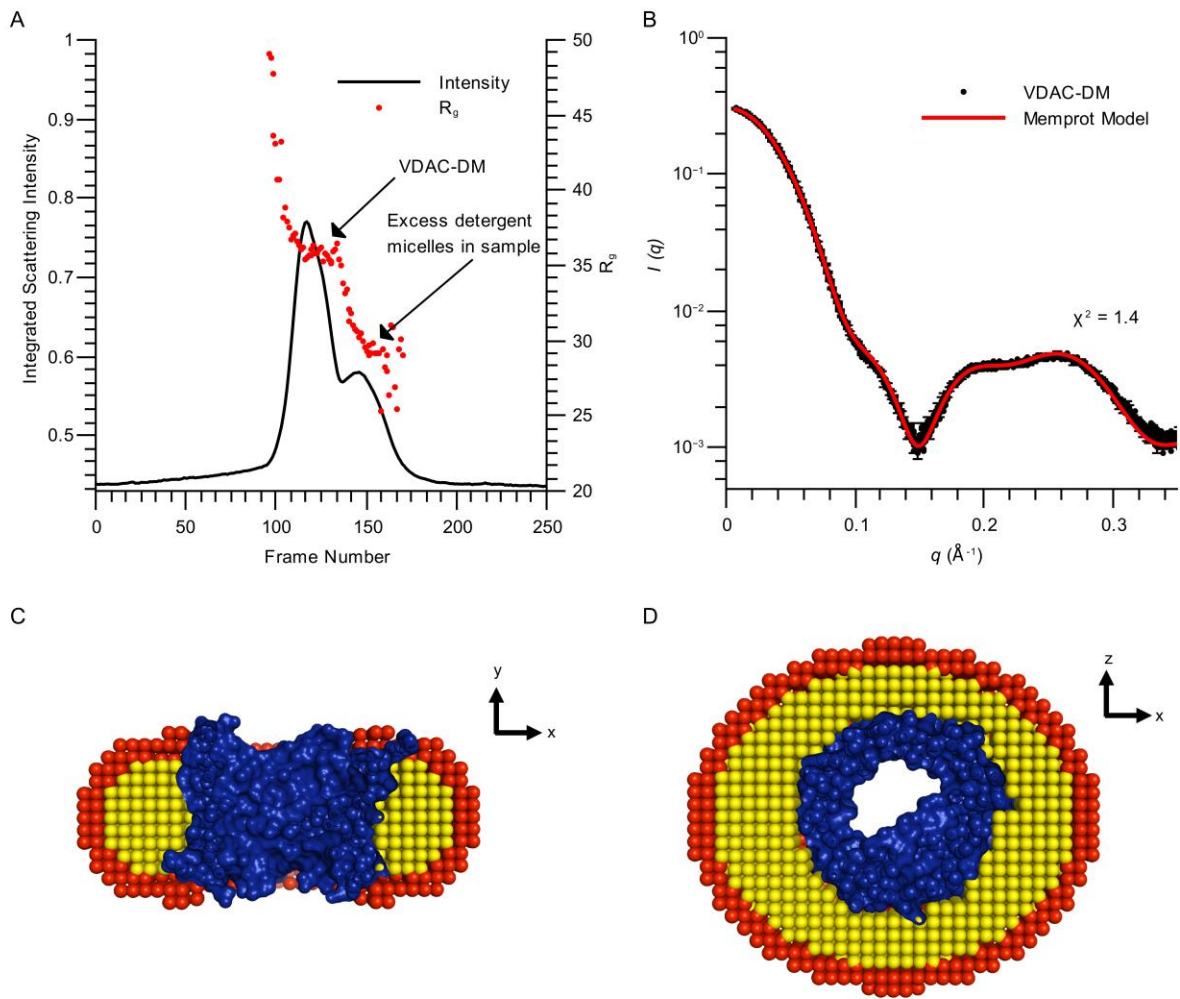


Figure 1.4. SEC-SAXS analysis of detergent solubilized IMPs.

Figure 1.4. SEC-SAXS analysis of detergent solubilized IMPs. A) Total Integrated scattering intensity of each frame plotted against frame number of a SEC-SAXS elution of *Neurospora* VDAC solubilized in the detergent DM (black line) and the radius of gyration determined from each frame with integrated intensity greater than the 0.45 baseline (red circles). B) Averaged scattering curve of the VDAC-DM complex (black circles) obtained by subtracting the buffer scattering contribution from each frame and then scaling and averaging each frame containing the VDAC-DM complex (region of the elution containing VDAC is indicated in panel (A)). The red line depicts the calculated scattering curve of a VDAC-DM complex produced by the software memprot; the reduced χ^2 of the fit between the model and experimental data is shown on the plot. C) Cross section of the VDAC-DM model produced by memprot using the mouse VDAC crystal structure (PDB: 3EMN) as the input model. D) The same VDAC-DM memprot model rotated 90° around the x-axis relative to panel (C). In panels (C) and (D) the mouse VDAC crystal structure is colored in blue, the beads corresponding to the detergent hydrophobic tails are colored in yellow and the beads corresponding to the hydrophilic headgroups are colored red.

exciting improvement to the treatment of SAXS data, which is currently modeled using coarse grain beads of uniform electron density (35, 48). The basic principles behind this approach show great promise for improvement of IMP-detergent complex SAXS data analysis as it would require no prior information as with memprot (36, 47). However, great care should be taken when using this new method as it should be noted that the current algorithm for the direct calculation of electron density from SAXS data, Denss (47), by the nature of its design will not consider components with negative electron density contrast (negative density is forced to 0) (47). This is an important point to consider as many commonly used detergents contain hydrophobic layers with negative electron density in contrast to water (45). Therefore, in order to use the Denss algorithm with an IMP data set great care must be taken to ensure the detergents used have an electron density higher than water (45, 47). Overall SAS methods can provide low resolution but important information about the organization of IMPs solubilized in detergents.

1.5 Combined Biophysics Approach

MST, AUC and SEC-SAXS are powerful techniques for the examination of IMPs as has been discussed above. The advantages and disadvantages of each individual method with respect to IMPs have been described above; however, the use of all three methods together can provide crucial information for the interpretation of data. A suggested approach to the characterization of detergent solubilized IMPs or IMP containing complexes using these methodologies is summarized in Fig. 1.5. The general workflow is to screen for interactions or oligomerization using MST, if an interaction is identified MST can be used to determine the affinity of the interaction (K_d), then AUC or SEC-UV-MALS-RI at a protein concentration above the K_d can be used to determine the oligomeric state or complex composition of the protein(s) involved in the

interaction and finally with the known composition of the IMP complex a model can be constructed and validated with SEC-SAXS data. These biophysical characterizations can provide information on the behavior of IMPs at the molecular level in isolation. It is, however, important to consider that the *in vitro* data gathered pertaining to an IMP obtained through a biophysical analysis may not correlate directly to the *in vivo* behaviour of the protein. It is therefore paramount that the information obtained from these methods be correlated to *in vivo* experiments using methods such as co-localization, proteomics, activity assays and physiological analysis. The use of biophysical methods to gain insight into the structure and function of biological macromolecules has been a long-standing approach for soluble proteins; however, in the past membrane proteins presented many difficulties. In this work the use of three biophysical methods in combination MST, AUC and SAXS to characterized IMPs was discussed and advances in these methodologies have allowed for the accessible characterization of integral membrane proteins.

1.6 Voltage-Dependent Anion-Selective Channels

Voltage-dependent anion-selective channels (VDACs) are integral membrane proteins which facilitate the transfer of ions and small molecules across the mitochondrial outer membrane (49). VDACs are ubiquitous to aerobic eukaryotes (50, 51), with some organisms expressing multiple VDAC isoforms (52). VDACs play an essential role in metabolism evidenced by a lethal phenotype in mouse VDAC2 knockout strains, partial lethality in mouse VDAC1 knockout strains, infertility in mouse VDAC3 knockout strains and extreme growth defects in *Neurospora crassa* VDAC knockout strains (53-56). VDACs form large aqueous channels approximately 1.4 nm in diameter at the smallest point (57, 58). Although the pore

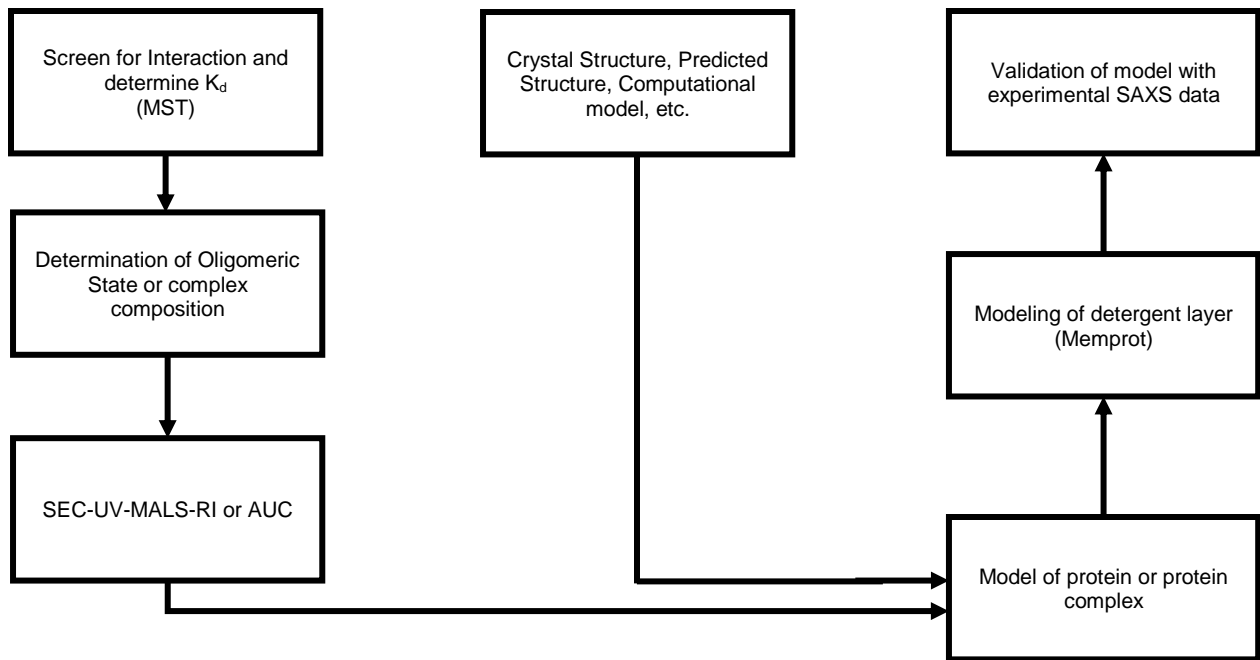


Figure 1.5. Summary of the biophysics pipeline for the *in vitro* characterization of IMPs.

formed by VDAC is quite large and it acts a general-purpose pore allowing for the passive diffusion of many kinds of molecules across the membrane there is evidence of direct interaction of nucleotides with the VDAC channel (58-60). VDACs are predicted to have high structural similarity although the sequence variability of proteins in the family is quite large (50, 51). Pore formation is accomplished by a β -barrel transmembrane domain consisting of 19 antiparallel β -strands with the first and last strands arranged in parallel (See Chapter 3 for a cartoon representation of the predicted *N. crassa* VDAC structure, Fig. 3.1). Aside from the transfer of small molecules across the mitochondrial outer membrane VDAC self-association (61), interactions with hexokinase (62-64) and bcl-2 family proteins (65), are involved in mitochondrial-mediated apoptotic signaling events ultimately leading to the release of cytochrome c, smac/diablo and apoptosis inducing factor (AIF) from mitochondria (61, 62, 65). VDAC's involvement in apoptotic signaling and metabolism will be discussed in more detail in chapter 2 and 3 respectively. As the major interface between the cytoplasm and the mitochondrial interior and playing a role in mitochondrial-mediated apoptotic signaling VDAC is an important member of a complex system of protein-protein interactions making it the ideal candidate for the combined biophysics approach coupled with physiological analysis.

1.7 Thesis Objectives

A methodology for the *in vitro* characterization of IMPs has been described above. The *in vitro* characterization of IMPs is an important step towards the understanding of IMP structures and functions; however, the information determined from these methods must be considered in a biological context. Therefore, it is important to also consider biological and physiological

information to better understand the relevance of the physical information. The main objective of this work was to develop a biophysics pipeline to investigate the *in vitro* physical characteristics of *Neurospora crassa* voltage dependent anion-selective channel (VDAC), an integral mitochondrial outer membrane protein and relate those physical characteristics of VDAC to physiological data. This protein is a 19-stranded β -barrel that acts as a channel and regulator of cellular metabolism; it is described in detail in Chapters 2 and 3. To achieve this objective two approaches were utilized:

- 1) Biophysical characterization of the effect of cholesterol analogues on *N. crassa* VDAC solubilized in detergent (Chapter 2)
- 2) Physiological and proteomic analysis of a *N. crassa* mutant expressing a VDAC deletion variant (Chapter 3)

Approach 1 utilized the methodology described above, a combination of microscale thermophoresis, analytical ultracentrifugation and size exclusion chromatography small angle x-ray scattering to probe the effect of a cholesterol analogue on the oligomeric state of VDAC, the organization of these oligomers and VDAC-hexokinase complex formation. Approach 2 focused on the effect of a VDAC mutation on the mitochondrial proteome and physiology using a mass spectrometry proteomic analysis, as well as biochemical assays to determine the overall effect of the mutation on mitochondrial function. The structural and functional analysis of *N. crassa* VDAC described will further the understanding of VDAC's role in metabolism and apoptosis.

Chapter 2: A Cholesterol Analogue Induces an Oligomeric Reorganization of VDAC

2.1 Publication Details and Author Contributions

Ferens F.G., Patel T.R., Oriss G., Court D.A., Stetefeld J. 2019. A Cholesterol Analog Induces an Oligomeric Reorganization of VDAC. *Biophysical Journal*, 116(5):847-859, DOI: 10.1016/j.bpj.2019.01.031

F.F. developed the biophysics pipeline. F.F., T.P., D.C. and J.S. designed the experiments. F.F. and T.P. performed the analytical ultracentrifuge experiments. G.O. performed initial VDAC^N solubilization and purification optimizations. F.F. performed all other experiments. F.F. analyzed the data. F.F., T.P., D.C. and J.S. prepared the manuscript.

2.2 Abstract

The oligomeric organization of the voltage-dependent anion-selective channel (VDAC) and its interactions with hexokinase play integral roles in mitochondrially mediated apoptotic signaling. Various small to large assemblies of VDAC are observed in mitochondrial outer membranes but they do not predominate in detergent solubilized VDAC samples. In this study, a cholesterol analogue, cholesteryl-hemisuccinate (CHS), was shown induce the formation of detergent soluble VDAC multimers. The various oligomeric states of VDAC induced by the addition of CHS were deciphered through an integrated biophysics approach using microscale thermophoresis, analytical ultracentrifugation and size exclusion chromatography-small angle X-ray scattering. Furthermore, CHS stabilizes the interaction between VDAC and hexokinase (K_d of $27 \pm 6 \mu\text{M}$), confirming the biological relevance of oligomers generated. Thus, sterols such as cholesterol in higher eukaryotes or ergosterol in fungi may regulate VDAC oligomeric state and may provide a potential target for the modulation of apoptotic signaling by effecting VDAC-

VDAC and VDAC-hexokinase interactions. In addition, the integrated biophysical approach described provides a powerful platform for the study of membrane protein complexes in solution.

2.3 Introduction

The characterization of integral membrane proteins in solution is often difficult relative to soluble proteins due to the necessity of adding amphipathic detergents to solubilize and stabilize them in solution (15). Nevertheless, their immense importance in biotechnology, structure-based drug design and medicine is evident from the fact that 59% of FDA approved drugs target transmembrane proteins (1). The potentially enormous impact of these drugs, coupled with the difficulty of studying the structure-function relationships of these membrane-localized drug targets, has created a pressing need for innovative methods to study integral membrane proteins. In this study we used a combination of existing technologies to probe the oligomeric states of an integral membrane protein VDAC.

Voltage-dependent anion-selective channels (VDACs) are a family of mitochondrial outer membrane proteins ubiquitous in aerobic eukaryotes and have garnered interest as possible targets for anticancer drugs (8, 66, 67). VDAC family proteins form large pores in the mitochondrial outer membrane, about 1.4 nm in diameter at the narrowest point (57, 58). The primary function of VDAC is the exchange of ions and metabolites across the mitochondrial outer membrane (49). VDAC interacts with proteins involved in apoptotic signaling, specifically through hexokinase dissociation (62, 63), interactions with bcl-2 family proteins (61, 62) and it is possibly involved in the release of cytochrome c and apoptosis-inducing factor (AIF) from mitochondria (61). The reorganization of VDAC into units larger than monomers and the

disassociation of the VDAC-hexokinase complex have been linked to mitochondrial mediated apoptosis (61).

Crystal structures of VDACs have provided insights into possible oligomeric organizations in the form of crystal packing; however, the biological relevance of these VDAC organizations is still being debated (57, 68, 69). Interestingly, many of the detergent-solubilized VDACs examined to date seem to adopt a monomeric configuration except for zebrafish VDAC2 and mouse VDAC1 (at low pH) which adopted dimeric configurations in detergent solutions (57, 58, 70, 71). Multimeric VDAC assemblies purified from native membranes have been observed using electron microscopy and atomic force microscopy; however, the components of the lipid environment that conserved the native VDAC oligomeric states were not identified (60, 72).

Here we utilized an integrated approach combining (i) microscale thermophoresis (MST) for the determination of binding constants and relevant concentrations of proteins for oligomeric analyses, (ii) analytical ultracentrifugation (AUC) to determine oligomeric state and (iii) size-exclusion chromatography in conjunction with small angle x-ray scattering (SEC-SAXS) to model VDAC-detergent complexes. We use this pipeline to decipher the oligomeric organization of this essential integral membrane protein and begin to probe VDAC complex formation with hexokinases. The established MST-AUC-SEC-SAXS experiments allowed us to validate high resolution structures with solution scattering data and to determine the oligomeric organizations of VDAC in detergent complexes (36, 46).

2.4 Materials and Methods

2.4.1 Plasmids, Strains and Reagents

Native purification of *N. crassa* VDAC was performed using a strain in which the VDAC gene was replaced via homologous recombination with a cDNA copy of the gene with a C-terminal 6x his tag, as described previously (73). The resulting strain was named Por-his₆.

Denaturing purification of the *N. crassa* VDAC was conducted utilizing a codon-optimized sequence for expression in *E. coli*. A 6x his-tag was engineered onto the C-terminus of the protein sequence. The gene was synthesized and cloned into the vector pET21b via the NdeI and BamHI sites by GenScript (Piscataway, NJ, USA). The resulting pET21b-VDAC-his₆ plasmid was transformed into *E. coli* strain BL21(c43) (74) for VDAC overexpression.

n-decyl- β -d-maltopyranoside (DM, Anagrade) was purchased from Anatrace, (Maumee, OH, USA) and cholesteryl-hemisuccinate (CHS) was purchased from Sigma-Aldrich Canada (Oakville, ON, Canada). All buffer solutions used in this study were adjusted to pH 7.0 unless otherwise specified.

2.4.2 VDAC^N Purification

Cultivation of *N. crassa* was conducted as per standard methodologies (75). 20 L of Por-his₆ culture was grown at 30°C for 22 h and mycelia were harvested via filtration using a paper filter. Mitochondria were isolated as previously described (73, 76) and diluted to a total protein concentration of 10 mg/ml. The suspension of mitochondria was mixed 1:1 with a solution of 20 mM MOPS, 300 mM NaCl, 2% DM, 2 mM 4-(2-aminoethyl)benzenesulfonyl fluoride hydrochloride (AEBSF) and mixed at 4°C for 1 hour and then applied to 5-mL of Ni-NTA resin (Thermo-Fisher Canada, Mississauga, ON, Canada) and allowed to bind in batch with mixing

overnight at 4°C. The Ni-NTA resin was washed with 4 column volumes of 20 mM MOPS, 100 mM NaCl, 0.3% DM, followed by 2 column volumes of 20 mM MOPS, 100 mM NaCl, 20 mM imidazole, 0.3% DM and then was eluted with 20 mM MOPS, 100 mM NaCl, 300 mM Imidazole, 0.3% DM. VDAC^N was then concentrated utilizing a 50-kDa cutoff concentrator and applied to a 24 ml capacity Superdex 200 Increase column (GE Healthcare Canada, Mississauga, ON, Canada) equilibrated with 20 mM MOPS, 100 mM NaCl, 0.3% DM. VDAC-containing fractions (Fig. 2.1A) were collected and pooled.

2.4.3 VDAC^R Overexpression, Purification and Refolding

A 25-ml overnight culture of BL21(c43) cells containing the pET21b-VDAC-his₆ vector was added to 500 mL of pre-warmed (37°C) LB media. The 500-mL culture was grown with shaking at 37°C for 1 h, after which time VDAC expression was induced with the addition of IPTG to a final concentration of 0.5 mM; the culture was grown for a further 4 hours. Cells were harvested via centrifugation for 5 min at 8000 rpm in a Sorvall SLA-3000 rotor. Harvested cells were resuspended in 30 mL of chilled (4°C) buffer (20 mM Tris, 300 mM NaCl, 1 mM AEBSF, pH 8.0). Resuspended cells were lysed via 3 passes through a french pressure cell at a pressure of 20,000 psi. VDAC inclusion bodies were harvested from cell lysate via centrifugation for 15 minutes at 16,000 rpm in a Sorvall SS-34 rotor. The resulting supernatant was discarded, and the pellet was resuspended in 20 mM MOPS, 150 mM NaCl, 6 M guanidine-HCl using a glass homogenizer. Insoluble material was removed via centrifugation at 20,000 rpm in a Sorvall SS - 34 rotor. The supernatant was applied to 3 mL Ni-NTA resin and binding of VDAC to the resin was done in batch with mixing overnight at 4°C. The Ni-NTA resin was washed with 10 column volumes of 20 mM MOPS, 150 mM NaCl, 6 M guanidine-HCl followed by 4 column volumes of

20 mM MOPS, 150 mM NaCl, 20 mM Imidazole, 6 M guanidine-HCl. VDAC was eluted with 10 mL of 20 mM MOPS, 150 mM NaCl, 600 mM Imidazole, 6 M guanidine-HCl.

Purified recombinant VDAC (VDAC^R) was refolded by rapid 1/10 dilution of denatured VDAC^R into 20 mM Tris, 300 mM NaCl, 1% DM pH 8.0 at 4°C. This mixture was dialyzed against 20 mM Tris, 300 mM, NaCl pH 8.0 overnight at 4°C using a dialysis membrane with a M_w cutoff less than 10 kDa. Dialyzed VDAC^R samples were then concentrated using a concentrator with a M_w cutoff of 50 kDa. Concentrated samples were loaded onto a 24 ml capacity Superdex 200 increase column equilibrated with 20 mM MOPS, 100 mM NaCl, 0.3% DM to separate aggregates from correctly refolded protein. For experiments containing CHS there was an additional SEC step to exchange the buffer via a 24 ml capacity Superdex 200 increase column equilibrated with 20 mM MOPS, 100 mM NaCl, 0.3% DM, 0.06% CHS. VDAC containing fractions were pooled and concentrated with a 50 or 100 kDa M_w cutoff concentrator. Purified VDAC activity was assessed using liposome swelling assays as described previously (77) (Fig. 2.1D).

2.4.4 Circular Dichroism Spectrapolarimetry (CD)

VDAC samples were exchanged into CD buffer (either 100 mM NaCl, 0.1% DM pH 7.0 or 20 mM MOPS, 100 mM NaCl, 0.1% DM 0.02% CHS pH7.0) and diluted to approximately 1 mg/ml in the same buffer. Final protein concentration was measured by UV absorbance at 280 nm (VDAC E_{0.1%}: 0.79, calculated from sequence). CD measurements were taken with a Jasco J-810 spectropolarimeter at 20°C in a 0.01-cm path length quartz cuvette. Raw data were converted to mean residue ellipticity (MRE) and secondary structure deconvolution was done using the CDSSTR algorithm and the SMP180 reference set on the Dichroweb server (78-80)

2.4.5 Analytical Ultracentrifugation (AUC)

VDAC was diluted to appropriate concentrations in 20 mM MOPS, 100 mM NaCl, 0.3% DM or 20 mM MOPS, 100 mM NaCl, 0.3% DM, 0.06% CHS, with the highest concentration of VDAC not exceeding 1 AU at 280 nm; final protein concentrations were determined directly from AUC absorbance data. Experiments were conducted using a Beckman-Coulter Proteome XL-I analytical ultracentrifuge and an An50Ti rotor.

Sedimentation velocity experiments were conducted at a rotor speed of 30,000 rpm and 20 mM MOPS, 100 mM NaCl (ρ : 1.004 g/ml, η : 0.01006 mPa) was used as the reference solution. Other values used in the analysis: VDAC \bar{v} of 0.733 was determined from the protein sequence using Sednterp (<http://www.jphilo.mailway.com/download.htm#SEDNTERP>), 0.187 was used as the VDAC dn/dc (29), VDAC $\epsilon_{0.1\%, 280}$ of 0.79 was determined from protein sequence, DM \bar{v} of 0.8 was reported by Zimmer *et al.*, 2006 (81), and DM dn/dc of 0.1457 was experimentally determined (data not shown). R_s values were determined by SEC elution volume relative to a standard curve of proteins with known R_s values. Sedimentation velocity $c(s)$ distribution analysis ($c(s)$ assumes a single frictional ratio, f/f_0 , for all species producing an s distribution of measured intensity) and $c(s, f/f_0)$ distribution analyses ($c(s, f/f_0)$ makes no assumptions about frictional ratio and produces a 2D distribution of the measured signal with s and f/f_0 dimensions) were conducted using the software sedfit (26). To gain additional resolution of VDAC species with similar S values in the VDAC^R+CHS samples 2D $c(s, f/f_0)$ distributions were calculated for the interference data sets (Fig. 2.2E). Due to the lower signal to noise ratio in the corresponding absorbance data sets of these samples it was not possible to produce meaningful $c(s, f/f_0)$ distributions from absorbance data. To produce comparable interference and absorbance distributions describing VDAC^R+CHS samples which retained the increased

resolution of VDAC species from the $c(s, f/f_0)$ distributions, we employed a Bayesian statistical analysis implemented in *sedfit* (82). This analysis was used to produce interference and absorbance $c(s)$ distributions of VDAC^R+CHS samples (Fig. 2.2F) using the prior knowledge of the distribution of VDAC species in these samples obtained from the $c(s, f/f_0)$ analysis of the interference data (Fig. 2.2E). Four VDAC concentrations were examined in the absence of CHS and in the presence of CHS so that sedimentation coefficients could be extrapolated to a protein concentration of 0 mg/ml to account for concentration dependent factors and to allow accurate determination of dn/dc_p values for the VDAC-detergent complexes. Before use for molecular weight determination, experimentally determined sedimentation coefficients ($S_{20, \text{buffer}}$: 20°C in sample buffer) were adjusted to standard conditions ($S_{20, \text{water}}$: 20°C in water).

Experimental theory and analysis of membrane protein samples and nomenclature are as previously described by Salvay et al., 2007 (27). A summary of the theory is as follows:

The mass of the protein detergent complex (M_{PD}) can be described by the equation:

$$M_{PD} = \frac{6\pi s N_A \eta R_s}{1 - \rho^\circ \bar{v}_{PD}} \quad (1.4)$$

Where N_A is Avogadro's number, η is the solvent viscosity, R_s is the hydrodynamic radius of the protein-detergent complex, s is the sedimentation coefficient, ρ° is the solvent density and \bar{v}_{PD} is the partial specific volume of the protein detergent complex. The \bar{v}_{PD} can be determined by the following equation:

$$\bar{v}_{PD} = \frac{\bar{v}_P + \delta_D \bar{v}_D}{1 + \delta_D} \quad (1.5)$$

Where \bar{v}_P and \bar{v}_D are the partial specific volumes of the protein and detergent respectively and δ_D is the ratio of detergent:protein (g:g) in the protein-detergent complex. δ_D can be determined

from the refractive index increment (dn/dc_p , change in refractive index relative to protein concentration) of the protein-detergent complex as follows:

$$\left(\frac{dn}{dc_p}\right)_{PD} = \left(\frac{dn}{dc_p}\right)_P + \left(\frac{dn}{dc_D}\right)_D \delta_D \quad (1.6)$$

Where $(dn/dc_p)_P$ is the refractive index increment of the protein and $(dn/dc_D)_D$ is the refractive index increment of the detergent. Finally the $(dn/dc_p)_{PD}$ can be determined from the absorbance at 280 nm and interference fringe displacement of the protein-detergent complex as follows:

$$\left(\frac{dn}{dc_p}\right)_{PD} = \frac{J\lambda}{cKl} \quad (1.7)$$

Where J is the interference fringe displacement, λ is the wavelength of light used, c is the concentration of protein determined from absorbance at 280 nm, K is the magnification of the lens used and l is the pathlength of the sample. Interference fringe displacement of a species can be directly determined from a $c(s)$ distribution of interference fringe displacement by integrating the area under the peak of the species being examined and the same is true for absorbance at 280 nm with the exception that a $c(s)$ distribution of absorbance data would be used instead.

Once the mass of the protein-detergent complex has been determined from the previous equations the mass of the protein and detergent components can be determined using δ_D :

$$M_P = \frac{M_{PD}}{1 + \delta_D} \quad (1.8)$$

$$M_D = M_{PD} - M_P \quad (2.1)$$

Where M_P and M_D are the masses of the protein and detergent components respectively.

2.4.6 Small-Angle X-ray Scattering (SAXS)

SEC-SAXS data was collected at beamline B21, Diamond Light Source (Didcot, UK).

VDAC-detergent complexes at VDAC concentrations of approximately 5-10 mg/ml in the

presence and absence of CHS were applied to a 2.4 ml superdex 200 increase column equilibrated with the appropriate buffer (20 mM MOPS, 100 mM NaCl with 0.1% DM or 0.1% DM+0.02% CHS) and the eluate was examined in-line. Data were collected with exposure to 1 Å wavelength x-rays. ScÅtter (<http://www.bioisis.net/scatter/>) and ATSAS (48) software packages were used to process collected SAXS data. Models were constructed using the crystal structure of mouse VDAC1 (PDB: 3EMN, 296 residues, 30% sequence identity to *N. crassa* VDAC, M_w : 32 kDa) (57, 69) or the crystal structure of zebrafish VDAC2 (PDB: 4BUM, 283 residues, 33% sequence identity to *N. crassa* VDAC, M_w : 30 kDa) (68) to describe the protein phase of the protein-detergent complex and the Memprot algorithm (36) to model the detergent corona around the protein. Memprot allows for the geometric modelling of an elliptical detergent layer around a fixed protein phase input in the form of a PDB file (protein electron density $0.42 \text{ e}^-/\text{Å}^2$) using 2 different types of detergent beads corresponding to detergent head groups (electron density $0.51 \text{ e}^-/\text{Å}^2$ for maltoside detergents (45)) and detergent tails (electron density $0.28 \text{ e}^-/\text{Å}^2$ for maltoside detergents (45))

2.4.7 Microscale Thermophoresis (MST)

VDAC was labeled with Alexa fluor 647 NHS ester dye (Thermo-Fisher Canada, Mississauga, ON, Canada) which labels lysine residues, VDAC samples were labeled with an efficiency of approximately 1 label per protein molecule as determined by absorbance measurements. Labeled VDAC was diluted to a concentration of 100 nM for hexokinase experiments or 20 nM for VDAC self-association experiments in 20mM MOPS, 100 mM NaCl, 0.3% DM or 20mM MOPS, 100 mM NaCl, 0.3% DM, 0.06% CHS which served as 2x working concentrations. Separated hexokinase isoforms were prepared from a mixture of *S. cerevisiae* hexokinases I and II (LS002512) obtained from Worthington Biochemical (Lakewood, NJ, USA)

using a well-established method relying on the different pIs of the isoforms (83). The hexokinase mixture was immobilized on a capto-Q anion exchange column (GE Healthcare Canada, Mississauga, ON, Canada) and hexokinases were separated by pI using a pH gradient formed by a linear gradient of a solution of 10 mM piperazine, 10 mM acetate, 10 mM formate at pH 5.5 and the same buffer solution at pH 4.0 (Fig. 2.7A & B). The isoforms were identified by the pH at which they eluted (Fig. 2.7A) (83). Purified HK-I and HK-II were exchanged into 20mM MOPS, 100mM NaCl, pH 7.0 buffer via dialysis. 2-fold serial dilutions (20 μ l) of concentrated separated hexokinases were prepared and each dilution was mixed 1:1 with the 100 nM stock solution of labeled VDAC for a final labeled VDAC concentration of 50 nM in each tube. For VDAC self-association experiments 2-fold serial dilutions (20 μ l) of concentrated unlabeled VDAC^R+CHS were prepared and each dilution was mixed 1:1 with the 20 nM labeled VDAC^R solution resulting in a final labeled VDAC concentration of 10 nM in each tube. MST experiments were conducted with a Nanotemper Monolith NT.115 in premium treated capillaries from Nanotemper Technologies (München, Germany). MST data was recorded at 40% maximum IR laser power. MST analysis was conducted using the “MO. Analysis” software from Nanotemper Technologies (München, Germany) and Palmist (20) using the K_d model. A brief description of the model is as follows:

The dissociation constant of a protein-protein complex consisting of two components, A and B, can be described by the following equation:

$$K_d = \frac{[A][B]}{[AB]} \quad (2.2)$$

Where K_d is the dissociation constant, [A] is the concentration of component A, [B] is the concentration of component B and [AB] is the concentration of the complex. For MST analysis

the fluorescence intensity of a sample after the activation of a localized heat source (F_{hot}) relative to the fluorescence intensity prior to the activation of the heat source (F_{cold}) is measured:

$$F_n = \frac{F_{hot}}{F_{cold}} \cdot 1000 \quad (2.3)$$

Where F_n is the resulting relative fluorescence of the sample. The measured F_n of a sample consisting of protein A, fluorescently labeled protein B and complex AB can be described by the equation:

$$F_n = \left(\frac{[B]}{B_{tot}} \cdot F_B \right) + \left(\frac{[AB]}{B_{tot}} \cdot F_{AB} \right) \quad (2.4)$$

Where B_{tot} is the total concentration of component B (bound and unbound), F_B is the F_n of protein B, and F_{AB} is the F_n of complex AB. The total concentrations of proteins A and B can be described by the following equations:

$$A_{tot} = [A] + [AB] \quad (2.5)$$

$$B_{tot} = [B] + [AB] \quad (2.6)$$

Using equations 2.2, 2.4, 2.5 and 2.6 we can describe F_n as a function of A_{tot} which can be fit to a series of MST measurements at different A_{tot} values (usually a 2-fold serial dilution) to determine K_d :

$$F_n(A_{tot}) = F_B + \frac{(F_{AB} - F_B) \left(A_{tot} + B_{tot} + K_d - \sqrt{(A_{tot} + B_{tot} + K_d)^2 - (4A_{tot}B_{tot})} \right)}{2B_{tot}} \quad (2.7)$$

Values for A_{tot} and B_{tot} are known as they are equivalent to the total input concentrations of each component for each measurement. Values for F_B , F_{AB} and K_d were determined by fitting the function to the experimental data if a full sigmoidal binding curve is observed over all measured values of A_{tot} (20). A more thorough examination of the theory and analysis of MST data on which this brief description was based is presented by Scheuermann, et al., 2016 (20).

2.5 Results

2.5.1 Evaluation of Recombinant *Neurospora crassa* VDAC

We established an isolation and characterization protocol for recombinantly expressed *Neurospora crassa* VDAC (VDAC^R) that was folded in n-decyl- β -d-maltopyranoside (DM). To evaluate the validity of VDAC^R as a biologically equivalent model protein, we performed the following experiments on VDAC^R and VDAC purified from *N. crassa* mitochondrial membranes (VDAC^N). In a first step, detergent-solubilized VDAC was assessed through size exclusion chromatography (Fig. 2.1A & B). Both, VDAC^N and VDAC^R elute as single symmetrical peaks with identical elution volumes of 14.2 mL indicating a R_s value of 4.2 nm from a calibration curve of proteins with known R_s values. These results suggest that, solubilized in DM, VDAC^R and VDAC^N exist in the same oligomeric state. In a second step, circular dichroism spectropolarimetry (CD) analysis suggests that VDAC from both sources have identical secondary structure compositions, which is largely consisting of β -strands (Fig. 2.1C), as observed previously (57, 58, 68). Deconvolution of the CD spectra reveals that the secondary structure compositions of VDAC^N and VDAC^R agree with the secondary structure present in the crystal structure of mouse VDAC1 (pdb-code: 3EMN) (Table 2.1) (57). Finally, liposome re-swelling assays show that VDAC^N and VDAC^R can both form pores large enough to accommodate the passage of poly ethylene glycol (average M_w 1000 Da, PEG1000) when reconstituted into lipid vesicles, indicating that they are functional (Fig. 2.1D). In addition, liposomes lacking any pores (pure lipid) as well as liposomes containing heat denatured VDAC were examined as negative controls (Fig. 2.1D). The liposomes containing heat denatured VDAC displayed a rapid increase in absorbance relative to the pure lipid liposomes indicating that the heat denatured VDAC was able to facilitate the rapid transfer of water molecules across

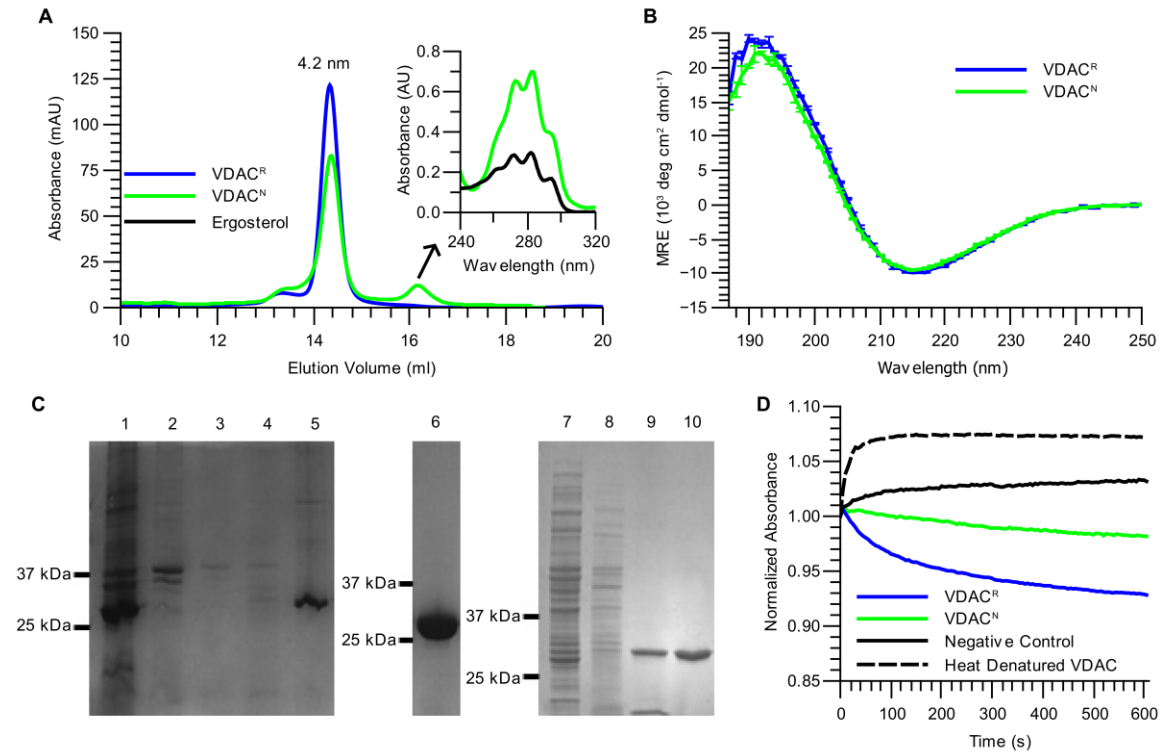


Figure 2.1 VDAC^R retains structural integrity and functionality relative to VDAC^N

Figure 2.1 VDAC^R retains structural integrity and functionality relative to VDAC^N.

(A) SEC profiles of VDAC^N (green), VDAC^R (blue) with the R_s calculated from the elution volumes of both samples displayed above the peaks. The inset depicts the UV spectrum of the small second peak in the VDAC^N elution (green) and the UV spectrum of the fungal sterol ergosterol (black). (B) CD-spectra of VDAC^N (Green) and VDAC^R (blue). Averages and standard deviations (error bars) of three measurements are displayed. See Table 2.1 for secondary structure deconvolution. (C) SDS-PAGE analysis of VDAC purification, cropped images of 3 gels are displayed for clarity with labeled lanes: 1: Inclusion bodies, 2-4: Ni-NTA Flow through, 5: Denatured VDAC^R elution, 6: Pooled SEC fractions of refolded VDAC^R, 7: Mitochondria, 8: DM solubilized mitochondrial proteins, 9: Ni-NTA purified VDAC^N, 10: Pooled SEC fractions of VDAC^N. Images of the full region of interest of each gel including protein M_w ladders are provided in the supplementary information (Fig. 5.3A-C). (D) Liposome re-swelling assays of VDAC^N and VDAC^R. Pore formation is observed through changes in the amount of scattered light that accompany reswelling of proteo-liposomes. The scattered light is measured by absorbance and is displayed as values normalized to the first absorbance measurement in each curve.

Table 2.1 VDAC secondary structure contributions obtained from deconvolution of CD data

Sample	α-Helix (%)	β-Strand (%)	β-Turn (%)	Other (%)	NRMSD
VDAC ^N	5	60	7	28	0.017
VDAC ^R	6	63	6	25	0.015
VDAC ^R +CHS	5	56	9	29	0.029
Mouse VDAC1 ^a	3	62	- ^b	35 ^b	-

^aValues for mVDAC1 (3EMN) obtained from the RCSB Protein Data Bank (57),

^bValues for β -turn content are grouped with “other” structural features on the PDB

the membrane upon the addition of solute to the exterior of the liposomes. There was no subsequent reduction in absorbance in the heat denatured liposomes indicating that any pores formed by the misfolded VDAC were too small to allow for the passage of PEG1000. It should be noted that the liposome size distribution in each individual reswelling assay reported in this work was not determined therefore the results of these assays are qualitative and the pore forming activity of each form of VDAC should not be quantitatively compared. In summary, VDAC^R is advantageous for our structural and biophysical studies as it retains structural integrity and functionality in comparison to VDAC^N while the purification and refolding procedure yields significantly higher quantities of VDAC relative to VDAC^N (~7.5 mg/L culture for VDAC^R and ~0.025mg/L culture for VDAC^N). With the methods used the only difference noticed between the two VDAC samples observed was a small second peak that eluted after VDAC^N during SEC (Fig. 2.1A and insert). This peak absorbed UV light at 280 nm; however, it did not contain protein as detected by SDS-PAGE analysis (data not shown). The far UV spectrum of the peak as well as previous evidence of co-purification (60, 84), suggests that the compound is ergosterol, a fungal sterol. Since ergosterol or cholesterol (85) was known to co-purify with VDACs derived from fungal or higher eukaryotes respectively, we became interested in investigating the effects that these sterols may have on VDAC. For this purpose, VDAC^R seemed to be an ideal platform as the denaturing purification from bacterial source would preclude the co-purification of any sterols which could have interfered with the investigation.

2.5.2 CHS Alters the Oligomeric State and Secondary Structure of VDAC^R

Attempts to introduce ergosterol or cholesterol to the sterol-free DM solubilized VDAC^R samples failed due to the insolubility of these sterols in the detergent DM (data not shown).

Therefore, to study the effects of sterols on VDAC solubilized in DM, we utilized cholesteryl-hemisuccinate (CHS), a cholesterol analogue soluble in maltoside detergents (86). Addition of CHS to VDAC^R drastically altered the behavior of the protein. Refolded VDAC in the presence of CHS (VDAC^R+CHS) eluted as three overlapping peaks during SEC. All three VDAC^R+CHS peaks eluted at much lower volumes than the protein in the absence of CHS (Fig. 2.2A). This result suggested the formation of at least three different VDAC oligomers, all of which had R_s values (5.9 nm, 6.9 nm and 7.7 nm) significantly greater than that of VDAC^R in the absence of CHS (4.2 nm) (Table 2.2). In addition, the CD spectrum of VDAC^R+CHS was slightly altered relative to VDAC^R (Fig. 2.2B) indicating that there is a conformational change in the secondary structure of the protein. Deconvolution of the CD spectrum suggested a reduction of β -strand content by 7% relative to VDAC^R (Table 2.1); although, it should be noted that the accuracy of computed secondary structure contributions from CD spectra is approximately ± 5 -10% under optimal conditions (87, 88). The change in VDAC^R+CHS oligomeric state was observed to be dependent on the concentration of VDAC^R+CHS (Fig. 2.2C). The binding was detected by change in fluorescence intensity of Alexa Fluor 647 labeled VDAC^R+CHS titrated against unlabeled VDAC^R+CHS; the K_d value of the change in state was determined to be $0.6 \pm 0.2 \mu\text{M}$ using MST (Fig. 2.2C). In the absence of CHS an increase in fluorescence was also observed upon the addition of 100 μM VDAC^R to Alexa fluor 647 labeled VDAC^R, however, an identical shift in fluorescence intensity also occurred upon the addition of 100 μM egg white lysozyme (Fig. 2.3D) indicating that this change was due to loss of fluorescent protein in the absence of a high overall protein concentration (likely caused by sticking of the labeled protein to pipette tips or sample tubes). The addition of 100 μM egg white lysozyme to Alexa Fluor 647 labeled VDAC^R in the presence of CHS had no effect on fluorescence intensity indicating that the

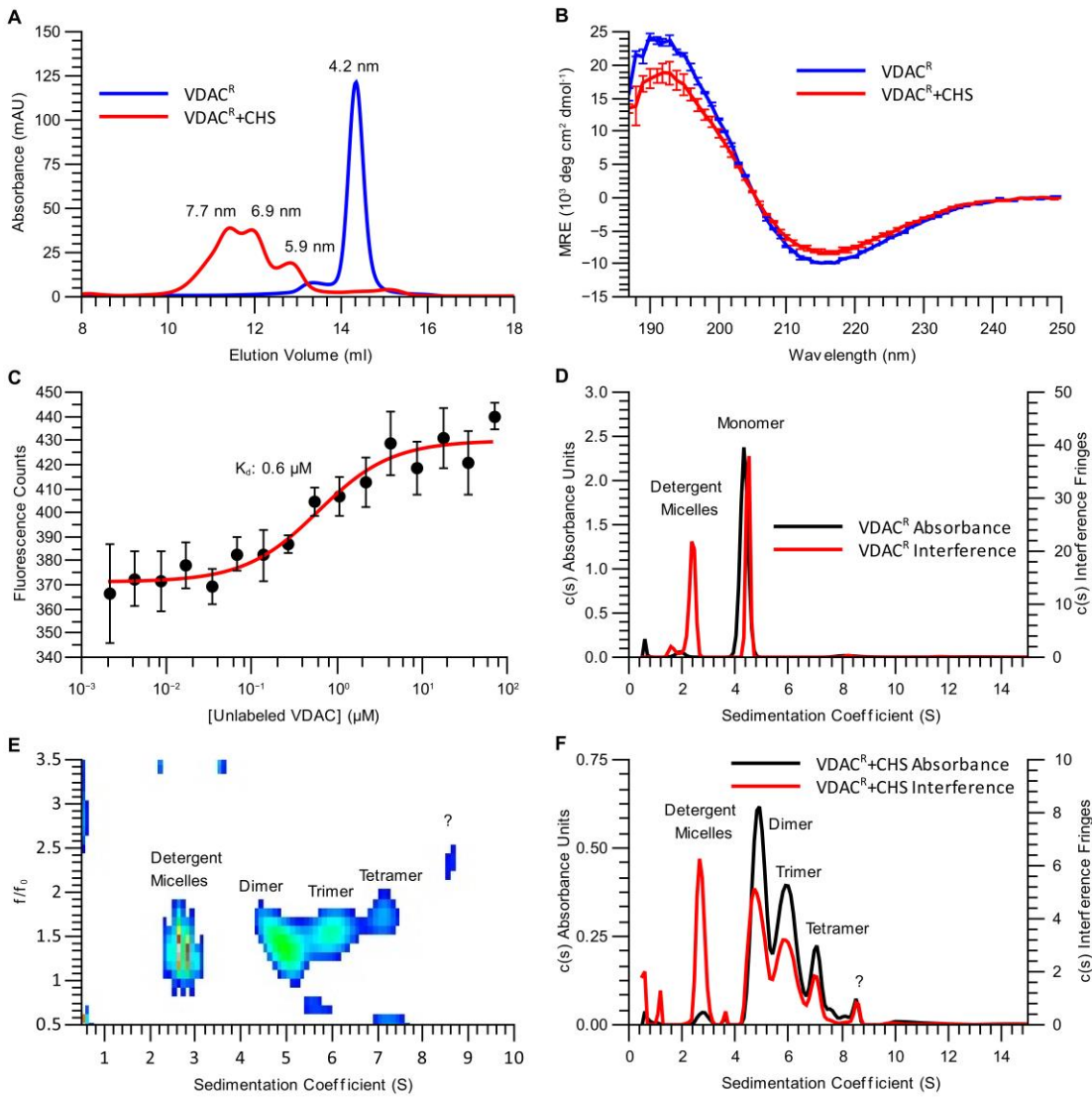


Figure 2.2. CHS alters the oligomeric state and secondary structure of VDAC^R

Figure 2.2. CHS alters the oligomeric state and secondary structure of VDAC^R.

(A) SEC of VDAC^R (blue) and VDAC^R+CHS (red), the calculated R_s values are displayed above each peak. (B) Averaged CD-spectra of VDAC^R (blue) and VDAC^R+CHS (red) with standard deviations of 3 measurements displayed as error bars. For secondary structure deconvolution see Table 2.1. (C) Microscale thermophoresis isotherm of 10 nM fluorescently labeled VDAC^R+CHS titrated against unlabeled VDAC^R+CHS. The K_d of the change in behavior is displayed on the plot. (D) $c(s)$ absorbance and interference distributions of VDAC^R at 0.98 mg/ml. Peaks corresponding to free detergent micelles and the VDAC^R monomer are indicated on the plot. (E) $c(s, f/f_0)$ interference distribution of VDAC^R+CHS at 0.99 mg/ml used to resolve the three VDAC species present in solution. Peaks corresponding to the free detergent micelles, VDAC dimer, trimer and tetramer and a peak of unknown composition are indicated on the plot. (F) Absorbance and interference $c(s)$ distributions of VDAC^R+CHS at 0.99 mg/ml. Peaks corresponding to free detergent micelles and VDAC dimer, trimer, tetramer and a peak of unknown composition are labeled on the plot. The $c(s, f/f_0)$ distribution in (E) was reduced into a 2D $c(s, *)$ distribution and was used as prior probabilities to resolve the three VDAC species in the $c(s)$ fitting procedure displayed in (F). Peaks corresponding to free detergent micelles and VDAC dimer, trimer, tetramer and a peak of unknown composition are labeled on the plot. In all AUC distributions detergent peaks were assigned using detergent-only control samples (data not shown).

Table 2.2 Parameters of VDAC-detergent species determined from sedimentation velocity experiments.

	dn/dc_p^a	δ_D^b (g/g)	\bar{v}^c (ml/g)	$S_{20, \text{water}}^a$	R_s^d (nm)	$M_{PD}^{e,f}$ (kDa)	$M_P^{e,f}$ (kDa)	$M_D^{e,f}$ (kDa)
VDAC^R Monomer	0.48±0.01	1.99±0.04	0.78±0.02	4.8±0.05	4.2±0.3	107±7	36±3	71±5
VDAC^R+CHS Dimer	0.43±0.03	1.7±0.1	0.78±0.07	5.3±0.03	5.9±0.3	170±30	60±10	100±20
VDAC^R+CHS Trimer	0.37±0.02	1.32±0.07	0.77±0.06	6.4±0.07	6.9±0.4	220±20	100±10	120±20
VDAC^R+CHS Tetramer	0.42±0.02	1.15±0.07	0.77±0.06	7.3±0.06	7.7±0.4	290±30	130±20	150±20
DM Micelles	-	-	-	2.4±0.02	2.8±0.2	-	-	39±3
DM+CHS Micelles	-	-	-	3.0±0.1	3.36±0.02	-	-	59±2

^a dn/dc_p and $S_{20, \text{water}}$ were determined from AUC $c(s)$ distributions (Table 5.1, Fig. 5.1)

^b δ_D was determined using Equation 1.6

^c \bar{v} of the protein-detergent complex was calculated from the protein (\bar{v}_p) and detergent (\bar{v}_D) using Equation 1.5

^d R_s was determined by SEC elution volume relative to elution volumes of proteins with known R_s values

^e M_{PD} , M_p and M_D values were calculated using Equations 1.4, 1.8 and 2.1 respectively

^fMW of VDAC^R monomer from sequence is 30.3 kDa

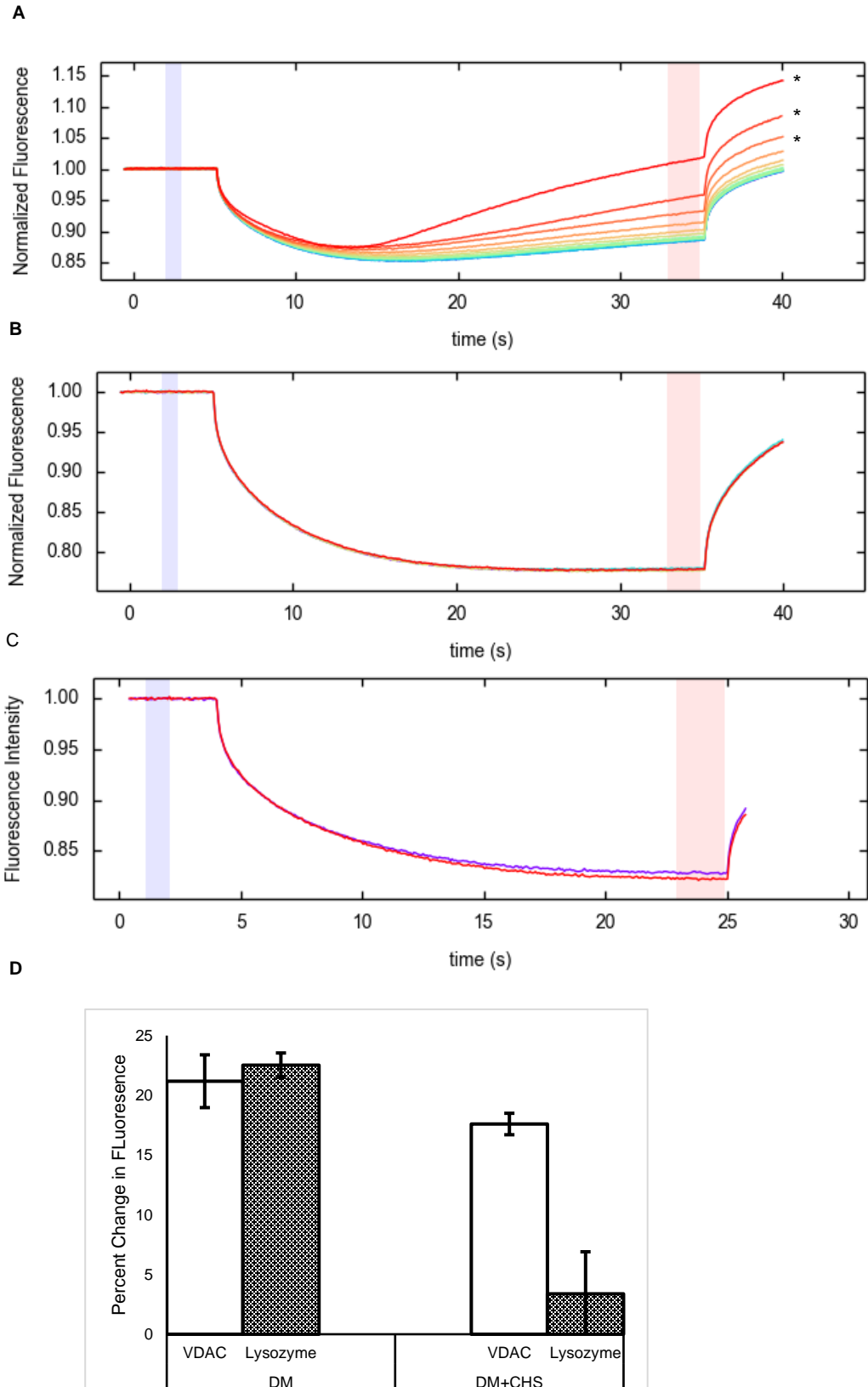


Figure 2.3. Microscale thermophoresis screening and controls

Figure 2.3. Microscale thermophoresis screening and controls. (A) MST time traces of VDAC^R+CHS+HK-I in a 0.15% DM solution. Under these conditions the protein aggregated once the MST IR laser was activated resulting in an increase in the fluorescence over time. At high HK-I concentrations aggregates were visible in the sample capillaries after the run, the curves corresponding to capillaries with visible aggregates are indicated with a *. (B) MST time traces for screening of VDAC^R+CHS+HK-2 binding. No difference in VDAC motion due to the temperature gradient was observed between samples with and without 90µM HK-II (C)VDAC^R MST time traces in DM solution in the absence and presence of 100 µM egg white lysozyme showing no aggregation. (D) Change in fluorescence intensity due to the addition of VDAC or egg white lysozyme in the absence and presence of CHS normalized to the fluorescence intensity of VDAC in the absence of any additional protein.

change in fluorescence observed upon the addition of unlabeled VDAC^R was due to a specific interaction (Fig. 2.3D).

To investigate the composition of the VDAC-detergent complexes and determine the oligomeric state of VDAC in the presence and absence of CHS, we employed AUC using both absorbance and interference optics (Fig. 2.2D, E & F). A clear difference was observed between the VDAC^R and VDAC^R+CHS samples. The VDAC^R sample contained two species which can be attributed to the monomeric VDAC-detergent complex and free detergent micelles (Fig. 2.2D). In contrast, the VDAC^R+CHS sample contained three VDAC species as well as free detergent micelles (Fig. 2.2E & F). We could clearly distinguish three distinct VDAC-detergent complexes and free detergent micelles in a $c(s, f/f_0)$ distribution (Fig. 2.2E) of interference data; however we were unable to obtain the same resolution in a $c(s, f/f_0)$ distribution of the corresponding absorbance data. Therefore we used the interference $c(s, f/f_0)$ distributions as prior probabilities for the determination of $c(s)$ distributions of both interference and absorbance data (Fig. 2.2F). The sedimentation coefficients of the three VDAC^R+CHS species are all higher than the VDAC-detergent complex in the VDAC^R sample (Table 2.2). These results confirm the SEC experiments (Fig. 2.2A) showing that CHS induces the formation of three different VDAC species. Determination of the composition of the VDAC-detergent complexes revealed that the VDAC^R sample contained exclusively monomers of VDAC, whereas the VDAC^R+CHS sample contained a mixture of VDAC dimers, trimers and tetramers (Table 2.2).

2.5.3 SEC-SAXS Modelling Supports Previously Proposed VDAC Multimer Arrangements

SEC-SAXS data collected of VDAC^R samples revealed only one VDAC-detergent complex present in solution (R_g of 35 Å) (Fig. 2.4 & Fig. 5.4A). The low chi square value for the

fit ($\chi^2=1.4$) of the scattering curve of the monomeric VDAC model confirms that the crystal structure of mouse VDAC1 resembles the assembly of VDAC^R in solution (57). The best fitting monomeric VDAC model produced is displayed in Fig. 2.4C & D.

Due to the heterogeneous nature of the VDAC^R+CHS sample (Fig 5.4B & C), the collection of data corresponding to specific oligomeric states was more challenging. Initial SEC-SAXS experiments using a VDAC sample pre-equilibrated with CHS provided clear separation of only one VDAC^R+CHS complex with an R_g of 70 Å (Fig. 2.6A). This species could be modelled as hexameric arrangement derived from crystal contacts of the mouse VDAC1 and produced a model with a χ^2 of 1.5 (Fig. 2.6B-D). The hexameric arrangement of VDAC^R+CHS used to construct the model is similar to previously observed organizations of VDAC isolated from native membranes (60, 72) and was previously suggested as a possible biological assembly (69); however, due to the antiparallel arrangement of the molecules in the mVDAC1 crystal structure the biological relevance of this arrangement is questionable.

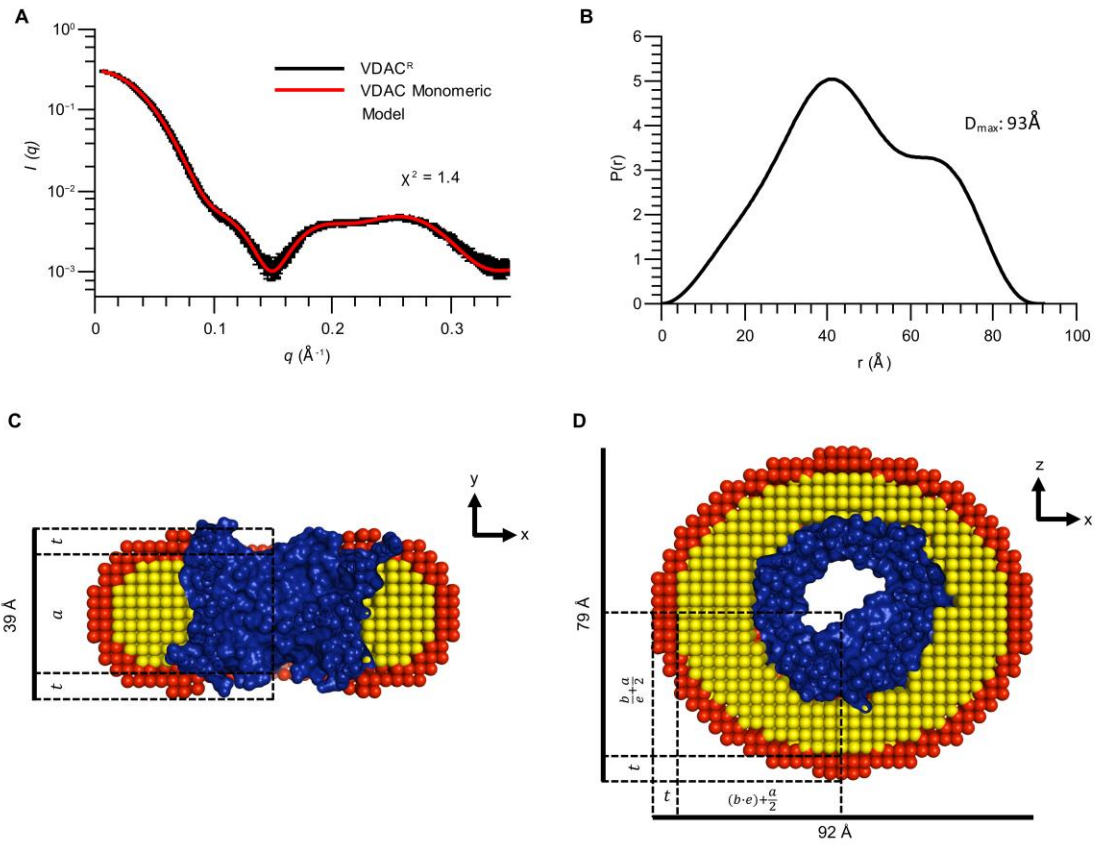


Figure 2.4. SEC-SAXS model of monomeric VDAC^R fits experimental scattering data

Figure 2.4. SEC-SAXS model of monomeric VDAC^R fits experimental scattering data.

(A) Experimental scattering data of SEC eluted VDAC^R in 0.3% DM solution (black) and calculated scattering curve of monomeric VDAC detergent complex (red); error bars represent standard deviation of averaged curves. The χ^2 of the fit of the calculated curve to the experimental data is displayed on the plot. (B) P(r) plot determined from experimental scattering data of VDAC^R. The determined D_{\max} value is shown on the plot. (C) Cross section of the monomeric VDAC^R model through the lumen of the VDAC pore and (D) rotated 90° around the x-axis. Dimensions of the model are shown and individual fitted parameters corresponding to the detergent component of the model are depicted relative to the total distances. These parameters (a, b, t and e) are depicted to aid in visualization of their relationship to the model of the protein-complex. In both panels, the protein component of the model is colored in blue, the hydrophobic layer of the detergent is colored yellow and the hydrophilic layer of the detergent is colored red. Values for the parameters a, b, t and e for all VDAC models are reported in Table 2.3.

Clearer separation of the VDAC dimer species was achieved when CHS was introduced to the VDAC sample during the SEC step of the SEC-SAXS experiment. This VDAC^R+CHS species had a R_g of 40 Å (Fig. 2.5A). The P(r) distribution of the protein detergent complex clearly demonstrate a D_{\max} value of 131 Å. (Fig. 2.5B) The best fitting model (χ^2 value of 4.7) was a dimeric zebrafish VDAC2 (pdb-code: 4BUM) (Fig. 2.5C and D). Parameters describing the detergent layer of each model are summarized in Table 2.3.

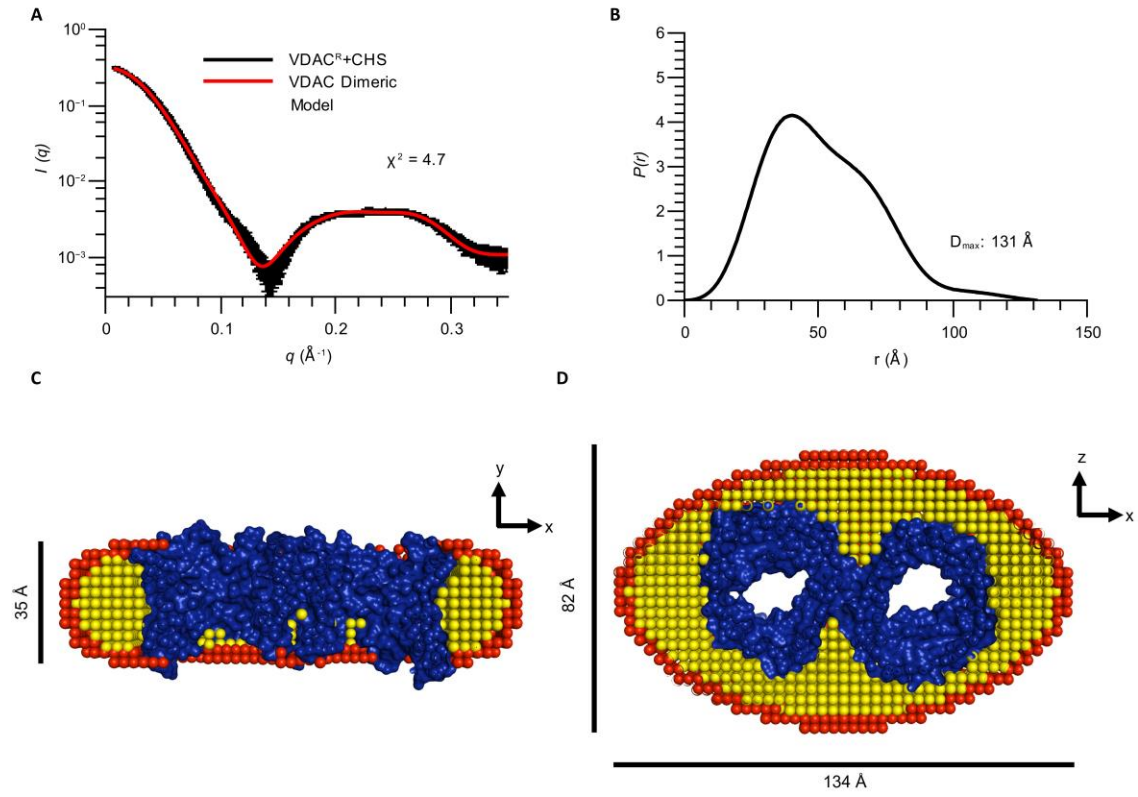


Figure 2.5. SEC-SAXS model of dimeric VDAC^R+CHS fits experimental scattering data

Figure 2.5. SEC-SAXS model of dimeric VDAC^R+CHS fits experimental scattering data (A) Experimental SAXS data (black) and calculated scattering curve of a dimeric VDAC detergent complex (red); error bars represent standard deviation of averaged curves. The χ^2 of the fit of the model to the experimental data is shown on the plot. (B) P(r) function calculated from experimental data of VDAC^R+CHS dimer. Determined D_{max} value is shown on the plot. (C) Cross section of the dimeric VDAC^R+CHS model through the lumen of the pore and (D) rotated 90° around the x-axis. Dimensions of the model and the orientation relative to the real space axes are displayed in each panel. The protein component of the model is colored in blue, the hydrophobic layer of the detergent is colored yellow and the hydrophilic layer of detergent is colored in red. Best fitting parameters of the detergent layer of the models are reported in Table 2.3 and a visualization of how each parameter relates to the model can be seen in Fig. 2.4.

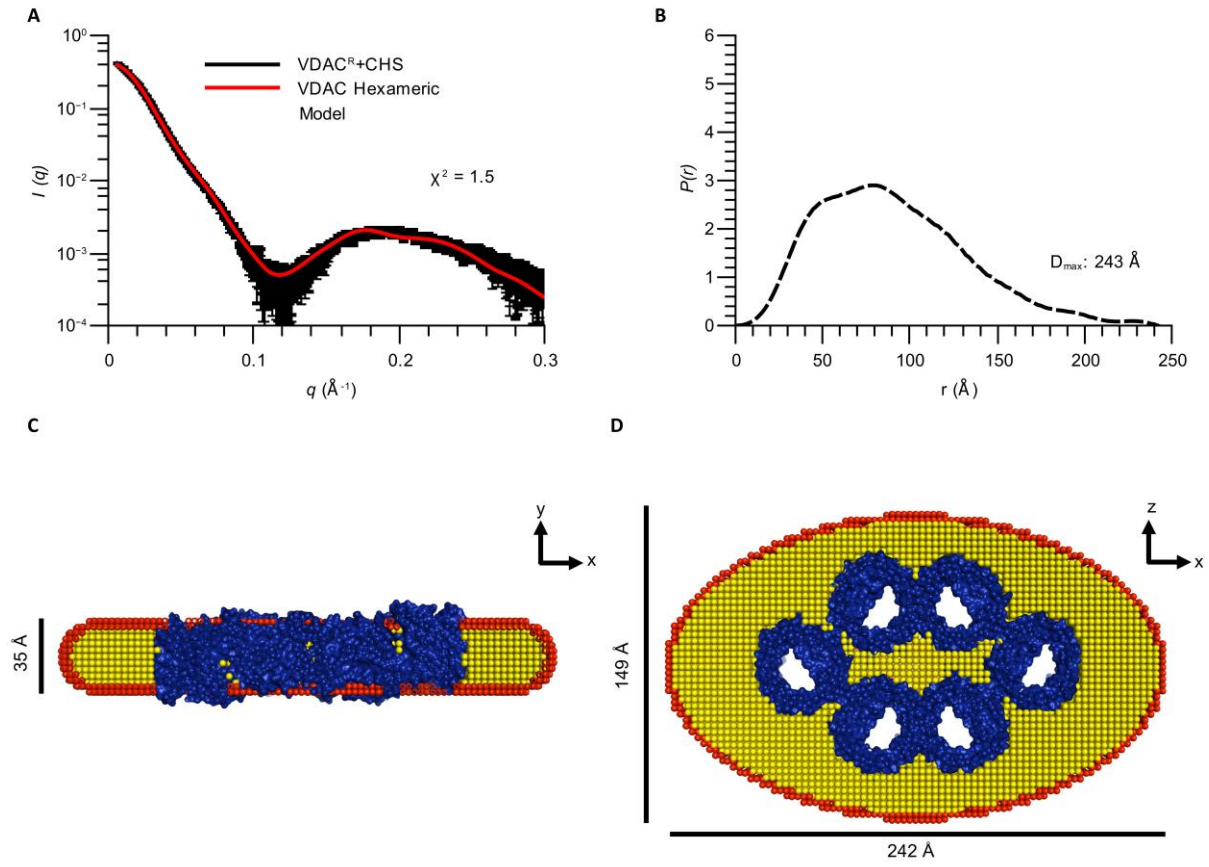


Figure 2.6. Anti-parallel Hexameric VDAC model fit to experimental SAXS data

Figure 2.6. Anti-parallel Hexameric VDAC model fit to experimental SAXS data. (A) Experimental SAXS data (black) and calculated scattering curve of a hexameric VDAC detergent complex model (red) error bars represent standard deviation of averaged curves. The χ^2 of the fit of the model to the data is shown on the plot. (B) P(r) function calculated from experimental data of VDAC^R+CHS hexamer. Determined D_{\max} value is shown on the plot. (C) Cross section of the hexameric VDAC^R+CHS model through the model with 4 of the pores visible and (D) rotated 90° around the x-axis. Dimensions of the models and the orientation relative to the axes are displayed in each panel. The protein component of the model is colored blue, the hydrophobic layer of the detergent is colored yellow and the hydrophilic layer of detergent is colored in red. Best fitting parameters of the detergent layer of the models are reported in Table 2.3 and a visualization of how each parameter relates to the model can be seen in Fig. 2.4.

Table 2.3 Parameters of best fitting VDAC-detergent complex models

	R_g^a (Å) (Guinier/Model)	D_{max}^b (Å) (P(r)/Model)	a^c (Å)	b^c (Å)	t^c (Å)	e^c (°)
VDAC^R (Monomer)	36/35	93/92	29	23	5	1.16
VDAC^R+CHS (Dimer)	40/40	131/134	27	34	4	1.45
VDAC^R+CHS (Hexamer)	70/71	243/242	27	77	4	1.35

^aExperimental R_g was determined via the Guinier method using the ATSAS software package (48), model R_g was determined with Crysol (48). Guinier analyses for each species can be found in Fig. 5.2.

^b D_{max} from P(r) distributions was determined using the software gnom, model D_{max} was determined from detergent parameters of models (see Fig. 2.4, 2.5 & 2.6)

^cParameters a, b, t, e describe the dimensions of the detergent component of the protein-detergent complex and were determined by the software Memprot (36). Visualization of the parameters and their relation to the dimensions of the final model can be seen in Fig. 2.4.

2.5.4 CHS Allows for a Stable VDAC-Hexokinase Interaction

Previous reports have linked apoptosis to the oligomeric state of VDAC, and to its interactions with hexokinase (61, 63). To gain insight into the onset of apoptosis triggered by the disassociation of the VDAC-hexokinase complex we performed microscale thermophoresis (Fig. 2.7). Our established experimental setup provides an excellent opportunity to study integral membrane protein complexes while also providing novel information on the role VDAC plays in apoptosis (62). To determine the binding behavior, we used full-length native-source hexokinase isoforms I and II from *S. cerevisiae* (HK-I and HK-II respectively) (Fig. 2.7A & B). Whereas HK-II did not show any binding (Fig. 2.3), it was determined that the stable interaction of HK-I with VDAC^R is strictly dependent upon addition of CHS to the sample. VDAC^R-HK-I mixtures showed signs of aggregation when the MST IR laser was activated, and the rate of aggregation seemed to be dependent on the HK-I concentration, a behavior which does not occur in the presence of other proteins such as egg white lysozyme (Fig 2.3D). As this behavior was not observed in the absence of HK-I or in the presence of egg white lysozyme, this result suggests that a thermally unstable VDAC-HKI complex was formed. In VDAC^R+CHS+HK-I mixtures aggregation was not observed. A binding constant for VDAC^R+CHS+HK-I of $27 \pm 6 \mu\text{M}$ was determined (Fig. 2.7C) from the thermophoresis profiles of a HK-I titration.

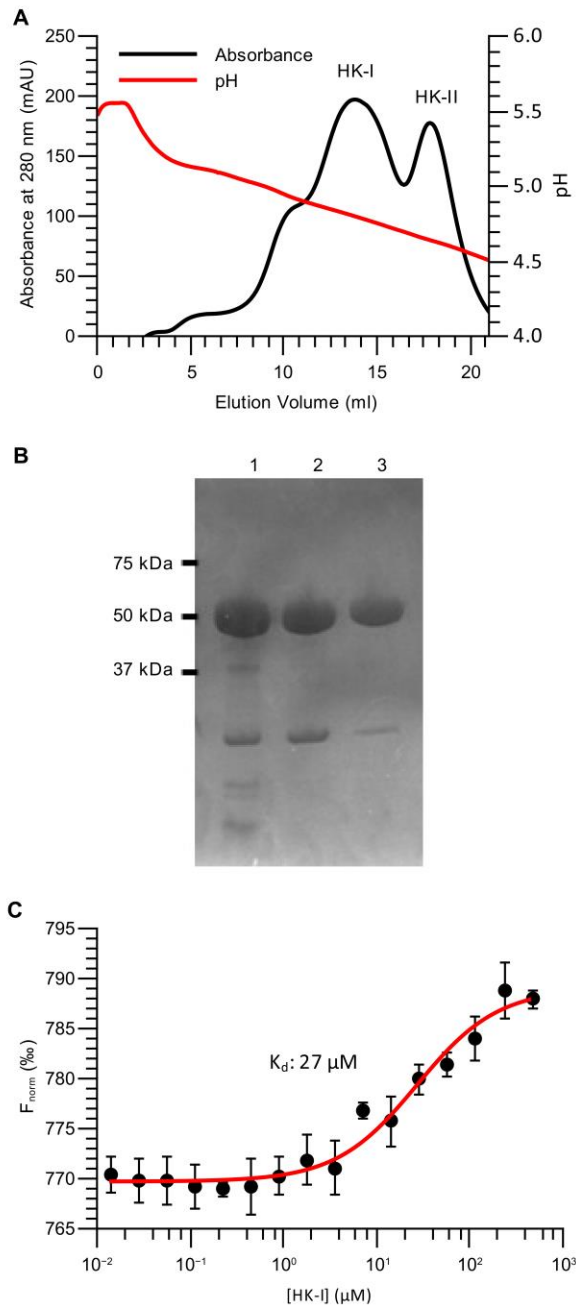


Figure 2.7. CHS allows for the formation of a stable VDAC-Hexokinase complex

Figure 2.7. CHS allows for the formation of a stable VDAC-Hexokinase complex.

(A) Separation of yeast HK-I and HK-II isoforms via pH gradient. Protein elution was monitored by absorbance at 280 nm (black) and the pH of the eluate was monitored in line with elution (red). Peaks corresponding to the hexokinase isoforms are indicated on the plot. (B) SDS-PAGE analysis of pooled HK-I (lane 2) and HK-II (lane 3) fractions relative to starting mixture (lane 1). An image of the full region of interest of the gel including the protein M_w ladder is provided in the supplementary information (Fig. 5.3D). (C) Titration of unlabeled HK-I against a constant concentration of fluorescently labeled VDAC^R+CHS resulted in a change in VDAC motion due to the generated temperature gradient. Experimentally determined average values are shown by black circles with error bars representing standard deviation. The K_d of the interaction and the fitted curve (red) used to determine the K_d are shown on the plot.

2.6 Discussion

The methods discussed in this study were used to gain an understanding of the self-association of VDAC induced by the cholesterol analogue CHS and to generate a platform for exploring the formation of the protein-protein complexes that include integral membrane proteins and drive essential biological processes. VDAC NMR (58) and crystal structures (57, 68, 70) focused on the arrangement of the VDAC polypeptide, which was a critical first step in understanding the structure-function relationships of VDAC and formed the basis of future work probing the protein function. However, the isolated protein cannot be studied in aqueous environments and studies of the function of VDAC are carried out in artificial membranes (49, 89) and membrane mimetic systems (60, 70). Evidence suggests that VDAC interacts with many proteins including proteins involved in apoptotic signaling, and thorough studies of these interactions will be most readily achieved using refolded VDAC solubilized in detergent; therefore, a detailed understanding of the complete protein-detergent system is critical to interpretation of structure-function relationships (61, 63, 90).

Previous works have adapted AUC and SAXS to the analysis of detergent-solubilized membrane proteins (27, 36). AUC provides information pertaining to molecular weight, shape, composition of oligomers and complexes and the relative abundance of distinct species present in a mixture (30). The analysis of membrane proteins via AUC sedimentation velocity can be achieved via the solubilizing of the membrane protein in detergent; however the interpretation of the data obtained from these experiments is complicated by the presence of detergent bound to the solubilized membrane protein, adding mass and obscuring the shape and composition of oligomers of the protein (27). SAXS allows for the low-resolution modeling of macromolecules in solution from x-ray scattering intensities. The main complications in the analysis of detergent-

solubilized membrane proteins via SAXS is the presence of free detergent micelles in the solution and the detergent layer surrounding the membrane protein (36).

To overcome these obstacles, we have established a new combination of i) MST to investigate the concentration dependence of VDAC oligomerization and the interaction of VDAC with hexokinase ii) AUC sedimentation experiments to investigate the composition of the VDAC-detergent complexes and iii) SEC-SAXS studies to create models of detergent micelles and VDAC-detergent complexes. Previous studies have shown that VDAC function is altered by the surrounding lipid environment through the modulation of its oligomeric state, which can influence apoptotic signaling (60, 91). There is some previous evidence for VDAC multimers in detergent solutions; however, evidence toward a detailed understanding of the regulation of these assemblies was not obtained (68). In this study the oligomerization of the VDAC was shown to be dependent on VDAC^R concentration in the presence of CHS via MST analysis and a K_d value of $0.6 \pm 0.2 \mu\text{M}$ ($\sim 0.02 \text{ mg/ml}$) was determined implying that the protein readily forms larger than monomer units in the presence of CHS. This contrasts with the behavior of the protein in the absence of CHS as only monomers of VDAC were observed. It should be noted that the K_d model used in this work to describe the self-association of VDAC is likely too simple of a model to accurately describe the self-association of an integral membrane protein in detergent solution and also is unlikely to completely represent the self-association of VDAC in a lipid bilayer. This is due to several complications, the main issue being the confinement of VDAC in the “detergent micelle phase” of the solution, drastically reducing the volume of the solution that VDAC molecules can possibly occupy. A more suitable model may be suggested by incorporating the volume of available detergent micelles into the model; however this approach itself would be too simplistic as the AUC results presented in this work (Table 2.2) as well as information presented

by others (27, 92) have demonstrated that integral membrane proteins do not associate with the same mass of detergent as is in a single detergent micelle. In the case of VDAC a further complication arises with different oligomers of VDAC associating with different quantities of detergent (Table 2.2). Never the less the K_d model used in this work can describe a relative binding constant for the comparison of VDAC self-association in the same detergent environment, establishing a baseline for the examination of the self-association of VDAC mutants or VDAC sequences from other organisms.

Dimeric organizations of VDAC have been suggested from previous crystal packing arrangement of mouse VDAC1 (antiparallel molecules) and zebrafish VDAC2 (parallel molecules) (57, 68, 69) and furthered by the examination these two molecules in solution by electron paramagnetic resonance (EPR) revealing two different dimeric interfaces (68, 71). The previously mentioned EPR experiments revealed that a parallel mouse VDAC1 dimer was formed at low pH and depended on the protonation state of residue E73, in contrast to the antiparallel mouse VDAC1 crystal packing arrangement (71). The EPR studies of zebrafish VDAC2 supported the parallel arrangement observed in the zebrafish VDAC2 crystal asymmetric unit (68). In this study we observed dimers, trimers, tetramers and possibly hexamers of VDAC in the presence of CHS via AUC and collected SEC-SAXS data corresponding to a VDAC dimer in the presence of CHS. The dimeric VDAC model produced from SEC-SAXS data in this study fit best utilizing the dimeric zebrafish VDAC2 organization for the protein phase of the model implying that the *N. crassa* VDAC^R dimer is organized in this way in detergent solution in the presence of CHS. The two alternative models for VDAC dimer arrangements which come from mouse VDAC1 data (57, 71) are unlikely arrangements of the *N. crassa* VDAC^R dimer observed in this study considering that one arrangement contains

antiparallel VDAC molecules which is likely a crystal packing artifact (57, 69) and the other relies on the protonation state of E73 which corresponds to a proline residue in the aligned *N. crassa* VDAC sequence (49).

The hexameric VDAC^R in the presence of CHS modeled from SEC-SAXS data was not observed by AUC sedimentation velocity experiments; however a possible explanation for this is the low concentrations of VDAC^R used in AUC (0.5 - 1 mg/ml) relative to SEC-SAXS (5 - 10 mg/ml) experiments. Interestingly, there is a small peak in the AUC $c(s)$ and $c(s, f/f_0)$ distributions of VDAC^R+CHS samples at a larger S value than the VDAC^R tetramer (Fig. 2.2D); however, the concentration of this species was too low to accurately determine its composition. Ultimately the data describing the hexameric species was limited relative to the other species examined in this study; as well the only available crystallographic model for a VDAC hexamer arrangement (mouse VDAC1, PDB: 3EMN) is comprised of anti-parallel barrels leading to the suggestion that this is a biologically irrelevant model. It is possible however, that due to the low resolution of models produced by SAXS analysis that the data represents a similarly arranged parallel-barrel hexamer as similar VDAC arrangements have been observed by atomic force microscopy of mitochondrial membranes (72). Future work in this area should focus on establishing the orientation of *N. crassa* VDAC molecules in these oligomers; this could be accomplished using the aforementioned EPR methods used to analyze the arrangement of mouse VDAC1 (71) and zebrafish VDAC2 (68) in solution.

The change in oligomeric organization of VDAC^R induced by the addition of CHS could be attributed to the direct binding of the sterol to VDAC. Direct binding of cholesterol to human VDAC1 has been described using NMR spectroscopy (58) and is supported by evidence of co-purification of VDAC proteins with ergosterol or cholesterol (60, 85). The binding of sterols to

VDAC could therefore be a possible target for drugs that could influence the oligomeric state of VDAC, if direct binding of CHS to VDAC is the cause of the change in behavior. Such a drug could be designed to block or promote the binding of sterols to VDAC to influence apoptosis. However, biological systems are more complex, precluding direct extrapolation of our *in vitro* results to biological systems. The accumulation of cholesterol in mitochondria is observed in some cancer cell lines (93) and as well, the accumulation of cholesterol in mitochondria has been shown to inhibit the activity of the pro-apoptotic protein BAX (94), suggesting that increased cholesterol content has an anti-apoptotic effect. The ability of CHS to promote the formation of VDAC oligomers is interesting as oligomerization is thought to have a pro-apoptotic effect (61). The relevance of the effect of cholesterol on mitochondrial mediated apoptosis is further enhanced by evidence suggesting that some VDACS also interact directly with BAX (65). These data suggest an intricate system with many factors at play. Overall, the roles of VDAC and mitochondrial cholesterol content in apoptotic signaling warrant future study.

An alternative explanation for the change in VDAC behavior is that CHS may impact the detergent components of the system. CHS is known to alter the size and shape of DDM micelles and CHS addition to maltoside detergents has been shown to stabilize solubilized G protein-coupled receptors (GPCRs) (86, 95). CHS has also been shown to be required for the retention of ligand recognition by detergent solubilized and purified GPCRs such as the adenosine A_{2a} receptor (95). This contrasts with VDAC as in isolation this protein showed no signs of instability in DM solutions. The VDAC-Hexokinase complex, however, was stabilized by the presence of CHS (Fig. 2.7 & 2.3). In addition, the restoration of the ability for VDAC to form oligomers by the introduction of CHS provides another interesting parallel with the effect of cholesterol on some GPCRs as works using molecular dynamic simulations of the β 2-Adrenergic

Receptor (96) and the chemokine receptor type 4 (97) have shown that the dimerization of these proteins is modulated by cholesterol. It is possible that the change in size and shape of the detergent micelles is affecting the oligomeric reorganization of VDAC through changes to the structure of the molecule. Indeed, a change to the secondary structure was observed by our CD measurements which could be due to the change in surrounding detergent environment.

The localization of hexokinase to the surface of mitochondria has been observed in mammalian and yeast cells (98, 99). Interestingly, the hexokinase could be detached from the mitochondrial surface by the introduction of a peptide consisting of the first 15 amino acids of the hexokinase, identifying the N-terminus as a possible VDAC binding site (62, 98). In this work, the binding of full-length *S. cerevisiae* HK-I with VDAC was reported and an interaction between *S. cerevisiae* HK-II and VDAC was not detected. The relevance of this isoform specificity is supported by the up-regulation of HK-I and down-regulation of HK-II during respiration relative to fermentative growth in *S. cerevisiae* (100). However, as both *S. cerevisiae* hexokinases have identical N-termini, the differential binding behavior of the two isoforms would imply that the N-terminus of hexokinase is required but not sufficient for binding of full-length hexokinase to VDAC and that there is likely at least one other site of contact between the two proteins that is required for specific binding. Subcellular localization data for *S. cerevisiae* HK-I and II under fermentative growth conditions place both proteins in the cytoplasm; however, HK-I does associate with the mitochondria after treatment with rapamycin, which causes an increase in HK-I expression (99).

A combination of MST, AUC and SEC-SAXS have revealed the most detailed picture of VDAC-detergent complexes and the effect of CHS on VDAC oligomeric organization. The identification of CHS as an effector of VDAC oligomeric organization and the detection of a

VDAC-HK-I binding event will provide a platform for the further investigation of this system as well as lending the use of these methods in the examination of other membrane protein complexes.

Chapter 3: A Deletion Variant Partially Complements a Porin-Less Strain of *Neurospora crassa*

3.1 Publication Details and Author Contributions

Ferens F.G., Spicer V., Krokhin O.V., Motnenko A., Summers W.A.T., Court D.A. 2017. A deletion variant partially complements a porin-less strain of *Neurospora crassa*. *Biochemistry and Cell Biology*, 95(2): 318-327

V.S. and O.K. performed LC-MS of the mitochondrial protein samples and raw data reduction for the mitochondrial proteome data sets. W.S. created the Δ Por-1 and the 238Por strains of *Neurospora crassa*. F.F. and A.M. created the database of mitochondrial proteins. F.F. performed all other experiments. F.F. analyzed the data and performed statistical analyses. F.F., D.C., and O.K. prepared the manuscript.

3.2 Abstract

Mitochondrial porin, the voltage-dependent anion channel, plays an important role in metabolism and other cellular functions within eukaryotic cells. To further the understanding of porin structure and function, *Neurospora crassa* wild-type porin was replaced with a deletion variant lacking residue 238-242 (238porin). 238porin was assembled in the mitochondrial outer membrane, but the steady state levels were only about 3% of those of the wild-type protein. The strain harbouring 238porin displayed cytochrome deficiencies and expressed alternative oxidase. Nonetheless, it exhibited an almost normal linear growth rate. Analysis of mitochondrial proteomes from a wild-type strain FGSC9718, a strain lacking porin (Δ Por-1) and that expressing 238porin revealed that the major differences between the variant strains were in the levels of subunits of the NADH:ubiquinone oxidoreductase (complex I) of the electron transport chain, which were reduced only in Δ Por-1 strain. These, and other proteins related to electron flow and mitochondrial biogenesis, are differentially affected by relative porin levels.

3.3 Introduction

Mitochondrial porin forms a highly abundant, voltage-dependent anion-selective channel (VDAC) in the outer membrane of mitochondria. The aqueous channel formed by the 19-stranded β -barrel (101), (102), (57), (103), (68)) allows for the passage of small metabolites, thereby mediating efficient introduction of substrates and release of products to and from mitochondria (reviewed by (104)). In artificial membranes, porin exhibits voltage-dependent gating that shifts the pore between a slightly anion-selective open state and a slightly cation-selective, semi-closed state (105), (106).

Mitochondrial porin has been shown to interact with many other cellular proteins (for example see (107)), including those involved in the regulation of apoptosis in mammalian cells (reviewed by (108)), and as a result the structure and function of porin are of great interest. Human VDAC1 (hVDAC1; (101), (102)), and VDAC2 (hVDAC2, (103)), mouse VDAC1 (57) and zebrafish VDAC2 (68) each form a novel barrel consisting of 19 anti-parallel transmembrane β -strands. The structure also contains a N-terminal α -helix, which in the solved structures resides within the pore, although electrophysiological data using native VDAC have been interpreted to indicate that the N-terminal helix forms part of the barrel (see (109) for discussion). Although structural data for non-vertebrate VDAC are not currently available, a 19- β -strand barrel was suggested for *Neurospora crassa* porin through secondary structure prediction analyses (50) that align well with the structures of vertebrate VDAC ((104), Fig. 3.1).

Recent work has shown that porin is non-essential for mitochondrial function in *N. crassa* (110). This haploid organism is an obligate aerobe that expresses only one porin isoform, allowing straightforward assessment of the effects of a porin variant on the cell. Although strains lacking porin (Δ Por) are viable, they exhibit extremely inhibited growth rates and mitochondrial dysfunction, demonstrating the necessity of porin for normal mitochondrial and cellular function (110). In this study, to further the understanding of the structure and functions of mitochondrial porin, a deletion variant, 238porin, was examined *in vivo*.

The 238porin variant contains a five-amino acid deletion (residues: NDRGV, (111)) at positions 238-242 (highlighted region in Fig. 3.1B), which according to predictions based on the solved structures encompasses the loop or turn between β -strands 16 and 17. The corresponding sequence in hVDAC1 and hVDAC2 is NNSSL, and is well conserved in vertebrate VDAC isoforms 1 and 2 (see (68) for examples). These residues encompass the link between β -strands

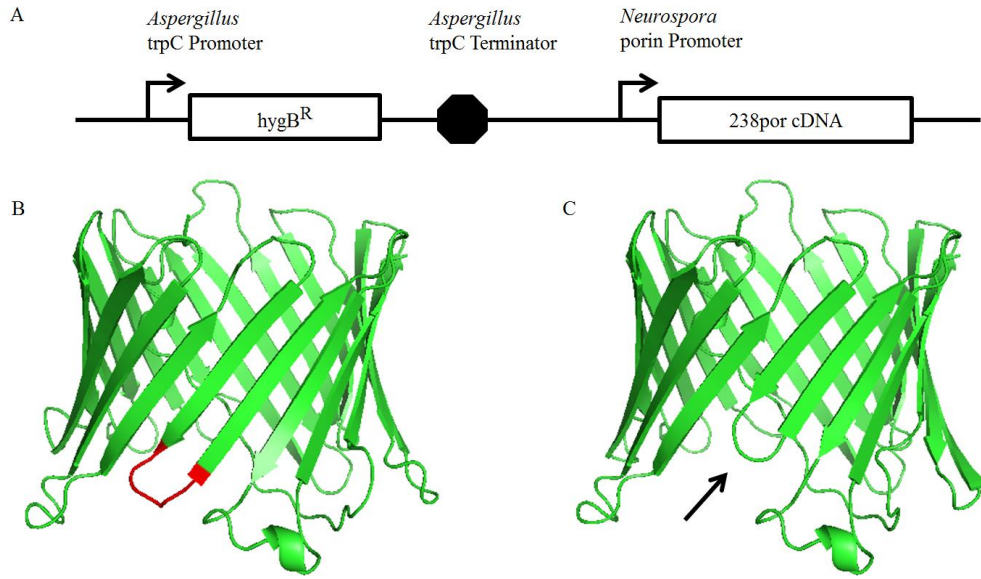


Figure 3.1. Porin variant used in this study.

Figure 3.1. Porin variant used in this study. **A)** Schematic diagram of the construct used to replace the wild-type porin gene to create the 238porin strain. The hygromycin-resistance cassette (HygB^R) and the flanking promoter and transcription termination regions were obtained from pCNS44 (Staben et al. 1989). The 238por cDNA was amplified from cloned DNA described in (111). **B)** Model of wild-type and 238porin. The structures of wild-type *N. crassa* porin (left panel, P07144) and 238porin (right panel, (111)) were predicted using Phyre² (112) and the human VDAC1 structure (left panel, (101), PDB 2K4T). The residues absent from 238porin are indicated in red in the wild-type structure, and the shortened α -strands resulting from the absence of residues 238-242 are indicated by the arrow in the 238por structure. Images were created in the PyMOL Molecular Graphics System, Version 1.7.4.

16 and 17 in all models published to date (see above for references). 238porin was initially created for the purposes of examining essential components of necessary for VDAC pore formation (89). 238porin was identified as a pore forming mutant by a previous study using small deletions to examine the location of β -strands in the VDAC sequence (111). At the time this was an intriguing result as the deletion was believed to be within a β -strand and should have disrupted the VDAC structure; however, subsequent structural information has revealed that this region of the VDAC sequence is a short loop connecting two β -strands (57, 58, 89). Nevertheless, this deletion variant was found to have pore properties, such as aqueous channel conductance and gating behaviour, similar to those of the wild-type porin. Therefore, it has the potential to form pores in mitochondria, and was chosen as a starting point for the analysis of the roles of specific segments of the VDAC sequence *in vivo*.

3.4 Materials and Methods

3.4.1 Strains and Growth Conditions

The strains of *Neurospora crassa* used in this study are detailed in Table 3.1. Strains with FGSC designations were obtained from the Fungal Genetics Stock Center, Kansas City, KS (113). The generation of the cDNA encoding *N. crassa* 238porin is described in (111) and the nomenclature used in therein has been used in the current work. A recombination-based method derived from that used by Colot et al. (2006) was used to introduce the 238porin coding sequence into the *Neurospora* genome. In brief, segments of DNA flanking the native porin gene (NCU04304) in strain FGSC 9720 (114), the 238porin cDNA (111) and the hygromycin-resistance cassette (115) were amplified by PCR using the primers listed in Supplementary Table 3.1, and used to construct the plasmid shown in Fig. 3.1A. The transformation cassette was

Table 3.1 *Neurospora crassa* strains utilized and their respective genotypes

Strain	Relevant Genotypes	Reference
FGSC 9718	<i>mus-51::bar mat a</i>	(114)
FGSC 9720	<i>mus-52::bar his-3 mat A</i>	(114)
238Por (FGSC 9718 background)	<i>238por hph⁺</i>	This work
Δ Por-1 (FGSC 9718 background)	<i>Δpor1::hph⁺</i>	(110)

removed from the plasmid by digestion with PvuII, purified and transformed into FGSC 9718 as described in Colot et al. (2006). A hygromycin-resistant isolate was obtained and purified by repeated subculturing. The gene replacement in the resulting 238Por strain was confirmed by PCR and DNA sequence analyses of the junctions and internal segments of the 238porin coding sequence. *Neurospora* cultures were maintained on Vogel's minimal medium (VMM) and linear growth rates were determined in race tubes as described by (116); race tubes were obtained from the FGSC.

3.4.2 Analysis of Mitochondria

Mitochondria were isolated from mycelia grown at 30°C in liquid VMM with shaking for 18 h (FGSC 9718a) or 21 h (238Por), using the procedure of (117). Protein concentrations were determined by a Bradford assay (BioShop, Burlington, ON).

Proteins were analyzed by SDS-PAGE using 12% acrylamide gels, and transferred to nitrocellulose, according to the manufacturer's instructions (Bio-Rad, Mississauga, ON). Primary antibodies against *N. crassa* porin, Tom40 and Tom70 were kindly provided by Drs. Roland Lill and Walter Neupert, Universität München. The secondary antibody used was a mouse α -rabbit-IgG-alkaline phosphatase (Sigma-Aldrich, Oakville, ON). Membrane bound complexes were isolated from membranes by resuspending mitochondria (100 μ g protein) in 50 μ l 1% (w/v) n-Dodecyl β -D-maltoside (DDM) and incubating on ice for 30 min followed by microcentrifugation at 13,000 rpm for 30 min to remove insoluble material (110) and the TOM complex was detected using antibodies against TOM40 (118). Complexes were analyzed by Red-Native-PAGE in the presence of Ponceau S (119) using a 6%-13% acrylamide gradient and

western blotting. An in-gel NADH dehydrogenase activity assay was performed as described (120).

Cytochrome spectra were determined as previously described (110); the reduced minus oxidized difference spectrum is presented (121). Expression of alternative oxidase was confirmed as described by Summers et al. (2012), using an Oxygraph-2k (Oroboros Instruments, Innsbruck, Austria).

For imaging of mitochondria, *N. crassa* cultures were grown on solid VMM for 12-16 hours at 30°C. Staining with 0.1 ng/ml of MitoTracker Green FM (Life Technologies, Burlington ON) was performed as described by (122), except that hyphae were grown directly on the microscope slide. Images were collected with a Zeiss Observer Z1 inverted microscope (Carl Zeiss Microscopy GmbH, Göttingen, Germany).

3.4.3 Proteomic Analysis of Mitochondria

Crude mitochondrial samples were prepared from *N. crassa* strains as above. To avoid any damage to the mitochondrial outer membranes and loss of intermembrane space proteins caused by further purification of mitochondria, the samples were utilized directly in this state. The proteomic analysis was conducted as described (123), using liquid chromatography (LC) and tandem mass spectroscopy (MS/MS). The resulting data sets contained many non-mitochondrial protein contaminants due to the use of crude mitochondrial preparations. These contaminant proteins inherently vary in abundance between samples and therefore were removed from the data sets prior to analysis to avoid skewing the data. To identify mitochondrial proteins in the data sets a reference set of mitochondrial proteins was constructed as follows: i) proteins

predicted from genes annotated as “mitochondrial” in the Broad Institute’s *N. crassa* genome database (<http://www.broadinstitute.org/annotation/genome/neurospora/GenomesIndex.htm>), ii) *N. crassa* proteins annotated as mitochondrial in the UniProt database (<http://www.uniprot.org/>), iii) proteins known to reside in the mitochondrial outer membrane of *N. crassa* (124) and iv) all sequences of detected proteins that were submitted to the TargetP subcellular localization prediction server (125) and any sequence scoring a mitochondrial probability ≥ 0.9 was identified as mitochondrial.

The resulting data sets of mitochondrial proteins were used to identify differential expression of proteins in the *N. crassa* VDAC mutants. Log_2 difference values were calculated for each pair of proteins and each set of values was normalized to generate a mean near zero and standard deviation near one. z -scores were calculated for proteins detected in both the wild-type and mutant strains. A minimum of 95% confidence was used to identify proteins that have differences in expression between two strains ($-1.96 > z > 1.96$, (123)). These data are presented in Tables 6.2 ($\Delta\text{Por-1}$ vs. wild-type); 6.3 (238Por vs. wild-type) and 6.4 ($\Delta\text{Por-1}$ vs. 238Por). This approach focuses on the population of differences in expression, rather than the absolute degrees of difference, and is used because the sensitivity of cells to the levels of each protein is unknown. Protein functional data was extracted from the Clusters of Orthologous Groups database (COG; <http://www.ncbi.nlm.nih.gov/COG/>) and the Kyoto Encyclopedia of Genes and Genomes databases (KEGG; <http://www.genome.jp/kegg/>).

3.5 Results and Discussion

In order to assess the *in vivo* function of 238porin, a cDNA coding sequence (111), linked to an upstream hygromycin-resistance cassette (Fig. 3.1A) was used to replace the wild-type porin gene in *N. crassa*. The resulting strain, 238Por, harbours a very low level of the variant (Fig. 3.2 and Table 3.4), indicating that the molecule either is not expressed efficiently at the transcriptional or translational levels, and/or is not effectively targeted to or assembled in the mitochondrial outer membrane (MOM). In mitochondria, 238porin is resistant to externally added protease (data not shown), suggesting that the small amount present is correctly assembled (see (126)).

Unexpectedly, the low levels of 238porin in mitochondria were not linked to significant growth defects (Table 3.2). The 238Por strain grew at more than 85% of the wild-type (FGSC 9718) rate at both 22°C and 30°C. This is in contrast to the severe reduction in growth rates observed in Δ Por mutants, particularly at lower temperatures ((110), Table 3.2). Thus, the very low levels of 238porin variant are able to partially complement the lack of wild-type porin.

One characteristic of the porin-less strains of *N. crassa* is a deficiency in the cytochromes assembled with mitochondrially-encoded polypeptides (110); these types of defects also arise when mitochondrial translation is blocked (127) and in other nuclear and mitochondrial mutants of *N. crassa* (for example see (121)). Similarly, the 238Por strain displays deficiencies in cytochromes *aa₃* and *b*, and an increased level of cytochrome *c* (Fig. 3.3). It also displays cyanide-resistant, SHAM-sensitive oxygen consumption (Table 3.2), characteristic of strains expressing alternative oxidase (128).

In principle, these differences between wild-type and 238Por cells could reflect low levels of porin, expression of a mutant porin, or a combination of the two. Attempts were made

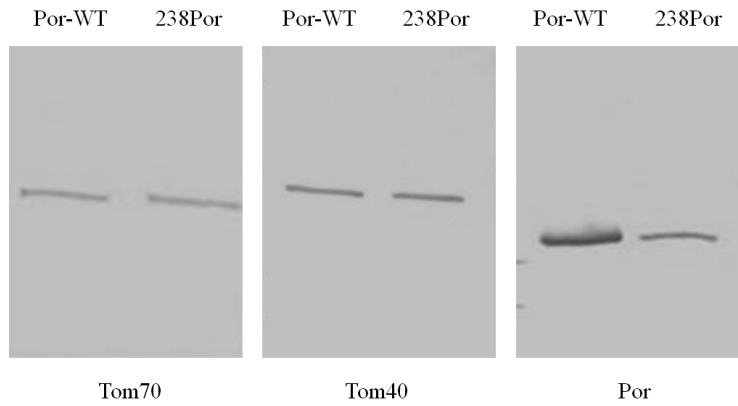


Figure 3.2. Western blot analysis of wild-type (Por-WT) and 238por-containing mitochondria. 30 μ g of mitochondrial protein from each strain was analyzed by western blotting with antibodies against the proteins indicated below each panel.

Table 3.2 Linear growth rates and cyanide-resistant respiration of *Neurospora crassa* strains on Vogel's minimal medium

Strain	Linear Growth Rates		Relative O ₂ consumption (%)		
	22°C (cm/day) [percentage of wild-type rate]	30°C (cm/day) [percentage of wild-type rate]	No additions	With KCN	With SHAM ^a
FGSC 9718	7.8 ± 0.4 [100]	11.4 ± 0.3 [100]	100	10.2	n/d
238Por	6.9 ± 0.1 [88]	9.8 ± 0.2 [86]	100	90.3	3.2
ΔPor1	1.3 ± 0.3 [17]	3.2 ± 1.4 [28]	100	95.6	12.0

^a SHAM, Salicylhydroxamic acid

Error values represent the standard deviation of 3 replicate experiments

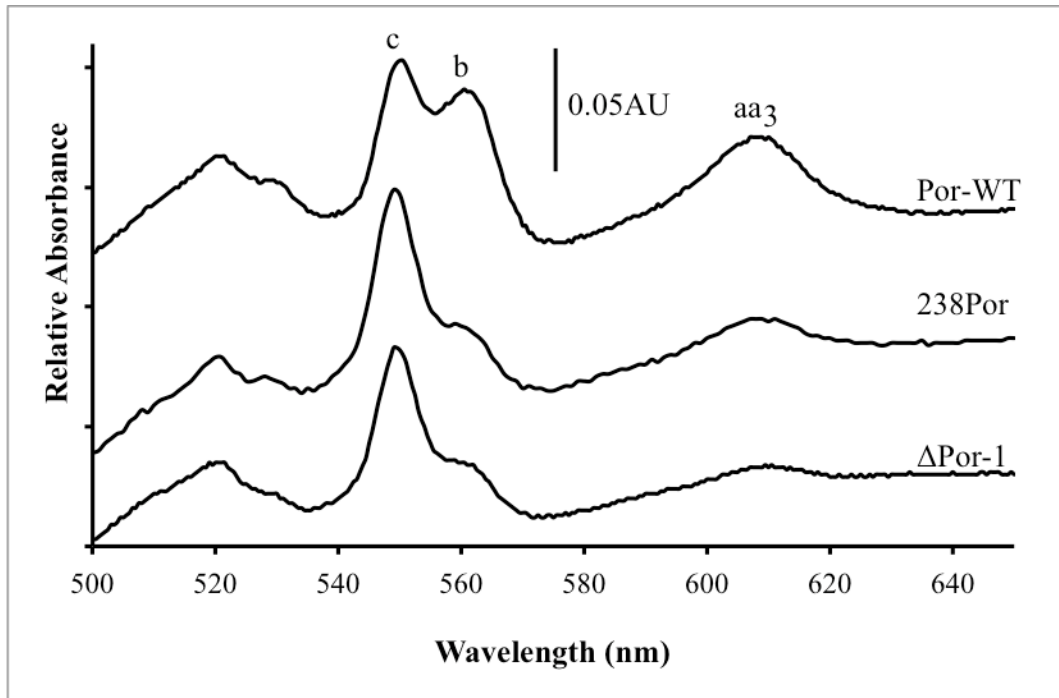


Figure 3.3. The reduced minus oxidized difference spectra obtained from wild-type (Por-WT), 238por, and Δ Por-1 mitochondria. Peaks representing absorbance by cytochromes *c*, *b*, and *aa₃* are indicated.

to generate a strain expression low levels of wild-type porin. Reduction of porin to 30-60% of wild-type levels was not associated with any detectable changes in growth rate, cytochrome profile, or expression of alternative oxidase (129), but very low levels of porin corresponding to those in 238Por (<5%) were not achieved. Given the ability of 238Por to generate an apparently wild-type pore in artificial membranes, the defects in 238Por may be most reflective of the low amount of porin. Nonetheless, it was predicted that further analysis of 238Por variant would reveal cellular changes responsible for almost wild-type growth rates in the absence of a normal mitochondrial bioenergetics. To that end, the proteomes of 238Por, Δ Por-1 and Por-WT strains were assessed.

3.5.1 1-Dimensional LC MS/MS analysis of the mitochondrial proteomes

Proteins were extracted from partially purified mitochondria and subjected to LC MS/MS. Peptides from a total of 1102 different proteins were detected, and slightly more than half of the proteins identified from each strain were predicted to reside in mitochondria (summarized in Table 3.2). The proteomic approach used in the current study detected a similar number of proteins (509) as was detected from *N. crassa* mitochondria through the use of iTRAQ from sucrose-gradient purified organelles (260, (130)) and (488, (110)). In the latter study, there were a number of intermembrane space proteins that were present in significantly reduced amounts in Δ Por-1, in spite of relatively normal levels of the corresponding mRNA (110). These proteins include TIM8, ketol-acid reductoisomerase, nucleoside diphosphate kinase-1, adenylate kinase, and ubiquinone cytochrome *c* reductase hinge. They were not reduced in the Δ Por-1 organelles used in the current study (Table 6.2). Thus, it appears that the

outer membranes of Δ Por-1 organelles were disrupted during the sucrose-gradient purification step in the iTRAQ studies.

The outer membrane proteome was well represented in the current study; 29 of the 30 proteins identified by Schmitt et al. (2006) in purified outer membranes were detected in the current study in wild-type mitochondria (Table 3.2). The exception was a mitochondrial import protein 1 (MIM1, NCU01101), a 130-amino acid protein required for assembly of TOM20 into the outer membrane (131). In contrast to the previous iTRAQ study (110), TOB55, a β -barrel in the topogenesis of mitochondrial outer membrane β -barrels (TOB) complex was detected in the current work, and there was a non-significant reduction its levels in Δ Por-1 and 238Por (\log_2 ratios of -0.3 and -0.5, respectively). Thus, as for the case for another β -barrel, TOM44 of the translocase of the outer membrane (see (110) and Fig. 3.2), upregulation of the TOB55 β -barrel was not increased as a mechanism for compensating for the absence of VDAC. The remaining predicted MOM β -barrel, MDM10 has yet to be detected in any large-scale proteomic analysis.

3.5.2 Electron Transport Chain

Both Δ Por-1 and 238Por display defects in cytochromes associated with mitochondrially encoded polypeptides and express alternative oxidase (Fig. 3.3 and Table 3.3). Proteomic analysis further revealed defects in NADH:Ubiquinone oxidoreductase (complex I) in Δ Por-1 (Table 3.4), which are supported by changes in the high molecular weight complexes detected by in-gel NDAH dehydrogenase assays (Fig. 3.4)

One of the main differences between the proteomes of Δ Por-1 and 238Por mitochondria is in the levels of subunits of complex I, which oxidizes NADH and translocates hydrogen ions

Table 3.3 Protein identification by LC-MS/MS. See tables 6.2-6.4 for details

Strain	Total proteins	Predicted mitochondrial proteins	OM proteins (of 30)^a
FGSC 9718	965	546	29
238Por	977	548	28
Δ Por	922	542	28

^aOf the proteins detected in isolated outer membranes of *N. crassa* ((124)

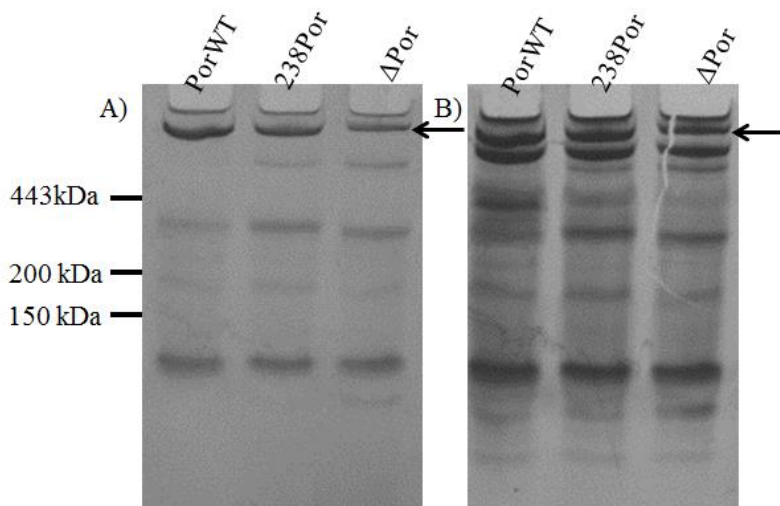


Figure 3.4. Red-Native PAGE of DDM-solubilized mitochondrial membrane complexes. A) In gel NADH dehydrogenase activity assay. B) The same gel stained with Coomassie Brilliant Blue. Arrows indicate bands corresponding to complex I. The intensity of the lower bands of the Coomassie-stained gel were used to confirm that similar amounts of DDM-solubilized material were present in each lane of the gel.

Table 3.4 Proteins detected in altered levels in Δ Por1 mitochondria. (Full data set in Appendix 2, Table 6.2)

Elevated in ΔPor				
Accession Number	Protein Description	Expression Difference (Log₂)	COG Group	Additional Descriptions (KEGG)
NCU03558	Hypothetical protein	3.35	None	Eukaryotic F-type ATPase ϵ -subunit
NCU01140	NAD(P) Transhydrogenase	2.94	Energy production and conversion	None
NCU05850	Rubredoxin-NAD ⁺ Reductase	2.63	General function prediction only	Similar to pyridine nucleotide-disulphide oxidoreductase
NCU06546	Hypothetical Protein	2.36	None	K17983 sensitive to high expression protein 9
NCU05495	CVNH Domain-Containing Protein	2.29	None	None
NCU00865	Oxalate Decarboxylase OxdC	2.12	General function prediction only	None
NCU01650	Hypothetical Protein	1.83	None	Large subunit ribosomal protein MRP49
NCU00122	Aspartyl Aminopeptidase	1.82	Amino acid transport and metabolism	None
NCU04578	ATP-Dependent Clp Protease Proteolytic Subunit	1.65	Intracellular trafficking, secretion, and vesicular transport	None
NCU04764	Hypothetical Protein	1.59	None	Methyltransferase OMS1
Reduced in ΔPor1				
NCU03802	Trimethyllysine Dioxygenase	-3.05	None	None
NCU05338	Hypothetical Protein	-3.22	None	None
NCU08561	Succinate/Fumarate Mitochondrial Transporter	-3.36	None	None
NCU01633	Hexose Transporter HXT13	-3.4	None	Similar to hexose transporter
NCU02564	Cysteine synthase 2	-3.56	Amino acid transport and metabolism	None
NCU04946	Hypothetical protein	-3.73	None	None

NCU00436	GTPase FZO1	-4.11	None	Hydrolases. Acting on acid anhydrides. Acting on GTP; involved in cellular and subcellular movement.
NCU04781	NADH:Ubiquinone Oxidoreductase 9.8 kDa Subunit	-4.23	None	None
NCU09345	Thiamine Biosynthesis Protein NMT-1, Variant 2	-5.07	Inorganic ion transport and metabolism	Pyrimidine precursor biosynthesis enzyme
NCU06110	Thiazole Biosynthetic Enzyme	-5.39	Coenzyme transport and metabolism	similar to stress-responsive gene product
NCU09143	Hypothetical Protein	-5.72	None	F-Type ATP synthase e-subunit
NCU09460	NADH:Ubiquinone Oxidoreductase 20.1kD Subunit	-5.86	None	None
NCU01024	Hypothetical Protein	-6.45	None	Altered inheritance of mitochondria protein 5

into the intermembrane space. None of the 27 subunits of complex I detected were present in significantly reduced levels (\log_2 difference < -1.6) in 238Por (Table 6.3), suggesting that this complex was functional. In contrast, in Δ Por-1 mitochondria, the levels of the 9.8- and 20.1-kDa subunits (NCU04781 and NCU09460) were significantly lower than in wild-type (Table 3.4), and levels of these proteins and the 40-kDa subunit were significantly different when the data from the two mutant strains were compared (Table 6.4). A nuo9.8 mutant lacking the former subunit fails to assemble the membrane-bound and peripheral arms of complex I (132), suggesting that assembly of this complex would be impaired in Δ Por-1. In fact, fifteen of the 27 other complex I subunits detected were present at levels 2.5- to 5-fold lower than in wild-type, although these differences were statistically insignificant (see Table 6.2). The differences in complex I activity are supported by the NADH dehydrogenase in-gel assay (Fig. 3.4).

Neurospora expresses four alternative NAD(P)H dehydrogenases allowing bypass of complex I, oxidizing NAD(P)H without proton translocation. Of these, NDE2 (133) and NDI1 (134) are essential for the viability in the absence of functional complex I. The relative levels of these proteins were not significantly changed in the Δ Por-1 mitochondria. Another alternative enzyme, NDE1, was unchanged and NDE3 (135) was not detected. Thus, the reduced levels of several subunits of the NADH dehydrogenase complex are not associated with overexpression of the alternative dehydrogenases in Δ Por-1 mitochondria and the defects in complex I may contribute to the very slow growth of Δ Por-1 in comparison to 238Por (Table 3.2).

The reduction in complex I subunits in Δ Por-1, and the reduced levels of cytochromes *b* and *aa₃* in both variant strains might contribute to suboptimal ratios of NAD(P)H/NAD(P)⁺, leading to changes in expression of proteins that impact these ratios. The increased levels of an NAD(P)H transhydrogenase (NCU01140, (136)), and a short chain dehydrogenase (NCU02097)

in both strains (Tables 3.4 and 3.5) may be involved in optimizing NAD⁺/NADH levels, particularly in Δ Por-1. Both variant strains harbour relatively high levels of an annotated rubredoxin reductase (NCU05850, Table 3.5). It has been identified as a homologue of apoptosis-inducing factor (137), an oxidoreductase that may be expressed in response to abnormal NAD⁺/NADH ratios.

There are no obvious differences between the variant and wild-type strains in terms of the nuclear-encoded co-enzyme Q: cytochrome *c* oxidoreductase (complex III) and cytochrome *c* oxidase (complex IV) proteins that were detected, and the mitochondrially encoded proteins associated with cytochromes *aa₃* in complex IV and *b* in complex III were not detected in any mutant strain in this and other studies (110), (130). Two proteins related to biogenesis of the electron transport chain, OMS1 (NCU04764, (138)) and OXA2 (139) are increased in Δ Por-1 (Table 3.4 and Table 6.2), indicating a response at the level of the proteome are related to the assembly of these complexes. As expected in cells with defective electron transport chains (128), cyanide-resistant alternative oxidase (AOD) activity was detected in both variant strains (Table 3.2) and both AOD-1 and AOD-3 proteins were detected in the Δ Por-1 proteome but not that of the wild-type (Table 6.2). However, transcription of *aod-1* is induced in *N. crassa* treated with chloramphenicol, while that of *aod-3* is not (140), suggesting that the two genes are regulated independently, and the inducers for both are present in Δ Por-1. However, alternative oxidase activity is not observed in *aod-1* mutants (discussed in Tanton et al. 2003), suggesting that the AOX-3 polypeptide detected in this study is non-functional. In spite of the cyanide-resistant respiration observed, neither alternative oxidase protein was detected in 238Por, suggesting that their levels were sufficient for biological activity but were below detection by the methods used.

Table 3.5 Proteins detected in altered levels in 238por mitochondria. (Full data set in Appendix 2, Table 6.3)

Elevated in 238Por				
Accession Number	Protein Description	Expression Difference (Log₂)	COG Group	Additional Descriptions (KEGG)
NCU01140	NAD(P) Trans Hydrogenase	3.91	Energy production and conversion	None
NCU05495	CVNH Domain-Containing Protein	3.47	None	None
NCU06546	Hypothetical Protein	2.84	None	K17983 sensitive to high expression protein 9
NCU05850	Rubredoxin-NAD ⁺ Reductase	2.79	General function prediction only	Similar to pyridine nucleotide-disulphide oxidoreductase
NCU00122	Aspartyl Aminopeptidase	2.52	Amino acid transport and metabolism	None
NCU09263	Anchored Cell Wall Protein 4 (Hypothetical)	2.51	None	None
NCU07021	Peptide Chain Release Factor 3	2.36	Translation, ribosomal structure and biogenesis	None
NCU06880	AhpC/TSA Family Protein	2.23	Posttranslational modification, protein turnover, chaperones	Atypical 2-Cys peroxiredoxin
NCU03929	Acyl-CoA Synthetase	2.18	Lipid transport and metabolism	Similar to Fum16p
NCU03796	Pyruvate Dehydrogenase Kinase	2.17	None	None
NCU04578	ATP-Dependent Clp Protease Proteolytic Subunit	2.16	Intracellular trafficking, secretion, and vesicular transport	None
NCU09285	Zinc-Containing Alcohol Dehydrogenase	2.12	General function prediction only	None
NCU03006	Sterol 24-C-Methyltransferase	2.12	Coenzyme transport and metabolism	None
NCU16657	Tryptophanyl-tRNA Synthetase	2.11	Translation, ribosomal structure and biogenesis	None
NCU10021	MFS Monosaccharide Transporter	2.11	None	None
NCU05558	3-Ketoacyl-CoA Thiolase	2.1	Lipid transport and metabolism	None

NCU06958	Mito Ribosomal Protein S21	2.03	None	None
NCU02802	Mitochondrial Ornithine Carrier Protein	1.98	None	None
NCU07858	DUF498 Domain-Containing Protein	1.94	Function unknown	None
NCU00264	Hypothetical Protein	1.91	Signal transduction mechanisms	None
Reduced in 238Por				
NCU02936	Proline Oxidase	-1.84	None	None
NCU06189	5-Aminolevulinate Synthase	-1.86	Coenzyme transport and metabolism	None
NCU00107	Mitochondrial Inner Membrane Protease ATP-23	-2.41	None	None
NCU02504	DUF1640 Domain-Containing protein	-2.62	None	None
NCU00565	Lipoic Acid Synthetase	-2.82	Coenzyme transport and metabolism	None
NCU08354	Hypothetical Protein	-2.84	None	None
NCU01024	Hypothetical Protein	-2.9	None	altered inheritance of mitochondria protein 5
NCU09143	Hypothetical Protein	-3.93	None	F-type H ⁺ -transporting ATP synthase e-subunit
NCU04304	Outer Mitochondrial Membrane Protein Porin	-4.96	None	Voltage-dependent anion channel protein 2

In terms of the F₁F₀-ATP synthase (complex V), in ΔPor-1 (Table 3.4), there was a higher level of a protein (NCU03558) that is similar to the ε-subunit (Atp15p, (141)) and an inner membrane protease involved in maturation of subunit 6 (NCU00107, ATP-23, (142)) was less abundant in 238Por (Table 3.5) and not detected in ΔPor-1. In both variant strains, there was a significant deficit in the putative e-subunit of the F₀ subcomplex (NCU09143, Tables 3.4 and 3.5), which will be discussed below.

3.5.3 Oxidative Stress

Oxidative stress is a predictable outcome in cells lacking complete electron transport chains and several of the differences between the proteomes of the wild-type and variants indicate direct or indirect responses to oxidative stress. Both variants express higher levels of alternative oxidase, which acts on reduced ubiquinone (143) and a Zn-dependent alcohol dehydrogenase (NCU09285, MIG-6, Tables 3.4 and 3.5, (110)). Expression of this open reading frame is induced by menadione. Only 238Por showed an increased levels of the protein predicted to encode an atypical 2-Cys peroxiredoxin (NCU06880), associated with resistance to hydrogen peroxide in mammalian cells (144).

In contrast, several proteins linked to reducing oxidative stress are in lower levels in one or both of the variant strains, including proline oxidase (NCU02936, (145)) and the thiamine thiazole synthase (146). Perhaps unexpectedly, there is over 8-fold less of the latter enzyme (NCU06110; CyPBP37) in ΔPor-1 than in the wild-type and 238Por strains, respectively (Table 3.4 and Table 6.4). Another thiamine biosynthetic enzyme, NMT-1 (NCU09345) is drastically reduced only in ΔPor-1 (Table 3.4) and has been implicated in protection against oxidative stress in yeast (147). Finally, lipoic acid has antioxidant activity (discussed in (148)) and lipoic acid

synthase (NCU00565) is reduced only in 238Por only (Table 3.5). Other impacts of reduced lipoic acid levels are discussed with respect to the TCA cycle and heme biosynthesis below (Fig. 3.7).

Both strains show evidence of increased responses to misfolded proteins, which could result from the effects of reduced ATP levels on chaperone activity. Δ Por-1 and 238Por have low-level overexpression of the proteolytic subunit of the Clp protease (NCU4578, Tables 3.4 and 3.5), which participates in the mitochondrial unfolded protein response (reviewed by (149)). Aspartyl aminopeptidase (NCU00122) also is present in higher levels in both variant strains, and aminopeptidases may “moonlight” as chaperones ((150), (151), (152)). Three other proteases, carboxypeptidase Y (NCU00477), the mitochondrial AAA ATPase (NCU05459), and the intermembrane space AAA protease IAP-1 (NCU03359) are present in elevated levels in Δ Por-1 compared to 238Por (Table 6.4). The latter protease is part of the mitochondrial protein quality control system (153), again suggesting increased protein misfolding in Δ Por-1.

Several of the differentially expressed proteins are linked to the TCA cycle, through the generation of cofactors or substrates, or utilization of TCA intermediates as substrates (Fig. 3.7). In mitochondria, the pyruvate dehydrogenase complex (PDC) converts pyruvate into acetyl-CoA, which can then enter the TCA cycle (Fig. 3.7A). Lipoic acid is a PDC cofactor (154). Increased levels of pyruvate dehydrogenase kinase (PDK, NCU03796), which inactivates PDC (155), and reduced lipoic acid synthase (LAS, NCU00565) in 238Por (Table 5) suggest lower levels of PDC activity in 238Por, which might optimize ratios of its substrates (pyruvate, NAD^+ and coenzyme A) and products (acetyl-CoA and NADH^+ and H^+). A second potential link to acetyl-CoA production is through the 3-ketoacyl CoA thiolase (NCU05558), which participates in both fatty acid degradation and fatty acid elongation. The slightly higher levels of acyl-CoA synthase

(NCU03929) might drive higher levels of fatty acid biosynthesis and ensure release of acetyl-CoA. Finally, the carnitine shuttle is involved in movement of acetyl groups between peroxisomes and mitochondria (reviewed by (156)). In Δ Por-1, the lower levels of trimethyllysine dioxygenase (TMLD, NCU03802), involved in carnitine biosynthesis, could potentially influence the shuttle and the acetyl-CoA levels in the organelle.

Several proteins present in lower levels only in Δ Por-1 are linked to intermediates of the TCA cycle (Fig. 3.7B). TMLD consumes α -ketoglutarate and generates succinate, bypassing a step that reduces NAD^+ . A putative succinate/fumarate mitochondrial transporter (Sfc1p homologue, NCU08561) and the lower levels of this protein would potentially drive matrix succinate levels lower, without increasing levels of ROS via a backlog of reduced ubiquinone. The yeast homologue of the transporter, Sfc1p (or Acr1p) is required for acetyl-CoA synthetase activity (157) again linking changes in Δ Por-1 with reduced acetyl-CoA levels.

Both mutant strains harbour lower levels of 5-aminolevulinate synthase (ALAS, NCU006189, Tables 3.4 and 3.5), which is involved in heme biosynthesis (reviewed by (158)) and may be a response to reduced heme requirements due to reduced levels of cytochromes *aa3* and *b* in the porin variants. Reduction in ALAS activity would also prevent diversion of succinyl-CoA from the TCA cycle (Fig. 3.7B). Conversely, α -ketoglutarate dehydrogenase (KGD), which generates succinyl-CoA, requires lipoic acid (159) and lipoic acid synthase is reduced in 238Por.

3.5.4 Mitochondrial Biogenesis

The translocase of the outer membrane (TOM complex) recognizes signals in mitochondrial pre-proteins and translocates the polypeptides across the outer membrane

(reviewed in (160)). The stability of the TOM complex is reduced in Δ Por mitochondria, as indicated by the increased migration rate of Tom40-containing complexes during non-denaturing PAGE ((110), Fig. 3.5). In contrast, the complex in 238Por migrates similarly to that of the wild-type strain, indicating that the small amount of 238Porin is sufficient for maintenance of the complex.

Depletion of mitochondrial porin also is associated with altered mitochondrial morphology (110). Staining of whole mitochondria with MitoTracker revealed similar morphology for 238Por and wild-type organelles (Fig. 3.6). However, there appeared to be a lower number of well-stained organelles per hyphal tip, and those observed generally were larger in the 238Por cells. Under the staining conditions used, long string-like mitochondria were not observed in hyphal tips in the wild-type.

With respect to different morphology, a potential Mdm33p homologue (NCU06546) is required for normal morphology and distribution of mitochondria (*mdm*; (161)) is relatively more abundant in Δ Por-1 and 238Por strains (Tables 3.4 and 3.5). FZO1 encoded by *uvs-5* (NCU00436) is a mitofusin homologue in the outer membrane (124)) is more than 8-fold reduced in Δ Por-1 mitochondria (Table 3.4), but was present in almost normal levels in 238Por organelles. This defect in Δ Por-1 may contribute to the small mitochondria seen Δ Por-1 strains (110), as *uvs-5* strains have fragmented mitochondria (162).

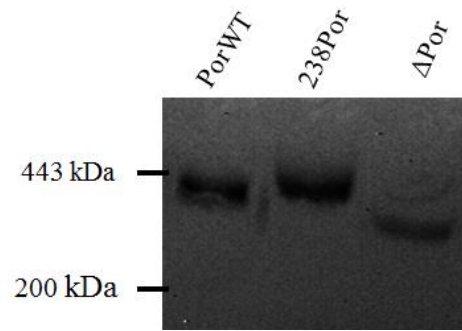


Figure 3.5. Western blot detection of the Translocase of the Outer Membrane (TOM) complex from Red-Native PAGE of DDM-solubilized mitochondrial membrane complexes. Antibodies against the TOM complex 40-kDa subunit (TOM40) were used to identify the TOM complex.

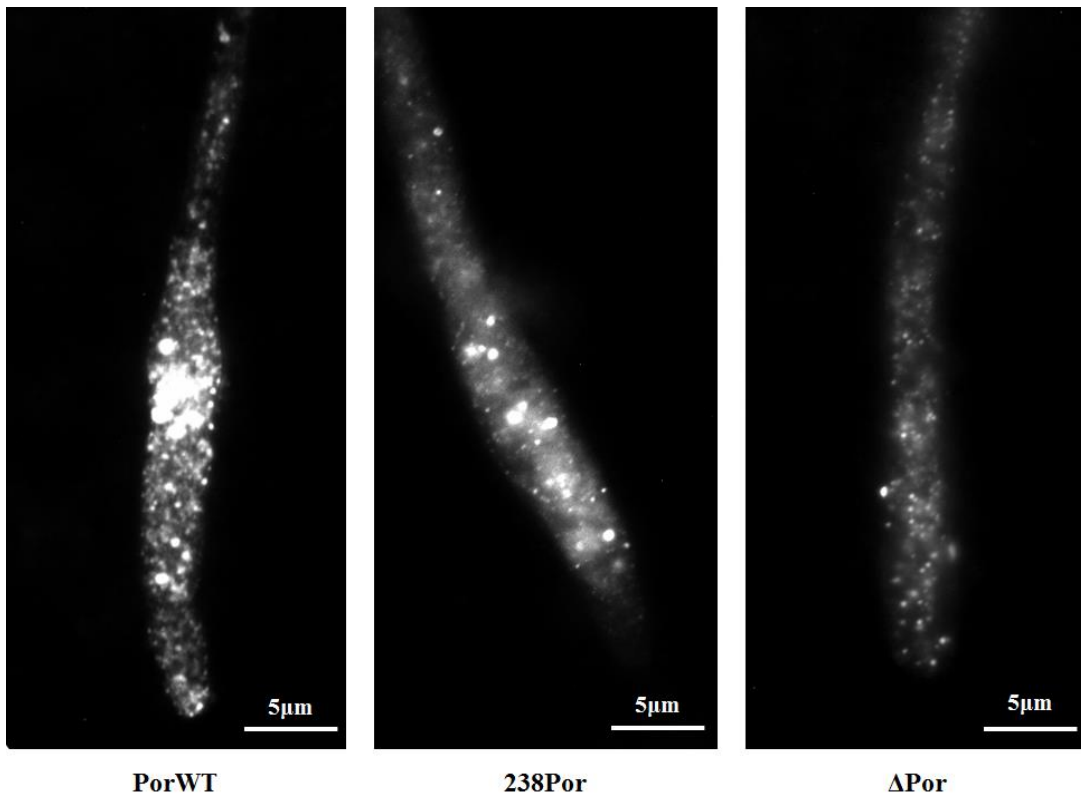


Figure 3.6. Fluorescence microscopy of *N. crassa* mitochondria. Hyphae of wild-type (left) and 238Por (middle) and Δ Por1 (right) were stained with MitoTracker and observed at 1000x magnification.

In both strains, there was a significant deficit in the putative e-subunit (NCU09143) of the F_o ATPase synthase subcomplex (Tables 3.4 and 3.5). This subunit, Atp21p in *S. cerevisiae*, is involved in the formation of monomers of the F₁F_o-ATP synthase that are competent for dimerization (163) and the dimers in turn appear to contribute to the curvature of the inner membrane (164). The mitochondrial organizing structure (MitOS) of the inner membrane is proposed to interact with the ATP synthase dimers and contribute to the development of normal morphology. The putative homologue (NCU01024) of one component of the yeast MitOS, Aim5p, is expressed at lower levels in Δ Por-1 mitochondria (Table 3.4), perhaps contributing to the abnormal morphology. Interestingly, porin is linked to MitOS through genetic interactions (165) although the nature of the interaction is unknown.

Two variably expressed proteins participate in synthesis of the non-protein components of the outer membrane. The sterol 24-C methyltransferase (NCU03006) is involved in ergosterol biosynthesis, and is present at 3.0- to 4.6-fold higher levels in both strains. The full extent of the impact of porin defects on sterol biosynthesis is not known because the other enzymes in the pathway from zymosterol to ergosterol (ERG-2, ERG-3, ERG-5) were not detected in any strain, and ERG-6 was detected only in the wild-type strain. An enzyme involved in fatty acid biosynthesis, 3-oxoacyl-(acyl-carrier-protein) reductase (NCU01092) was not detected in the wild-type strain, but, in the variant strains, was present in almost 8-fold higher levels in Δ Por-1 (Table 3.4).

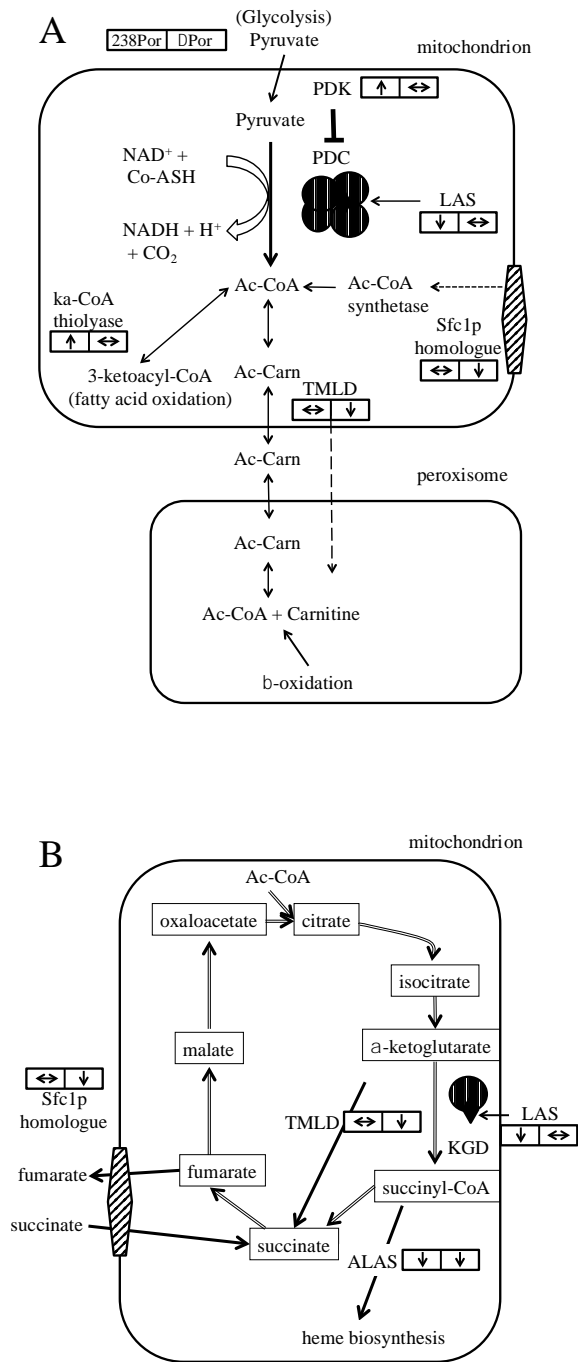


Figure 3.7 Connections among proteins present in different relative amounts in 238por and Δ Por-1 mitochondria.

Figure 3.7. Connections among proteins present in different relative amounts in 238por and Δ Por-1 mitochondria. A) Mitochondrial proteins. Proteins present in relatively high or low amounts are indicated by arrows directed upward or downward, respectively, in split boxes referring to 238Por (left) and Δ Por-1 (right). In the case of enzymes, the reactions they catalyze are represented by thin or thick arrows if the proteins are in low or high levels, respectively. The blunt arrow between PDK and PDC indicates an inhibitory interaction; all others are positive effects. The dotted line linking TMLD and carnitine in peroxisomes indicates that the mitochondrial enzyme TMLD is required for synthesis of carnitine, which participates in the carnitine shuttle between mitochondria and peroxisomes. The dotted arrow denotes an effect of Sfc1p on the activity of Ac-CoA synthetase as described in the text. PDC, pyruvate decarboxylase; PDK, PDC kinase; Ac-CoA synthase, acetyl-coenzyme A synthase; Carn, carnitine; ka-CoA, 3-ketoacetyl-CoA; TMLD, trimethyllysine dioxygenase. B) Links between differentially expressed proteins and the TCA cycle in 238porin. The TCA cycle is indicated by double arrows linking substrates/products (boxes). Reduction in lipoic acid synthase (LAS) levels, could reduce the amounts of lipoic acid (grey diamond), a cofactor of α -ketoglutarate dehydrogenase (KGD, speckled circle), potentially decreasing levels of succinyl-CoA. ALAS, 5-Aminolevulinate Synthase. For references, see text.

3.6 Conclusions

238porin is present in relatively low levels in the outer membrane, but nonetheless partially complements a porin-less strain of *Neurospora*. Its presence is associated with almost wild-type growth rate, although 238Por expresses alternative oxidase and suffers defects in the electron transport chain. The proteomic studies revealed links to altered electron flow, NADH metabolism and mitochondrial morphology in both Δ Por-1 and 238Por strains. The strain expressing 238Por appears to contain higher levels of complex I of the ETC, and the carbon flow through the TCA cycle in these cells may be different from that in Δ Por-1 organelles. Thus, the cellular response to the presence of a low level of 238Por allows more rapid hyphal growth.

4.1 Conclusions

In this work two approaches were used to further the understanding of VDAC function, biophysical analysis of a VDAC protein and physiology of a *N. crassa* strain expressing a VDAC mutant. These two complementary approaches produced data that led to the following conclusions:

- 1) VDAC oligomeric state is affected by CHS in detergent solutions (Fig. 2.1)
- 2) In the presence of CHS VDAC forms dimers, trimers, tetramers and possibly hexamers. (Table 2.2 and Fig. 2.2)
- 3) The *N. crassa* VDAC studied in this work has a similar structure to mouse VDAC1 and zebrafish VDAC2. (Fig. 2.4)
- 4) The *N. crassa* VDAC dimer observed in this work is arranged in a similar manner to the zebrafish VDAC2 dimer crystal structure. (Fig. 2.5)
- 5) The described biophysics approach to the characterization of detergent solubilized VDAC should be applicable to the characterization of other membrane proteins or membrane protein complexes.
- 6) The 238porin variant of *N. crassa* VDAC localizes to mitochondria and is protease resistant indicating that it inserts into the MOM.
- 7) 238porin partially compensates for a VDAC knockout in *N. crassa*.
- 8) 238porin expression level is 3% that of the wild-type VDAC sequence. (Table 3.5)
- 9) The 238porin variant causes differential expression of mitochondrial proteins of varied functions and the effect is different than that of a VDAC knockout. (Tables 3.4 and 3.5)

The development of a biophysics pipeline for the analysis of IMPs *in vitro* will provide a platform for the study of any detergent-solubilized membrane protein. Due to the difficulties in the study of these proteins this work will function as a guide to making the accessible characterization of IMPs possible. The results presented will further the understanding of VDAC behavior and function. VDAC self-assembly into units larger than a monomer has been linked to the induction of apoptosis through a proposed mechanism in which Smac/Diablo, cytochrome c and AIF are released from mitochondria by either the larger VDAC units or complexes of VDAC oligomers and Bax (61). The work described in this thesis work demonstrated that a cholesterol analogue (CHS) was able to induce the formation of VDAC oligomers in detergent solution. This finding is in line with other studies that indicate VDAC oligomeric state is sensitive to the surrounding lipid environment in their native membranes (60, 91) and therefore it is not surprising that this would also be the case in membrane mimetic systems such as detergent micelles. This implies that VDAC oligomeric state is regulated by the local composition of the mitochondrial outer membrane and cholesterol (or ergosterol) concentration. Furthermore, the proteomic data presented displayed increased expression of a rubredoxin-NAD⁺ reductase in the VDAC knockout and VDAC depleted strains of *N. crassa*, Δ Por and 238Por respectively. The rubredoxin-NAD⁺ reductase has been identified as a homologue of the higher eukaryotic Apoptosis Inducing Factor (AIF) (137), which as discussed above is suggested to be released by VDAC oligomers during the induction of apoptosis (61). In this light the reduced expression levels of 238porin may explain the increase in rubredoxin-NAD⁺ reductase expression in the 238Por strain as a mechanism to compensate for a reduced VDAC concentration in the MOM or the impaired ability of VDAC to form oligomers. The differential expression of an apoptosis inducing factor homologue due to alterations to the levels of VDAC in the MOM supports a link

between VDAC and the induction of apoptosis. As the study of the involvement of VDAC in mitochondrial-mediated apoptosis progresses, the data provided by this work will be paramount to the understanding of mechanisms by which VDAC oligomers are linked to programmed cell death.

4.2 Future Directions

Based on the results of this study, the steps in the study of the VDAC system should be focused into three main objectives:

- 1) The characterization of the VDAC-hexokinase complex and the involvement of the VDAC-hexokinase complex in mitochondrial-mediated apoptosis.
- 2) Further study into the regulation of VDAC oligomeric state
- 3) Examination of VDAC mutants using the biophysics approach
- 4) High resolution structural analysis

The binding of *N. crassa* VDAC to *S. cerevisiae* HK-I was demonstrated in Chapter 2 of this work (Fig. 2.7); this is only the first step in the characterization of this complex as the full biophysics pipeline should be applied to the complex to gain a more complete understanding of the makeup of the complex. Particularly of interest is structural information that SAXS could provide describing the complex. Due to the low resolution of SAXS models the structural information would not be able to provide the same insight into the structure as high-resolution methods; however, it would be sufficient to determine the organization of VDAC and hexokinase units within the complex.

The effect of CHS on the oligomeric state of detergent solubilized VDAC has been established by the work presented in this thesis; however, the next logical step in the study of this effect is to determine the specific nature and mechanism of this effect. An important area of interest will be determining if these oligomers exist as a dynamic population and if so the dynamics of this system could be probed by AUC sedimentation equilibrium experiments (30). In addition, it would be interesting to determine if the VDAC oligomeric transition induced by CHS is concentration dependent and if different concentrations of CHS alter the populations of oligomers formed via AUC sedimentation velocity experiments or SEC-MALS experiments. The use of the biophysics approach to examine VDAC mutants could provide an interesting tool to examine the relationship between biological data and structural features of VDAC. It would be interesting to use the biophysics method to determine if the 238porin mutation alters the ability of VDAC to form oligomers, which could aid in determining whether the differential expression of rubredoxin-NAD⁺ reductase is due to the lack of VDAC oligomers or reduced VDAC concentration in the MOM.

High resolution studies have been paramount in the understanding of protein structure-function relationships for the past 50+ years and therefore the analysis of these VDAC oligomers would benefit from high resolution information. A probable high-resolution structure of a VDAC dimer exists (68); however, structures of VDAC trimers, tetramers and hexamers are not yet available. While techniques such as x-ray crystallography and NMR may not be suited to tackling these structures due to crystallization difficulties and size limits respectively, recent advances in the field of cryogenic electron microscopy could provide a platform for structural analysis at high resolution. With these further explorations of the combined structural and

functional aspects of VDAC, the role VDAC plays in the complex processes leading to apoptosis will be revealed.

5. Appendix 1: Supporting Information for Chapter 2

Table 5.1 Raw Data obtained from AUC c(s) distributions

Detergent	Total VDAC Concentration (mg/ml)	VDAC Peak	$S_{20, \text{buffer}}^a$ (Absorbance/Interference)	A_{280}^b	J^c
0.3%DM	0.49	Monomer	4.53/4.57	0.40	3.29
	0.67	Monomer	4.41/4.56	0.61	5.44
	0.82	Monomer	4.38/4.52	0.72	6.33
	0.98	Monomer	4.33/4.48	0.84	7.66
0.3% DM + 0.06% CHS	0.48	Dimer	5.04/5.16	0.054	0.54
		Trimer	6.04/6.01	0.089	0.95
		Tetramer	7.19/7.35	0.229	1.83
	0.63	Dimer	5.01/5.11	0.091	0.99
		Trimer	6.07/6.01	0.172	1.38
		Tetramer	7.13/7.13	0.261	2.19
	0.84	Dimer	5/4.9	0.241	2.43
		Trimer	5.99/6.04	0.316	2.62
		Tetramer	7.08/7.06	0.179	1.34
	0.99	Dimer	4.94/ 4.84	0.414	3.89
		Trimer	5.93/ 5.95	0.319	2.75
		Tetramer	7.1/ 7.05	0.134	0.94

^a $S_{20, \text{buffer}}$: Sedimentation coefficient of peak in sample buffer

^b A_{280} : Absorbance at 280nm calculated by integration of species peak in the c(s) absorbance distribution

^c J : interference fringe displacement calculated by integration of species peak in the c(s) interference distribution

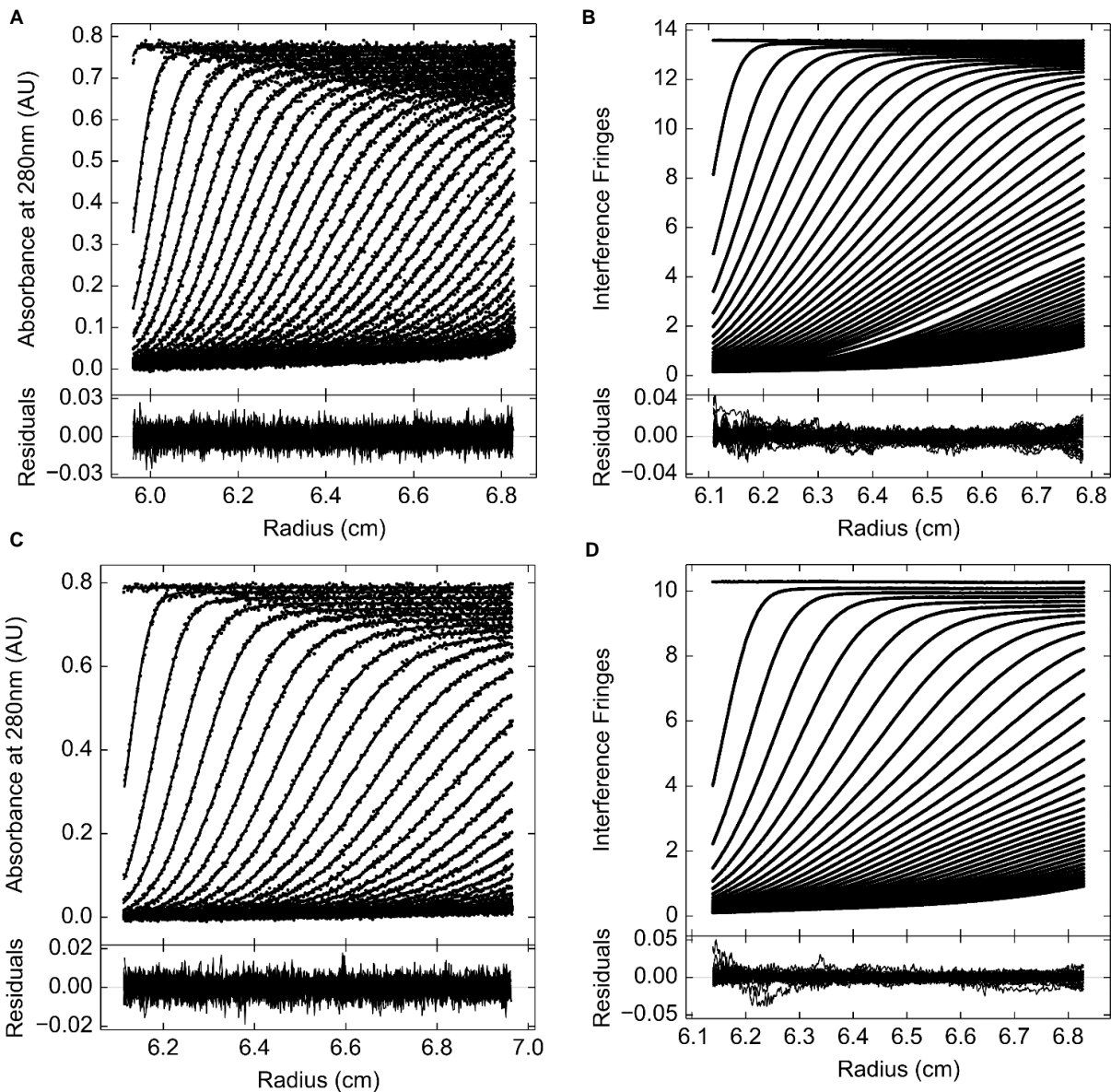


Figure 5.1 Representative sedimentation velocity experimental data and fitted curves used to calculate $c(s)$ or $c(s, f/f_0)$ distributions.

Figure 5.1 Representative sedimentation velocity experimental data and fitted curves used to calculate $c(s)$ or $c(s, f/f_0)$ distributions. (A) 0.82mg/ml VDAC^R solution measured by absorbance at 280nm. (B) 0.82mg/ml VDAC in DM solution measured by interference. (C) 0.84mg/ml VDAC^R+CHS solution measured by absorbance at 280nm (D) 0.84mg/ml VDAC^R+CHS solution measured by interference. In all panels data points are presented as black circles and fitted sedimentation boundaries are depicted as black lines. For clarity only every third time point is presented.

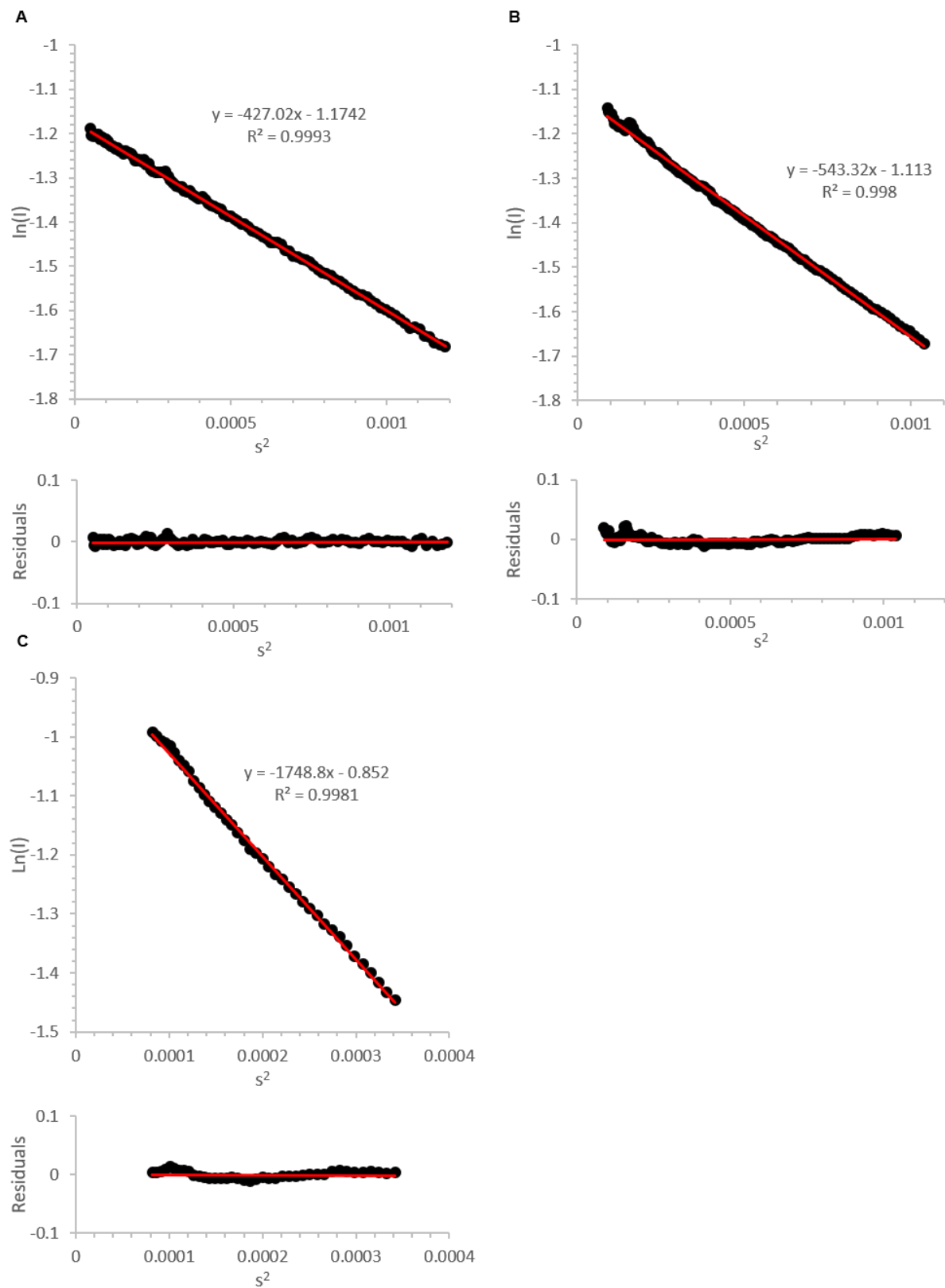


Figure 5.2. Guinier analyses of VDAC species examined in this study.

Figure 5.2. Guinier analyses of VDAC species examined in this study. (A) The upper panel depicts the Guinier region of the VDAC-monomer scattering curve (Fig 2.4) with the linear function fitted to the data displayed in red from which the R_g was determined. The bottom panel depicts the residuals between the experimental data and the fitted function with the red line indicating a value of 0. The fitted function and goodness of fit (R^2) are indicated in the upper panel. (B) The upper panel depicts the Guinier region of the VDAC-dimer scattering curve (Fig 2.5) with the linear function fitted to the data displayed in red from which the R_g was determined. The bottom panel depicts the residuals between the experimental data and the fitted function with the red line indicating a value of 0. The fitted function and goodness of fit (R^2) are indicated in the upper panel. (C) The upper panel depicts the Guinier region of the VDAC-hexamer scattering curve (Fig 2.6) with the linear function fitted to the data displayed in red from which the R_g was determined. The bottom panel depicts the residuals between the experimental data and the fitted function with the red line indicating a value of 0. The fitted function and goodness of fit (R^2) are indicated in the upper panel.

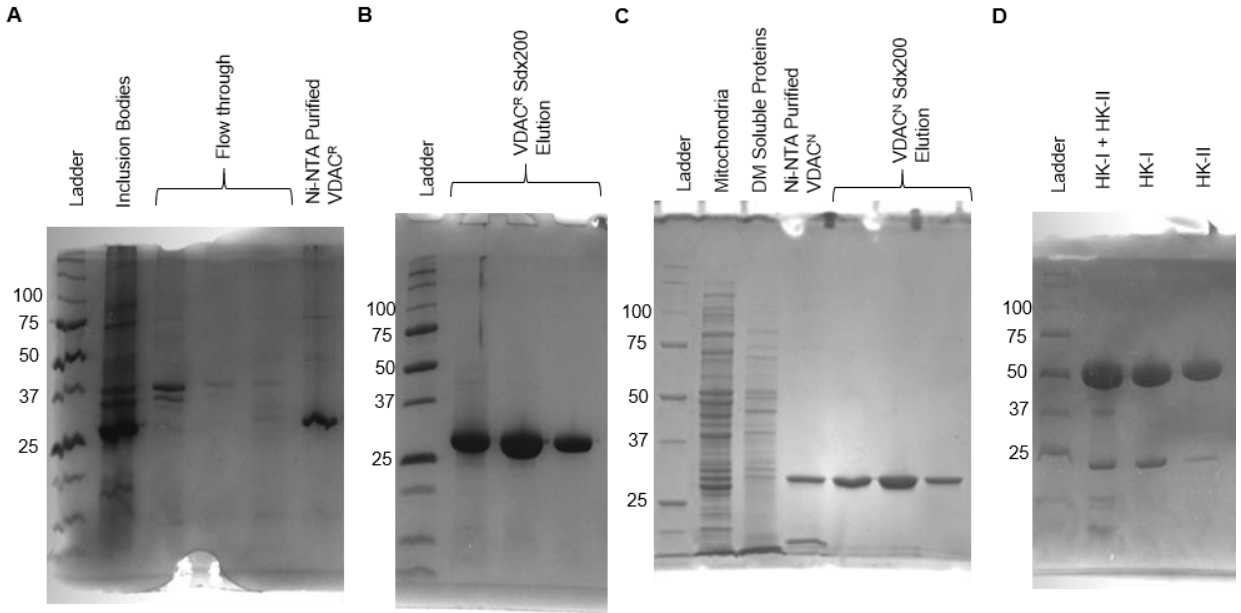


Figure 5.3. Full regions of interest of SDS-PAGE gels.

Figure 5.3. Full regions of interest of SDS-PAGE gels. (A) Denaturing Ni-NTA purification of VDAC^R from inclusion bodies (Left panel of Fig. 2.1A). (B) Refolded VDAC^R SEC fractions (Middle panel of Fig. 2.1B). (C) Native purification of VDAC^N (Right panel of Fig. 2.1A). (D) Separation of HK-I & HK-II (Fig. 2.7B). For all gels the contents of lanes are labeled directly above each lane. The M_w of relevant protein ladder bands are labeled to the right of each ladder lane.

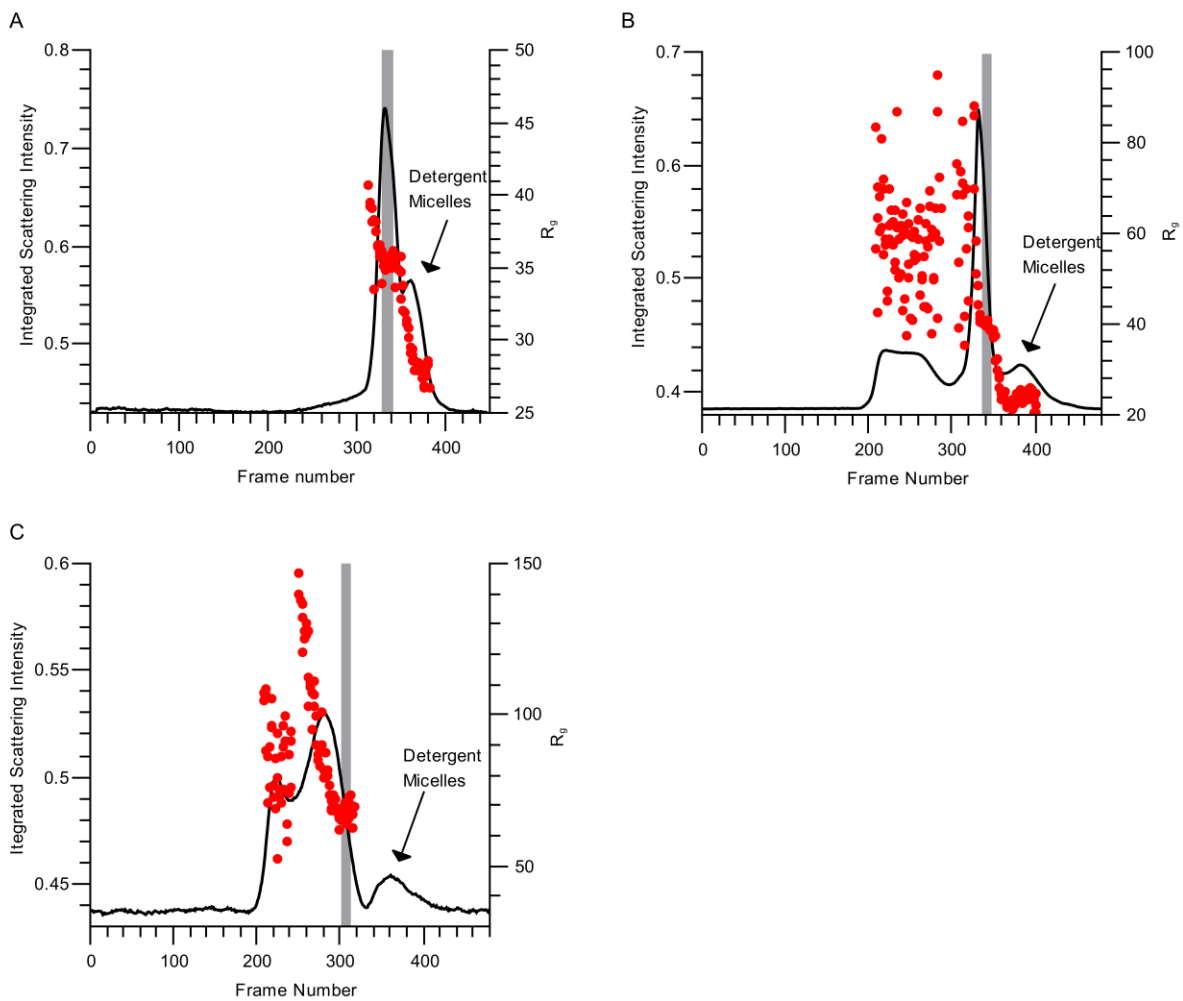


Figure 5.4. SEC-SAXS-Elution profiles of VDAC-detergent complexes

Figure 5.4. SEC-SAXS-Elution profiles of VDAC-detergent complexes. Elution profile of VDAC^R in the absence of CHS (A), VDAC^R with CHS in the column running buffer (B) and VDAC^R pre-equilibrated with CHS and with CHS in the running buffer (C). In all plots the integrated scattering intensity of each frame (black lines) and R_g determined from each frame (red circles) is plotted against the frame number. The R_g of frames with integrated scattering intensities <0.03 above the buffer baseline were not determined. Peaks corresponding to excess detergent micelles in the loaded samples are indicated on each plot, these peaks were identified as detergent micelles as they were absent from the UV absorbance trace of the elution and produced identical scattering curves to detergent only samples (data not shown). The frames used in the final analysis of the VDAC-detergent complexes are indicated by the area of the plots shaded in grey.

6. Appendix 2: Supporting Information for Chapter 3

Table 6.1 Primer sequences. The sequences of the 5' and 3' portions of each of the indicated primers are listed below.

	5' sequence for homology or restriction	3' sequence for priming [position with respect to porin ORF] ^a
5' Prom::pRS416	5'GTAACGCCAGGGTTTTCCCAG TCACGACGTTGTAAAACGA nt 1920-1959 of gb U03450.1 pRS416	ATCGGGATTACAATGCA GGG 3' SC5 ^b : 5561724-43 [-959]
3' Prom::Hyg	5'GCCCAAAAAGTGCTCCTTCAA TATCATCTTCTGTCGACGG (pCNS44 (Staben 1989)– TrpC terminator <i>Aspergillus nidulans</i> X02390.1 nt 912-886)	TTAGACGGAGTCGTGAT TGG 3' SC5: 5562339-58 [-344]
hphFnarI	5'AAAAAGGCGCC (<i>NarI</i> restriction site)	CCGTCGACAG AAGATGATATTGAAGGA GC 3' (pCNS44 (Staben 1989)– TrpC terminator <i>Aspergillus nidulans</i> X02390.1 nt 886-912)
hphRnarI	5'AAAAAGGCGCC (<i>NarI</i> restriction site in italics)	AGCTGACATCGACACCA ACG 3' (pCNS44 (Staben 1989)– TrpC promoter <i>Aspergillus nidulans</i> X02390.1 nt 3482-3463)
5'_por_ATG	'5ATGGCTGTTCCCGCTTTCTC (homology and priming on 238porin cDNA – Runke et al. 2006) SC5:5562683-5562702 [+1]	
3'_cDNA:porTerm	5'GTTCTGAAGGAATACTATTACGCCGCTGCTTCTTCA CATGT SC5:5564421-5564460	CTAAGACTCGAAGGTGA AGC 3' SC5: 5564387-5564406
por3'UTRF	5'GACGAATCTGGATATAAGATCGTTGGTGTCGATGT CAGCT (pCNS44 (Staben 1989)– TrpC promoter <i>Aspergillus nidulans</i> X02390.1 nt 3443-3482)	ACATGTGAAGAAGCAGC GGC 3' SC5: 5564421-5564440 [-15]
por3'UTRR	5'GCGGATAACAATTTACACAGGAAACAGCTATGA CCATGA (gb U03450.1 pRS416; nt 2197-2158)	GGCACCTGACTTCAACA GCG 3' SC5:5565823-5565814 [-1418]

^a the ORF for porin (NCU04303.7) is bp 5562683-5564406 in supercontig 5 of the Nc12 version of the *N. crassa* genome sequence; the transcript spans bp 5562346-5564796

^b *N. crassa* OR74A (NC12): Supercontig 5, accessed at

<https://www.broadinstitute.org/annotation/genome/neurospora/MultiHome.html>

Table 6.2 Levels of predicted mitochondrial proteins in Δ Por-1 relative to wild-type

Log2 differences that are statistically different are highlighted in blue.			
Locus	Description	log2 Difference	Z-Score
NCU03558	hypothetical protein	4.08	3.46
NCU01140	NAD(P) Transhydrogenase	3.67	3.11
NCU05850	rubredoxin-NAD	3.36	2.85
NCU06546	hypothetical protein	3.09	2.62
NCU05495	CVNH domain-containing protein	3.02	2.56
NCU00865	oxalate decarboxylase oxdC	2.85	2.41
NCU01650	hypothetical protein	2.56	2.17
NCU00122	aspartyl aminopeptidase	2.55	2.16
NCU04578	ATP-dependent Clp protease proteolytic subunit	2.38	2.02
NCU04764	hypothetical protein	2.32	1.97
NCU00831	extracellular serine carboxypeptidase, variant	2.24	1.90
NCU03006	sterol 24-C-methyltransferase	2.21	1.87
NCU06880	AhpC/TSA family protein	2.10	1.78
NCU09754	mitochondrial chaperone Frataxin	2.05	1.74
NCU07362	L-lactate ferricytochrome c oxidoreductase	2.00	1.69
NCU07549	mitochondrial ribosomal protein L43	1.96	1.66
NCU02948	non-anchored cell wall protein 4	1.94	1.64
NCU07858	DUF498 domain-containing protein	1.93	1.63
NCU07021	peptide chain release factor 3	1.90	1.61
NCU05459	mitochondrial AAA ATPase	1.85	1.57
NCU10226	mmf1	1.84	1.56
NCU06740	hypothetical protein	1.84	1.56
NCU05427	ATP-dependent Clp protease, variant	1.83	1.55
NCU01516	mitochondrial co-chaperone GrpE	1.79	1.52
NCU09285	zinc-containing alcohol dehydrogenase	1.78	1.51
NCU09263	anchored cell wall protein 4	1.77	1.50
NCU02128	D-arabinitol dehydrogenase	1.77	1.50
NCU00264	hypothetical protein	1.73	1.47
NCU06778	OXA-2	1.70	1.44
NCU01102	mitochondrial export translocase Oxa1	1.70	1.44
NCU02157	COQ4	1.67	1.41
NCU00316	peroxisomal adenine nucleotide transporter 1	1.66	1.41
NCU16657	tryptophanyl-tRNA synthetase	1.65	1.40
NCU03929	acyl-CoA synthetase	1.65	1.40
NCU03749	hydroxyacylglutathione hydrolase	1.64	1.39
NCU07298	CAIB/BAIF family enzyme	1.61	1.36

NCU04098	monothiol glutaredoxin-5	1.54	1.30
NCU03823	ABC1 protein	1.54	1.30
NCU04334	chaperonin	1.52	1.29
NCU06958	mito ribosomal protein S21	1.52	1.29
NCU00137	ssDNA binding protein	1.52	1.29
NCU02630	heat shock protein 78	1.50	1.27
NCU05558	3-ketoacyl-CoA thiolase	1.46	1.24
NCU05248	hypothetical protein	1.44	1.22
NCU07295	mitochondrial import inner membrane translocas	1.44	1.22
NCU06246	ATP-dependent RNA helicase mrh-4	1.42	1.20
NCU08138	cytochrome C1 heme lyase	1.41	1.19
NCU03338	hypothetical protein	1.40	1.19
NCU05828	hypothetical protein	1.40	1.19
NCU02273	vacuolar protease A	1.39	1.18
NCU09862	ubiquinone biosynthesis methyltransferase coq5	1.37	1.16
NCU00466	glutamyl-tRNA synthetase	1.36	1.15
NCU06403	hypothetical protein	1.30	1.10
NCU10732	mitochondrial dicarboxylate transporter	1.27	1.08
NCU03796	pyruvate dehydrogenase kinase	1.24	1.05
NCU00183	DUF185 domain-containing protein	1.21	1.02
NCU03893	short-chain dehydrogenase/reductase SDR	1.20	1.02
NCU00737	presequence translocated-associated moto	1.20	1.02
NCU05196	mitochondrial DnaJ chaperone	1.20	1.02
NCU07794	2Fe-2S iron-sulfur cluster bindin	1.19	1.01
NCU02701	dipeptidyl peptidase	1.19	1.01
NCU00905	N-acylethanolamine amidohydrolase	1.15	0.97
NCU05419	hydroxymethylglutaryl-CoA lyase	1.15	0.97
NCU03516	mitochondrial ribosomal protein subunit L32	1.14	0.97
NCU02705	F1F0 ATP synthase assembly protein Atp10	1.14	0.97
NCU05225	mitochondrial NADH dehydrogenase	1.13	0.96
NCU07871	hypothetical protein	1.13	0.96
NCU03217	MRS7 family protein	1.12	0.95
NCU12046	gamma-butyrobetaine dioxygenase	1.11	0.94
NCU04817	electron transfer protein 1	1.09	0.92
NCU02423	mitoferrin-1	1.09	0.92
NCU09517	hypothetical protein	1.08	0.91
NCU08998	4-aminobutyrate aminotransferase	1.07	0.91
NCU09266	methylmalonate-semialdehyde dehydrogenase	1.06	0.90
NCU09560	superoxide dismutase	1.05	0.89
NCU03229	mitochondrial inner membrane translocase subuni	1.05	0.89
NCU09602	heat shock protein 70	1.03	0.87

NCU05778	iron sulfur cluster assembly protein 1	1.01	0.86
NCU02639	argininosuccinate synthase, variant	1.01	0.86
NCU02887	voltage-gated potassium channel beta-2 subunit	1.01	0.86
NCU03155	hypothetical protein	1.00	0.85
NCU06307	multisynthetase complex auxiliary component p43	0.99	0.84
NCU05302	GTP-binding protein Obg	0.98	0.83
NCU04013	aldehyde dehydrogenase	0.96	0.81
NCU08909	beta-1,3-glucanosyltransferase	0.95	0.80
NCU03199	ATP synthase subunit H	0.94	0.80
NCU04837	mitochondrial 2-oxodicarboxylate carrier 1	0.93	0.79
NCU00599	mito ribosomal protein S22	0.92	0.78
NCU08005	NADPH-adrenodoxin reductase Arh1	0.91	0.77
NCU16742	hypothetical protein	0.91	0.77
NCU05772	TOM6	0.91	0.77
NCU07670	CYT-19 DEAD-box protein	0.91	0.77
NCU01473	mitochondrial large ribosomal subunit YmL35	0.91	0.77
NCU02545	hypothetical protein	0.91	0.77
NCU00378	aldehyde dehydrogenase	0.89	0.75
NCU05008	acp-1	0.88	0.75
NCU06017	thiosulfate sulfurtransferase	0.88	0.75
NCU01272	mitochondrial presequence protease	0.87	0.74
NCU02162	SURF-family protein	0.87	0.74
NCU09327	protein phosphatase	0.86	0.73
NCU04336	60S ribosomal protein L19	0.86	0.73
NCU05287	50S ribosomal protein L4	0.86	0.73
NCU02943	mitochondrial import inner membrane translocas	0.85	0.72
NCU09553	3-hydroxybutyryl CoA dehydrogenase	0.85	0.72
NCU09255	acetate non-utilizing protein 9	0.84	0.71
NCU08048	NAD dehydrogenase	0.83	0.70
NCU00673	serine protease p2	0.83	0.70
NCU02267	mitochondrial protein Fmp25	0.82	0.69
NCU02136	transaldolase	0.82	0.69
NCU03814	leucyl-tRNA synthetase	0.81	0.69
NCU03339	glutathione reductase	0.80	0.68
NCU06643	oleate-induced peroxisomal protein	0.80	0.68
NCU03231	mitochondrial chaperone BCS1	0.79	0.67
NCU01479	matrix AAA protease MAP-1	0.77	0.65
NCU08946	hypothetical protein	0.76	0.64
NCU08004	electron transfer flavoprotein alpha-subunit	0.75	0.63
NCU03031	succinate dehydrogenase cytochrome b smal	0.75	0.63
NCU02287	acyl-CoA dehydrogenase	0.71	0.60

NCU01512	phenylalanyl-tRNA synthetase	0.70	0.59
NCU05261	ATP-dependent protease La	0.69	0.58
NCU06536	hypothetical protein	0.69	0.58
NCU03637	CaaX prenyl protease Ste24	0.69	0.58
NCU00904	D-lactate dehydrogenase	0.69	0.58
NCU09403	NmrA family protein	0.68	0.58
NCU03310	prohibitin-2	0.68	0.58
NCU06086	regulatory protein suaprgal	0.65	0.55
NCU00477	carboxypeptidase Y	0.65	0.55
NCU02580	fumarate reductase Osm1	0.64	0.54
NCU05288	rab GDP-dissociation inhibitor	0.64	0.54
NCU03008	hypothetical protein	0.64	0.54
NCU04202	nucleoside diphosphate kinase	0.62	0.52
NCU11311	small zinc finger protein Tim8	0.61	0.52
NCU03177	sco1	0.60	0.51
NCU09058	enoyl-CoA hydratase	0.59	0.50
NCU01218	hypothetical protein	0.59	0.50
NCU02366	aconitase	0.58	0.49
NCU00405	glycyl-tRNA synthetase 1	0.58	0.49
NCU02291	glutaryl-CoA dehydrogenase	0.57	0.48
NCU03777	mitochondrial 3-hydroxyisobutyryl-CoA hydrolase	0.57	0.48
NCU06103	Mito Translation initiation factor	0.57	0.48
NCU06881	succinyl-CoA:3-ketoacid-coenzyme A transferas	0.57	0.48
NCU07682	acetylglutamate synthase	0.56	0.47
NCU00360	NAD dependent epimerase/dehydratase	0.56	0.47
NCU03094	hypothetical protein	0.55	0.47
NCU02451	mitochondrial hypoxia responsiv	0.54	0.46
NCU02807	hypothetical protein	0.54	0.46
NCU08877	glycine cleavage system H protein	0.53	0.45
NCU08861	hypothetical protein	0.52	0.44
NCU01528	glyceraldehyde 3-phosphate-dehydrogenase	0.52	0.44
NCU05515	mitochondrial import inner membrane translocas	0.52	0.44
NCU09732	acetyl-CoA acetyltransferase	0.49	0.41
NCU01546	coproporphyrinogen III oxidase	0.49	0.41
NCU05717	mito ribosomal protein S6	0.49	0.41
NCU01304	mitochondrial mRNA processing protein PET127	0.49	0.41
NCU07552	hypothetical protein	0.49	0.41
NCU07904	short chain dehydrogenase/reductase	0.49	0.41
NCU03759	methionine-tRNA synthetase	0.49	0.41
NCU05220	ATP synthase subunit F	0.48	0.41
NCU02481	mitochondrial 2-methylisocitrate lyase	0.48	0.41

NCU03020	IdgA domain-containing protein	0.47	0.40
NCU01564	calcium dependent mitochondrial carrier protein	0.47	0.40
NCU01328	transketolase	0.47	0.40
NCU02959	hypothetical protein	0.47	0.40
NCU06371	mitochondrial ATP-dependent RNA helicase Suv3	0.46	0.39
NCU03296	F1 ATPase assembly protein 11	0.46	0.39
NCU00775	isocitrate dehydrogenase subunit 1	0.46	0.39
NCU08291	ferrochelatase	0.45	0.38
NCU01006	complex I intermediate-associated protein CIA84	0.45	0.38
NCU03525	3-oxoacyl-[acyl-carrier-protein]-reductase	0.44	0.37
NCU07852	ribosomal protein L13	0.43	0.36
NCU01808	cytochrome c	0.43	0.36
NCU05279	hypothetical protein	0.43	0.36
NCU06469	54S ribosomal protein L12	0.43	0.36
NCU09539	40S ribosomal protein S13	0.43	0.36
NCU07550	triosephosphate isomerase	0.42	0.36
NCU00726	peptidyl-prolyl cis-trans isomerase	0.41	0.35
NCU05982	hexaprenyldihydroxybenzoate methyltransferase	0.41	0.35
NCU01657	cytochrome-c oxidase assembly protein	0.41	0.35
NCU03925	toxin biosynthesis protein	0.40	0.34
NCU03957	COQ7	0.39	0.33
NCU02064	hypothetical protein	0.38	0.32
NCU08329	mitochondrial ribosomal protein subunit L23	0.38	0.32
NCU04945	mitochondrial intermembrane space protein Mia40	0.37	0.31
NCU09025	glutamyl-tRNA	0.36	0.30
NCU04412	hypothetical protein	0.36	0.30
NCU02305	decaprenyl-diphosphate synthase subunit 1	0.35	0.30
NCU06270	mitochondrial-processing peptidase subuni	0.35	0.30
NCU06761	sphingosine-1-phosphate lyase	0.35	0.30
NCU00655	mitochondrial enoyl reductase	0.35	0.30
NCU04803	2-nitropropane dioxygenase famil	0.35	0.30
NCU01589	heat shock protein 60	0.34	0.29
NCU03173	HAD superfamily hydrolase	0.34	0.29
NCU06448	enoyl-CoA hydratase	0.33	0.28
NCU03158	alpha/beta hydrolase	0.33	0.28
NCU06749	60S ribosomal protein L3	0.32	0.27
NCU09594	seryl-tRNA synthetase	0.32	0.27
NCU06556	thioredoxin II	0.32	0.27
NCU08410	50S ribosomal protein L24	0.32	0.27
NCU07386	Fe superoxide dismutase	0.32	0.27
NCU02802	mitochondrial ornithine carrier protein	0.32	0.27

NCU04068	60S ribosomal protein L6	0.31	0.26
NCU02549	ubiquinol-cytochrome-c reductase subunit beta	0.31	0.26
NCU00103	hypothetical protein	0.31	0.26
NCU08693	hsp70-like protein	0.30	0.25
NCU08893	60S ribosomal protein L1	0.28	0.24
NCU00395	mRNA processing protein	0.28	0.24
NCU04212	hypothetical protein	0.26	0.22
NCU02955	elongation factor G 1	0.25	0.21
NCU09598	mitochondrial escape protein 2	0.24	0.20
NCU07560	50S ribosomal subunit L30	0.24	0.20
NCU02727	glycine cleavage system T protein	0.24	0.20
NCU00958	5-azacytidine resistance protein azr1	0.24	0.20
NCU08936	clock-controlled gene-15, variant	0.23	0.19
NCU02954	homoisocitrate dehydrogenase	0.22	0.19
NCU07756	succinate dehydrogenase cytochrome b560 subunit	0.22	0.19
NCU01023	50S ribosomal protein L17	0.22	0.19
NCU08471	succinyl-CoA ligase beta-chain	0.21	0.18
NCU02193	pyruvate decarboxylase	0.21	0.18
NCU07608	ribose 5-phosphate isomerase A, variant	0.21	0.18
NCU09826	RNase III domain-containing protein	0.20	0.17
NCU02566	alanyl-tRNA synthetase	0.19	0.16
NCU06244	mitochondrial import inner membrane translocas	0.18	0.15
NCU06211	malate dehydrogenase, variant	0.17	0.14
NCU03359	intermembrane space AAA protease IAP-1	0.17	0.14
NCU03908	fmp-52	0.16	0.13
NCU07465	mitochondrial phosphate carrier protein 2	0.16	0.13
NCU08120	mitochondrial ribosomal protein DAP3	0.16	0.13
NCU07697	isocitrate dehydrogenase subunit 2	0.15	0.13
NCU05633	stomatin family protein	0.15	0.13
NCU01255	mitochondrial dynamin GTPase	0.14	0.12
NCU05517	mitochondrial genome maintenance protein MGM101	0.14	0.12
NCU03347	kynurenine-oxoglutarate transaminase 1	0.14	0.12
NCU00952	mitochondrial ribosomal protein L44	0.14	0.12
NCU08002	carnitine acetyl transferase	0.13	0.11
NCU04171	50S ribosomal protein L5	0.13	0.11
NCU06309	hypothetical protein	0.13	0.11
NCU03979	biotin synthase	0.12	0.10
NCU01965	valyl-tRNA synthetase	0.12	0.10
NCU01306	hypothetical protein	0.12	0.10
NCU02514	mitochondrial ATP synthase alpha subunit	0.11	0.09
NCU04636	cysteine desulfurase	0.10	0.08

NCU06543	acyl-CoA dehydrogenase	0.10	0.08
NCU00484	NADH:ubiquinone oxidoreductase 18.4kD subunit	0.10	0.08
NCU06587	hypothetical protein	0.10	0.08
NCU03030	tyrosyl-tRNA synthetase	0.10	0.08
NCU01975	complex I intermediate-associated protein CIA30	0.09	0.08
NCU02063	mitochondrial intermediate peptidase	0.09	0.08
NCU06247	hypothetical protein	0.09	0.08
NCU06424	aminomethyl transferase	0.08	0.07
NCU02438	dihydrolipoamide succinyltransferase	0.08	0.07
NCU02804	mitochondrial 60S ribosomal protein L25	0.08	0.07
NCU01962	encodes anonymous transcript-5 protein, variant	0.08	0.07
NCU00951	inorganic pyrophosphatase	0.07	0.06
NCU00660	glutamyl-tRNA amidotransferase	0.06	0.05
NCU08707	iron sulfur assembly protein	0.06	0.05
NCU00680	2-methylcitrate dehydratase	0.06	0.05
NCU01606	ATP synthase subunit 5	0.06	0.05
NCU01485	hypothetical protein	0.04	0.03
NCU03297	cytochrome c peroxidase	0.03	0.02
NCU00030	mitochondrial nuclease	0.03	0.02
NCU00371	mitochondrial import inner membrane translocas	0.03	0.02
NCU04380	acyl-CoA synthetase	0.02	0.02
NCU04429	mitochondrial import protein mmp37	0.02	0.02
NCU06760	pyruvate dehydrogenase kinase	0.02	0.02
NCU00278	hypothetical protein	0.02	0.02
NCU00676	F1-ATP synthase assembly protein	0.01	0.01
NCU03737	elongation factor Tu	0.00	0.00
NCU01169	NADH:ubiquinone oxidoreductase 24	0.00	0.00
NCU00977	aconitate hydratase	-0.01	-0.01
NCU07263	carnitine/acyl carnitine carrier	-0.01	-0.01
NCU05425	2-oxoglutarate dehydrogenase E1 component	-0.02	-0.02
NCU03004	pyruvate dehydrogenase E1 component	-0.02	-0.02
NCU02407	dihydrolipoyl dehydrogenase	-0.03	-0.03
NCU05623	mitochondrial inner membrane translocase subuni	-0.03	-0.03
NCU08336	succinate dehydrogenase flavoprotein subunit	-0.04	-0.03
NCU06495	mitochondrial inner membrane organizatio	-0.04	-0.03
NCU02585	aspartyl-tRNA synthetase	-0.04	-0.03
NCU06647	enoyl-CoA hydratase/isomerase	-0.05	-0.04
NCU02734	citrate lyase beta subunit	-0.06	-0.05
NCU05430	ATP synthase beta subunit	-0.06	-0.05
NCU08477	small GTP-binding protein	-0.08	-0.07
NCU05805	serine hydroxymethyltransferase	-0.08	-0.07

NCU08980	alternative NADH-dehydrogenase	-0.08	-0.07
NCU01894	hypothetical protein	-0.09	-0.08
NCU01692	mitochondrial citrate synthase	-0.09	-0.08
NCU00959	succinate dehydrogenase iron-sulfur protein	-0.09	-0.08
NCU06695	cytochrome c oxidase polypeptide VI, variant	-0.09	-0.08
NCU05454	glycerol-3-phosphate dehydrogenase	-0.10	-0.09
NCU05971	xaa-Pro dipeptidase	-0.11	-0.09
NCU08541	hypothetical protein	-0.11	-0.09
NCU06441	D-lactate dehydrogenase 2	-0.12	-0.10
NCU04138	hypothetical protein	-0.13	-0.11
NCU03877	C-1-tetrahydrofolate synthase	-0.13	-0.11
NCU05890	hypothetical protein	-0.14	-0.12
NCU09770	acetyl-coa hydrolase	-0.15	-0.13
NCU00075	mitochondrial import inner membrane translocas	-0.15	-0.13
NCU01667	ornithine carbamoyltransferase	-0.15	-0.13
NCU10021	MFS monosaccharide transporter	-0.18	-0.15
NCU02044	GTP-binding protein	-0.19	-0.16
NCU08924	acyl-CoA dehydrogenase	-0.19	-0.16
NCU00431	mitochondrial import receptor subunit Tom22	-0.20	-0.17
NCU03112	NADH-cytochrome b5 reductase 2	-0.20	-0.17
NCU03857	tricarboxylic acid-5 protein, variant 2	-0.20	-0.17
NCU03653	hypothetical protein	-0.22	-0.19
NCU09477	ADP/ATP carrier protein, variant	-0.22	-0.19
NCU00051	hypothetical protein	-0.23	-0.20
NCU05029	iron-sulfur clusters transporter atm-1	-0.23	-0.20
NCU04280	aconitate hydratase	-0.23	-0.20
NCU04502	hypothetical protein	-0.23	-0.20
NCU09057	hypothetical protein	-0.23	-0.20
NCU03559	ubiquinol-cytochrome c reductase complex cor	-0.24	-0.20
NCU01474	60S ribosomal protein L4, variant	-0.24	-0.20
NCU03556	peroxisomal membrane protein Pmp47	-0.24	-0.20
NCU08728	mitochondrial ribosomal protein S19	-0.25	-0.21
NCU00894	hypothetical protein	-0.25	-0.21
NCU04806	hypothetical protein	-0.25	-0.21
NCU06518	NADH-cytochrome b5 reductase 2	-0.25	-0.21
NCU06482	pyruvate dehydrogenase E1 component alph	-0.26	-0.22
NCU08898	homoaconitase	-0.26	-0.22
NCU16833	hypothetical protein	-0.27	-0.23
NCU04899	malate dehydrogenase	-0.28	-0.24
NCU03343	37S ribosomal protein S25	-0.28	-0.24
NCU00502	ATP synthase subunit 4	-0.28	-0.24

NCU01767	phosphatase 2C family protein	-0.29	-0.25
NCU00050	pyruvate dehydrogenase X component	-0.30	-0.25
NCU01484	rho-type GTPase	-0.30	-0.25
NCU05593	mitochondrial outer membrane beta-barrel protein	-0.31	-0.26
NCU06450	mitochondrial ribosomal protein	-0.31	-0.26
NCU09223	protein disulfide-isomerase	-0.31	-0.26
NCU08949	hypothetical protein	-0.31	-0.26
NCU02623	mitochondrial hypoxia responsive	-0.32	-0.27
NCU06786	50S ribosomal protein L30	-0.32	-0.27
NCU08941	calcium-binding mitochondrial carrier protein	-0.32	-0.27
NCU05526	homocitrate synthase, variant 2	-0.33	-0.28
NCU05601	cytochrome c heme lyase	-0.33	-0.28
NCU01343	TPR repeat protein	-0.33	-0.28
NCU00565	lipoic acid synthetase	-0.34	-0.29
NCU03926	37S ribosomal protein Rsm24	-0.35	-0.30
NCU00114	30S ribosomal protein S10	-0.35	-0.30
NCU08299	60S ribosomal protein L3	-0.36	-0.31
NCU02482	2-methylcitrate synthase, variant 2	-0.37	-0.31
NCU07733	electron transfer flavoprotein beta-subunit	-0.37	-0.31
NCU07793	hypothetical protein	-0.38	-0.32
NCU01179	outer membrane translocase 40 kDa subunit	-0.38	-0.32
NCU08552	50S ribosomal protein L14	-0.38	-0.32
NCU01007	mitochondrial ribosomal protein S18	-0.38	-0.32
NCU00936	succinate semialdehyde dehydrogenase	-0.38	-0.32
NCU01550	adenylate kinase cytosolic	-0.39	-0.33
NCU04074	NADH:ubiquinone oxidoreductase 30.4 kDa subunit	-0.39	-0.33
NCU01227	succinyl-CoA ligase alpha-chain	-0.40	-0.34
NCU02403	ubiquinone biosynthesis protein COQ9	-0.41	-0.35
NCU05714	50S ribosomal subunit protein L15	-0.42	-0.36
NCU09119	ATP synthase subunit gamma	-0.43	-0.37
NCU03211	hypothetical protein	-0.43	-0.37
NCU07659	pyruvate dehydrogenase complex	-0.44	-0.37
NCU09886	hypothetical protein	-0.44	-0.37
NCU09228	aminopeptidase 2	-0.45	-0.38
NCU00562	hypothetical protein	-0.45	-0.38
NCU00895	RAB GTPase Ypt5	-0.46	-0.39
NCU01689	mitochondrial DNA replication protein YHM2	-0.46	-0.39
NCU01765	NADH:ubiquinone oxidoreductase 78	-0.47	-0.40
NCU06452	cysteine synthase	-0.47	-0.40
NCU02419	mitochondrial 37S ribosomal protein S17	-0.48	-0.41
NCU03230	mitochondrial ribosomal protein subunit S18	-0.49	-0.42

NCU08146	hypothetical protein	-0.49	-0.42
NCU03394	ribosomal protein S15	-0.53	-0.45
NCU07493	hypothetical protein	-0.54	-0.46
NCU07724	mitochondrial division protein 1	-0.55	-0.47
NCU09222	hypothetical protein	-0.56	-0.48
NCU05313	mitochondria fission 1 protein	-0.57	-0.48
NCU09810	succinyl-CoA synthetase subunit alpha	-0.58	-0.49
NCU00789	DUF221 domain-containing protein	-0.59	-0.50
NCU02534	NADH:ubiquinone oxidoreductase 49kD subunit	-0.62	-0.53
NCU00644	ATP synthase subunit G	-0.62	-0.53
NCU01241	mitochondrial carrier protein	-0.62	-0.53
NCU03156	NUO	-0.62	-0.53
NCU01454	mitochondrial hydrolase	-0.64	-0.54
NCU04588	hypothetical protein	-0.64	-0.54
NCU03739	protein disulfide-isomerase tigA	-0.65	-0.55
NCU08411	aspartate aminotransferase	-0.66	-0.56
NCU10468	arginine biosynthesis argJ	-0.67	-0.57
NCU07286	membrane-associated progesterone recepto	-0.67	-0.57
NCU03188	sugar 1,4-lactone oxidase	-0.68	-0.58
NCU08296	mito ribosomal protein S4	-0.69	-0.59
NCU08071	ribosomal protein S16	-0.70	-0.59
NCU04579	dihydroxy-acid dehydratase	-0.71	-0.60
NCU01666	acetolactate synthase small subunit	-0.72	-0.61
NCU02544	ABC transporter	-0.72	-0.61
NCU10042	enolase, variant	-0.72	-0.61
NCU04481	mitochondrial ATPase	-0.72	-0.61
NCU12023	mito ribosomal protein S2	-0.73	-0.62
NCU05552	hypothetical protein	-0.74	-0.63
NCU04100	vacuolar sorting protein 1	-0.74	-0.63
NCU01680	plasma membrane ATPase	-0.75	-0.64
NCU00567	Arg-6 protein, variant	-0.76	-0.64
NCU02269	mitochondrial carnitine/acylcarnitine carrie	-0.76	-0.64
NCU07112	hypothetical protein	-0.76	-0.64
NCU00584	hypothetical protein	-0.76	-0.64
NCU04768	electron transfer flavoprotein-ubiquinon	-0.77	-0.65
NCU08195	arginyl-tRNA synthetase	-0.77	-0.65
NCU06451	hypothetical protein	-0.80	-0.68
NCU01469	hypothetical protein	-0.81	-0.69
NCU00211	mitochondrial ribosomal protein subunit L31	-0.82	-0.70
NCU04287	hypothetical protein	-0.84	-0.71
NCU05457	cytochrome c oxidase subunit IV	-0.85	-0.72

NCU05027	hypothetical protein	-0.87	-0.74
NCU05813	mitochondrial large ribosomal subunit	-0.88	-0.75
NCU06632	outer mitochondrial membrane translocase 20	-0.89	-0.75
NCU00153	pyridine nucleotide-disulfide oxidoreductase	-0.89	-0.75
NCU01800	37S ribosomal protein S5	-0.89	-0.75
NCU04044	NADH2 dehydrogenase flavoprotein 1	-0.89	-0.75
NCU04245	outer mitochondrial membrane translocase	-0.90	-0.76
NCU05390	mitochondrial phosphate carrier protein	-0.90	-0.76
NCU04605	hypothetical protein	-0.90	-0.76
NCU07982	acetolactate synthase	-0.90	-0.76
NCU01467	NADH:ubiquinone oxidoreductase 10.4kD subunit	-0.91	-0.77
NCU06768	60S ribosomal protein L16	-0.92	-0.78
NCU09002	NADH:ubiquinone oxidoreductase 10.6kD subunit	-0.92	-0.78
NCU01360	NADH:ubiquinone oxidoreductase 11.5kD subunit	-0.92	-0.78
NCU04754	branched-chain-amino-acid aminotransferase	-0.94	-0.80
NCU09999	hypothetical protein	-0.94	-0.80
NCU05299	NADH:ubiquinone oxidoreductase	-0.95	-0.81
NCU02690	mitochondrial integral membrane protein	-0.96	-0.81
NCU04225	60S ribosomal protein L20	-0.96	-0.81
NCU08272	cytochrome b2	-1.01	-0.86
NCU03982	glucose-regulated protein	-1.01	-0.86
NCU10008	fumarate hydratase	-1.07	-0.91
NCU03076	delta-1-pyrroline-5-carboxylate dehydrogenase	-1.07	-0.91
NCU11345	hypothetical protein	-1.08	-0.92
NCU02013	hypothetical protein	-1.09	-0.92
NCU00605	ThiF domain-containing protein	-1.10	-0.93
NCU00536	homoserine O-acetyltransferase	-1.10	-0.93
NCU06924	kynurenine 3-monooxygenase	-1.11	-0.94
NCU03827	40S ribosomal protein S9	-1.12	-0.95
NCU01916	mitochondrial carrier protein RIM2	-1.13	-0.96
NCU03608	ketol-acid reductoisomerase	-1.16	-0.98
NCU05075	mitochondrial tricarboxylate transporter	-1.17	-0.99
NCU06550	pyridoxine 1	-1.17	-0.99
NCU01859	NADH:ubiquinone oxidoreductase 20.9kD subunit	-1.17	-0.99
NCU07057	hypothetical protein	-1.19	-1.01
NCU01821	alanine-glyoxylate aminotransferase	-1.20	-1.02
NCU02504	DUF1640 domain-containing protein	-1.21	-1.03
NCU03711	GTP-binding protein ypt7	-1.24	-1.05
NCU03695	phosphatidylserine decarboxylase proenzyme 1	-1.25	-1.06
NCU11258	LYR family protein	-1.25	-1.06
NCU05689	cytochrome c oxidase polypeptide IV	-1.28	-1.09

NCU02677	carbamoyl-phosphate synthase large subunit	-1.29	-1.09
NCU05221	NADH:ubiquinone oxidoreductase 21kD subunit	-1.29	-1.09
NCU02757	60S ribosomal protein L2	-1.30	-1.10
NCU08356	acetamidase	-1.31	-1.11
NCU03129	threonyl-tRNA synthetase	-1.33	-1.13
NCU00160	NADH:ubiquinone oxidoreductase 6.6kD subunit	-1.37	-1.16
NCU00564	mitochondrial 40S ribosomal protein MRP2	-1.38	-1.17
NCU05410	acetylornithine aminotransferase	-1.42	-1.20
NCU02812	uridylate kinase	-1.47	-1.25
NCU06606	ubiquinol-cytochrome c reductase iron-sulfu	-1.48	-1.25
NCU00385	ATP synthase subunit delta	-1.55	-1.31
NCU03561	mitochondrial carrier protein	-1.56	-1.32
NCU05009	NADH-quinone oxidoreductase chain I, variant	-1.57	-1.33
NCU09816	cytochrome-26	-1.58	-1.34
NCU11348	NADH-ubiquinone oxidoreductase B18 subunit	-1.58	-1.34
NCU03093	NADH:ubiquinone oxidoreductase 12.3kD subunit	-1.65	-1.40
NCU02070	peroxisomal biogenesis factor 2	-1.66	-1.41
NCU08940	ubiquinol-cytochrome c reductase comple	-1.66	-1.41
NCU07732	carbamoyl-phosphate synthase small subunit	-1.69	-1.43
NCU02472	NADH:ubiquinone oxidoreductase 20.8kD subunit	-1.71	-1.45
NCU02951	40S ribosomal protein S8	-1.72	-1.46
NCU02475	glycine dehydrogenase	-1.77	-1.50
NCU00418	NADH:ubiquinone oxidoreductase 14.8kD subunit	-1.78	-1.51
NCU01142	NADH:ubiquinone oxidoreductase 13.4kD subunit	-1.80	-1.53
NCU06189	5-aminolevulinate synthase	-1.81	-1.53
NCU00227	mitochondrial cation transporter	-1.81	-1.53
NCU04230	isocitrate lyase	-1.82	-1.54
NCU05226	ABC transporter	-1.84	-1.56
NCU00969	NADH:ubiquinone oxidoreductase 17.8kD subunit	-1.91	-1.62
NCU03340	cytochrome-c oxidase chain VIIC	-1.96	-1.66
NCU08947	ubiquinol-cytochrome-c reductase chain VIII	-1.97	-1.67
NCU04276	hypothetical protein	-2.06	-1.75
NCU00670	NADH:ubiquinone oxidoreductase 9.5kD subunit	-2.08	-1.76
NCU08930	NADH:ubiquinone oxidoreductase 21.3kD subunit A	-2.11	-1.79
NCU06741	cytochrome c oxidase subunit VIb	-2.14	-1.81
NCU03953	mitochondrial NADH-ubiquinone oxidoreductase 2	-2.25	-1.91
NCU09299	NADH:ubiquinone oxidoreductase 14kD subunit	-2.25	-1.91
NCU02373	NADH-ubiquinone oxidoreductase 40 kDa subunit	-2.26	-1.92
NCU02280	NADH:ubiquinone oxidoreductase 21.3kD subunit B	-2.26	-1.92
NCU01401	mitochondrial outer membrane protein, variant	-2.27	-1.92
NCU08661	pantoate-beta-alanine ligase	-2.30	-1.95

NCU03802	trimethyllysine dioxygenase	-2.32	-1.97
NCU05338	hypothetical protein	-2.49	-2.11
NCU08561	succinate/fumarate mitochondrial transporter	-2.63	-2.23
NCU01633	hexose transporter HXT13	-2.67	-2.26
NCU02564	cysteine synthase 2	-2.83	-2.40
NCU04946	hypothetical protein	-3.00	-2.54
NCU00436	GTPase FZO1	-3.38	-2.86
NCU04781	NADH:ubiquinone oxidoreductase 9.8 kDa subunit	-3.50	-2.97
NCU09345	thiamine biosynthesis protein NMT-1, variant 2	-4.34	-3.68
NCU06110	thiazole biosynthetic enzyme	-4.66	-3.95
NCU09143	hypothetical protein	-4.99	-4.23
NCU09460	NADH:ubiquinone oxidoreductase 20.1kD subunit	-5.13	-4.35
NCU01024	hypothetical protein	-5.72	-4.85

Table 6.3 Levels of predicted mitochondrial proteins in 238Por relative to wild-type

Log2 differences that are statistically different are highlighted in blue.			
Locus	Description	log2 Difference	Z-Score
NCU01140	NAD Trans hydrogenase	3.91	4.16
NCU05495	CVNH domain-containing protein	3.47	3.68
NCU06546	hypothetical protein	2.84	3.00
NCU05850	rubredoxin-NAD	2.79	2.95
NCU00122	aspartyl aminopeptidase	2.52	2.66
NCU09263	anchored cell wall protein 4	2.51	2.65
NCU07021	peptide chain release factor 3	2.36	2.48
NCU06880	AhpC/TSA family protein	2.23	2.34
NCU03929	acyl-CoA synthetase	2.18	2.29
NCU03796	pyruvate dehydrogenase kinase	2.17	2.28
NCU04578	ATP-dependent Clp protease proteolytic subunit	2.16	2.27
NCU09285	zinc-containing alcohol dehydrogenase	2.12	2.22
NCU03006	sterol 24-C-methyltransferase	2.12	2.22
NCU16657	tryptophanyl-tRNA synthetase	2.11	2.21
NCU10021	MFS monosaccharide transporter	2.11	2.21
NCU05558	3-ketoacyl-CoA thiolase	2.1	2.20
NCU06958	mito ribosomal protein S21	2.03	2.13
NCU02802	mitochondrial ornithine carrier protein	1.98	2.07
NCU07858	DUF498 domain-containing protein	1.94	2.03
NCU00264	hypothetical protein	1.91	2.00
NCU07295	mitochondrial import inner membrane translocas	1.79	1.87
NCU01516	mitochondrial co-chaperone GrpE	1.7	1.77
NCU10732	mitochondrial dicarboxylate transporter	1.66	1.73
NCU04098	monothiol glutaredoxin-5	1.64	1.71
NCU03516	mitochondrial ribosomal protein subunit L32	1.56	1.62
NCU02157	COQ4	1.53	1.59
NCU03893	short-chain dehydrogenase/reductase SDR	1.49	1.54
NCU02136	transaldolase	1.49	1.54
NCU04764	hypothetical protein	1.48	1.53
NCU01512	phenylalanyl-tRNA synthetase	1.4	1.45
NCU09754	mitochondrial chaperone Frataxin	1.36	1.40
NCU05288	rab GDP-dissociation inhibitor	1.36	1.40
NCU07871	hypothetical protein	1.35	1.39
NCU01328	transketolase	1.34	1.38
NCU02566	alanyl-tRNA synthetase	1.34	1.38
NCU01650	hypothetical protein	1.31	1.35
NCU10226	mmf1	1.29	1.33

NCU07550	triosephosphate isomerase	1.26	1.30
NCU06518	NADH-cytochrome b5 reductase 2	1.23	1.26
NCU00831	extracellular serine carboxypeptidase, variant	1.22	1.25
NCU07386	Fe superoxide dismutase	1.22	1.25
NCU05225	mitochondrial NADH dehydrogenase	1.19	1.22
NCU09602	heat shock protein 70	1.19	1.22
NCU07298	CAIB/BAIF family enzyme	1.14	1.17
NCU02193	pyruvate decarboxylase	1.1	1.12
NCU03338	hypothetical protein	1.08	1.10
NCU00137	ssDNA binding protein	1.08	1.10
NCU09255	acetate non-utilizing protein 9	1.08	1.10
NCU05279	hypothetical protein	1.07	1.09
NCU08877	glycine cleavage system H protein	1.04	1.06
NCU03759	methionine-tRNA synthetase	1.04	1.06
NCU00075	mitochondrial import inner membrane translocas	1.04	1.06
NCU00905	N-acylethanolamine amidohydrolase	1.01	1.03
NCU09266	methylmalonate-semialdehyde dehydrogenase	1	1.01
NCU00466	glutamyl-tRNA synthetase	0.99	1.00
NCU03823	ABC1 protein	0.99	1.00
NCU09553	3-hydroxybutyryl CoA dehydrogenase	0.98	0.99
NCU09810	succinyl-CoA synthetase subunit alpha	0.98	0.99
NCU05261	ATP-dependent protease La	0.97	0.98
NCU03347	kynurenine-oxoglutarate transaminase 1	0.97	0.98
NCU09594	seryl-tRNA synthetase	0.96	0.97
NCU06103	Mito Translation initiation factor	0.96	0.97
NCU02701	dipeptidyl peptidase	0.96	0.97
NCU01962	encodes anonymous transcript-5 protein, variant	0.95	0.96
NCU03094	hypothetical protein	0.94	0.95
NCU05196	mitochondrial DnaJ chaperone	0.94	0.95
NCU08998	4-aminobutyrate aminotransferase	0.93	0.94
NCU08004	electron transfer flavoprotein alpha-subunit	0.92	0.93
NCU02063	mitochondrial intermediate peptidase	0.92	0.93
NCU00153	pyridine nucleotide-disulfide oxidoreductase	0.92	0.93
NCU03031	succinate dehydrogenase cytochrome b smal	0.92	0.93
NCU07794	2Fe-2S iron-sulfur cluster bindin	0.91	0.92
NCU07362	L-lactate ferricytochrome c oxidoreductase	0.91	0.92
NCU01916	mitochondrial carrier protein RIM2	0.91	0.92
NCU02273	vacuolar protease A	0.91	0.92
NCU01528	glyceraldehyde 3-phosphate-dehydrogenase	0.9	0.91
NCU05419	hydroxymethylglutaryl-CoA lyase	0.88	0.88
NCU01564	calcium dependent mitochondrial carrier protein	0.86	0.86

NCU04287	hypothetical protein	0.86	0.86
NCU03749	hydroxyacylglutathione hydrolase	0.85	0.85
NCU02630	heat shock protein 78	0.85	0.85
NCU00378	aldehyde dehydrogenase	0.83	0.83
NCU05772	TOM6	0.81	0.81
NCU02128	D-arabinitol dehydrogenase	0.81	0.81
NCU05982	hexaprenyldihydroxybenzoate methyltransferase	0.8	0.80
NCU02545	hypothetical protein	0.8	0.80
NCU02267	mitochondrial protein Fmp25	0.8	0.80
NCU04202	nucleoside diphosphate kinase	0.79	0.79
NCU06247	hypothetical protein	0.79	0.79
NCU03155	hypothetical protein	0.79	0.79
NCU02943	mitochondrial import inner membrane translocas	0.78	0.78
NCU01102	mitochondrial export translocase Oxa1	0.78	0.78
NCU06469	54S ribosomal protein L12	0.78	0.78
NCU16742	hypothetical protein	0.77	0.77
NCU06086	regulatory protein suaprga1	0.77	0.77
NCU06246	ATP-dependent RNA helicase mrh-4	0.76	0.76
NCU04013	aldehyde dehydrogenase	0.76	0.76
NCU03814	leucyl-tRNA synthetase	0.75	0.74
NCU00951	inorganic pyrophosphatase	0.75	0.74
NCU08005	NADPH-adrenodoxin reductase Arh1	0.74	0.73
NCU06017	thiosulfate sulfurtransferase	0.74	0.73
NCU09057	hypothetical protein	0.74	0.73
NCU03525	3-oxoacyl-[acyl-carrier-protein]-reductase	0.73	0.72
NCU02366	aconitase	0.73	0.72
NCU12046	gamma-butyrobetaine dioxygenase	0.73	0.72
NCU08707	iron sulfur assembly protein	0.73	0.72
NCU02481	mitochondrial 2-methylisocitrate lyase	0.72	0.71
NCU06424	aminomethyl transferase	0.71	0.70
NCU00737	presequence translocated-associated moto	0.71	0.70
NCU09403	NmrA family protein	0.7	0.69
NCU02887	voltage-gated potassium channel beta-2 subunit	0.7	0.69
NCU05248	hypothetical protein	0.69	0.68
NCU05008	acp-1	0.69	0.68
NCU09732	acetyl-CoA acetyltransferase	0.69	0.68
NCU09560	superoxide dismutase	0.69	0.68
NCU03217	MRS7 family protein	0.69	0.68
NCU00599	mito ribosomal protein S22	0.68	0.67
NCU07608	ribose 5-phosphate isomerase A, variant	0.68	0.67
NCU03339	glutathione reductase	0.64	0.63

NCU01479	matrix AAA protease MAP-1	0.64	0.63
NCU08949	hypothetical protein	0.64	0.63
NCU03199	ATP synthase subunit H	0.64	0.63
NCU01218	hypothetical protein	0.64	0.63
NCU02948	non-anchored cell wall protein 4	0.63	0.61
NCU05526	homocitrate synthase, variant 2	0.63	0.61
NCU03177	sco1	0.63	0.61
NCU09327	protein phosphatase	0.62	0.60
NCU06550	pyridoxine 1	0.61	0.59
NCU01272	mitochondrial presequence protease	0.6	0.58
NCU09517	hypothetical protein	0.6	0.58
NCU04945	mitochondrial intermembrane space protein Mia40	0.59	0.57
NCU04336	60S ribosomal protein L19	0.59	0.57
NCU02287	acyl-CoA dehydrogenase	0.59	0.57
NCU08048	NAD dehydrogenase	0.58	0.56
NCU02549	ubiquinol-cytochrome-c reductase subunit beta	0.57	0.55
NCU09886	hypothetical protein	0.57	0.55
NCU08382	peroxisomal half ABC transporter	0.56	0.54
NCU03008	hypothetical protein	0.56	0.54
NCU04588	hypothetical protein	0.56	0.54
NCU06270	mitochondrial-processing peptidase subuni	0.55	0.53
NCU08471	succinyl-CoA ligase beta-chain	0.55	0.53
NCU05805	serine hydroxymethyltransferase	0.55	0.53
NCU08291	ferrochelatae	0.54	0.52
NCU04334	chaperonin	0.54	0.52
NCU06740	hypothetical protein	0.54	0.52
NCU02133	superoxide dismutase	0.53	0.51
NCU00405	glycyl-tRNA synthetase 1	0.52	0.50
NCU02580	fumarate reductase Osm1	0.52	0.50
NCU10311	mitochondrial ribosomal protein subunit S4	0.51	0.49
NCU05287	50S ribosomal protein L4	0.51	0.49
NCU02291	glutaryl-CoA dehydrogenase	0.49	0.46
NCU04817	electron transfer protein 1	0.49	0.46
NCU07904	short chain dehydrogenase/reductase	0.46	0.43
NCU07697	isocitrate dehydrogenase subunit 2	0.46	0.43
NCU05778	iron sulfur cluster assembly protein 1	0.46	0.43
NCU04415	hypothetical protein	0.46	0.43
NCU02951	40S ribosomal protein S8	0.46	0.43
NCU00775	isocitrate dehydrogenase subunit 1	0.45	0.42
NCU02423	mitoferrin-1	0.45	0.42
NCU03229	mitochondrial inner membrane translocase subuni	0.43	0.40

NCU06307	multisynthetase complex auxiliary component p43	0.43	0.40
NCU01304	mitochondrial mRNA processing protein PET127	0.42	0.39
NCU08936	clock-controlled gene-15, variant	0.42	0.39
NCU04636	cysteine desulfurase	0.42	0.39
NCU01473	mitochondrial large ribosomal subunit YmL35	0.41	0.38
NCU01808	cytochrome c	0.4	0.37
NCU06543	acyl-CoA dehydrogenase	0.4	0.37
NCU00904	D-lactate dehydrogenase	0.4	0.37
NCU08924	acyl-CoA dehydrogenase	0.4	0.37
NCU00726	peptidyl-prolyl cis-trans isomerase	0.39	0.36
NCU09770	acetyl-coa hydrolase	0.39	0.36
NCU06448	enoyl-CoA hydratase	0.38	0.34
NCU01546	coproporphyrinogen III oxidase	0.38	0.34
NCU07733	electron transfer flavoprotein beta-subunit	0.38	0.34
NCU03777	mitochondrial 3-hydroxyisobutyryl-CoA hydrolase	0.37	0.33
NCU00484	NADH:ubiquinone oxidoreductase 18.4kD subunit	0.36	0.32
NCU05971	xaa-Pro dipeptidase	0.36	0.32
NCU01006	complex I intermediate-associated protein CIA84	0.36	0.32
NCU06556	thioredoxin II	0.35	0.31
NCU03877	C-1-tetrahydrofolate synthase	0.34	0.30
NCU00183	DUF185 domain-containing protein	0.33	0.29
NCU02585	aspartyl-tRNA synthetase	0.33	0.29
NCU03020	IdgA domain-containing protein	0.33	0.29
NCU08693	hsp70-like protein	0.32	0.28
NCU06881	succinyl-CoA:3-ketoacid-coenzyme A transferase	0.32	0.28
NCU06403	hypothetical protein	0.31	0.27
NCU08946	hypothetical protein	0.31	0.27
NCU09058	enoyl-CoA hydratase	0.3	0.26
NCU08195	arginyl-tRNA synthetase	0.3	0.26
NCU01767	phosphatase 2C family protein	0.3	0.26
NCU08002	carnitine acetyl transferase	0.29	0.25
NCU03737	elongation factor Tu	0.29	0.25
NCU00959	succinate dehydrogenase iron-sulfur protein	0.29	0.25
NCU00360	NAD dependent epimerase/dehydratase	0.29	0.25
NCU03925	toxin biosynthesis protein	0.29	0.25
NCU05430	ATP synthase beta subunit	0.28	0.24
NCU02305	decaprenyl-diphosphate synthase subunit 1	0.27	0.23
NCU03211	hypothetical protein	0.27	0.23
NCU08541	hypothetical protein	0.27	0.23
NCU02807	hypothetical protein	0.27	0.23
NCU01606	ATP synthase subunit 5	0.27	0.23

NCU06643	oleate-induced peroxisomal protein	0.27	0.23
NCU06309	hypothetical protein	0.27	0.23
NCU02403	ubiquinone biosynthesis protein COQ9	0.26	0.22
NCU04380	acyl-CoA synthetase	0.25	0.20
NCU06211	malate dehydrogenase, variant	0.25	0.20
NCU06760	pyruvate dehydrogenase kinase	0.24	0.19
NCU08336	succinate dehydrogenase flavoprotein subunit	0.22	0.17
NCU09862	ubiquinone biosynthesis methyltransferase coq5	0.22	0.17
NCU02013	hypothetical protein	0.22	0.17
NCU04212	hypothetical protein	0.22	0.17
NCU00680	2-methylcitrate dehydratase	0.21	0.16
NCU01692	mitochondrial citrate synthase	0.21	0.16
NCU02482	2-methylcitrate synthase, variant 2	0.21	0.16
NCU00673	serine protease p2	0.21	0.16
NCU07852	ribosomal protein L13	0.2	0.15
NCU02064	hypothetical protein	0.19	0.14
NCU01965	valyl-tRNA synthetase	0.19	0.14
NCU03857	tricarboxylic acid-5 protein, variant 2	0.19	0.14
NCU01169	NADH:ubiquinone oxidoreductase 24	0.17	0.12
NCU03957	COQ7	0.17	0.12
NCU01255	mitochondrial dynamin GTPase	0.17	0.12
NCU07286	membrane-associated progesterone recepto	0.17	0.12
NCU01023	50S ribosomal protein L17	0.16	0.11
NCU03310	prohibitin-2	0.16	0.11
NCU01007	mito ribosomal protein S18	0.15	0.10
NCU03559	ubiquinol-cytochrome c reductase complex cor	0.15	0.10
NCU02954	homocitrate dehydrogenase	0.15	0.10
NCU07670	CYT-19 DEAD-box protein	0.15	0.10
NCU06587	hypothetical protein	0.14	0.09
NCU00584	hypothetical protein	0.14	0.09
NCU06786	50S ribosomal protein L30	0.13	0.07
NCU04429	mitochondrial import protein mmp37	0.13	0.07
NCU05425	2-oxoglutarate dehydrogenase E1 component	0.12	0.06
NCU09598	mitochondrial escape protein 2	0.12	0.06
NCU02734	citrate lyase beta subunit	0.12	0.06
NCU00395	mRNA processing protein	0.12	0.06
NCU05302	GTP-binding protein Obg	0.12	0.06
NCU02438	dihydrolipoamide succinyltransferase	0.11	0.05
NCU01360	NADH:ubiquinone oxidoreductase 11.5kD subunit	0.11	0.05
NCU02044	GTP-binding protein	0.11	0.05
NCU10042	enolase, variant	0.11	0.05

NCU03556	peroxisomal membrane protein Pmp47	0.1	0.04
NCU03231	mitochondrial chaperone BCS1	0.1	0.04
NCU02514	mitochondrial ATP synthase alpha subunit	0.09	0.03
NCU00936	succinate semialdehyde dehydrogenase	0.09	0.03
NCU00278	hypothetical protein	0.09	0.03
NCU08861	hypothetical protein	0.08	0.02
NCU03173	HAD superfamily hydrolase	0.08	0.02
NCU04605	hypothetical protein	0.08	0.02
NCU00655	mitochondrial enoyl reductase	0.08	0.02
NCU08138	cytochrome C1 heme lyase	0.07	0.01
NCU06778	OXA-2	0.07	0.01
NCU07756	succinate dehydrogenase cytochrome b560 subunit	0.07	0.01
NCU07560	50S ribosomal subunit L30	0.06	0.00
NCU08477	small GTP-binding protein	0.06	0.00
NCU00644	ATP synthase subunit G	0.05	-0.01
NCU01589	heat shock protein 60	0.05	-0.01
NCU00030	mitochondrial nuclease	0.05	-0.01
NCU01975	complex I intermediate-associated protein CIA30	0.05	-0.01
NCU00676	F1-ATP synthase assembly protein	0.05	-0.01
NCU07682	acetylglutamate synthase	0.04	-0.02
NCU05515	mitochondrial import inner membrane translocas	0.04	-0.02
NCU09119	ATP synthase subunit gamma	0.02	-0.04
NCU02373	NADH-ubiquinone oxidoreductase 40 kDa subunit	0.02	-0.04
NCU05881	DUF500 and UBA/TS-N domain-containing protein	0.02	-0.04
NCU06761	sphingosine-1-phosphate lyase	0.01	-0.05
NCU08909	beta-1,3-glucanosyltransferase	0	-0.07
NCU08898	homoaconitase	-0.01	-0.08
NCU05517	mitochondrial genome maintenance protein MGM101	-0.01	-0.08
NCU06695	cytochrome c oxidase polypeptide VI, variant	-0.01	-0.08
NCU06536	hypothetical protein	-0.02	-0.09
NCU06371	mitochondrial ATP-dependent RNA helicase Suv3	-0.02	-0.09
NCU06666	inositol-3-phosphate synthase	-0.02	-0.09
NCU02407	dihydrolipoyl dehydrogenase	-0.03	-0.10
NCU08120	mitochondrial ribosomal protein DAP3	-0.04	-0.11
NCU02472	NADH:ubiquinone oxidoreductase 20.8kD subunit	-0.04	-0.11
NCU01859	NADH:ubiquinone oxidoreductase 20.9kD subunit	-0.04	-0.11
NCU06069	hypothetical protein	-0.05	-0.12
NCU03637	CaaX prenyl protease Ste24	-0.05	-0.12
NCU06441	D-lactate dehydrogenase 2	-0.05	-0.12
NCU01469	hypothetical protein	-0.05	-0.12
NCU03296	F1 ATPase assembly protein 11	-0.05	-0.12

NCU03004	pyruvate dehydrogenase E1 component	-0.06	-0.13
NCU02955	elongation factor G 1	-0.07	-0.14
NCU00050	pyruvate dehydrogenase X component	-0.07	-0.14
NCU04280	aconitate hydratase	-0.07	-0.14
NCU02623	mitochondrial hypoxia responsiv	-0.07	-0.14
NCU01485	hypothetical protein	-0.07	-0.14
NCU04138	hypothetical protein	-0.09	-0.16
NCU00894	hypothetical protein	-0.1	-0.17
NCU04100	vacuolar sorting protein 1	-0.1	-0.17
NCU07659	pyruvate dehydrogenase complex	-0.11	-0.18
NCU05813	mitochondrial large ribosomal subunit	-0.11	-0.18
NCU06482	pyruvate dehydrogenase E1 component alph	-0.12	-0.20
NCU03297	cytochrome c peroxidase	-0.12	-0.20
NCU08411	aspartate aminotransferase	-0.12	-0.20
NCU00895	RAB GTPase Ypt5	-0.12	-0.20
NCU02959	hypothetical protein	-0.12	-0.20
NCU06914	histidyl-tRNA synthetase	-0.13	-0.21
NCU07423	hypothetical protein	-0.13	-0.21
NCU04803	2-nitropropane dioxygenase famil	-0.13	-0.21
NCU00431	mitochondrial import receptor subunit Tom22	-0.14	-0.22
NCU03112	NADH-cytochrome b5 reductase 2	-0.14	-0.22
NCU00502	ATP synthase subunit 4	-0.14	-0.22
NCU09228	aminopeptidase 2	-0.15	-0.23
NCU01667	ornithine carbamoyltransferase	-0.16	-0.24
NCU05220	ATP synthase subunit F	-0.16	-0.24
NCU01765	NADH:ubiquinone oxidoreductase 78	-0.16	-0.24
NCU04074	NADH:ubiquinone oxidoreductase 30.4 kDa subunit	-0.16	-0.24
NCU02070	peroxisomal biogenesis factor 2	-0.17	-0.25
NCU01550	adenylate kinase cytosolic	-0.17	-0.25
NCU01227	succinyl-CoA ligase alpha-chain	-0.17	-0.25
NCU02657	s-adenosylmethionine synthetase, variant	-0.18	-0.26
NCU03979	biotin synthase	-0.19	-0.27
NCU08980	alternative NADH-dehydrogenase	-0.19	-0.27
NCU04044	NADH2 dehydrogenase flavoprotein 1	-0.2	-0.28
NCU04171	50S ribosomal protein L5	-0.2	-0.28
NCU01467	NADH:ubiquinone oxidoreductase 10.4kD subunit	-0.21	-0.29
NCU06632	outer mitochondrial membrane translocase 20	-0.22	-0.30
NCU00562	hypothetical protein	-0.22	-0.30
NCU09477	ADP/ATP carrier protein, variant	-0.23	-0.31
NCU04899	malate dehydrogenase	-0.24	-0.32
NCU05454	glycerol-3-phosphate dehydrogenase	-0.25	-0.34

NCU00567	Arg-6 protein, variant	-0.26	-0.35
NCU00969	NADH:ubiquinone oxidoreductase 17.8kD subunit	-0.26	-0.35
NCU01474	60S ribosomal protein L4, variant	-0.26	-0.35
NCU00952	mitochondrial ribosomal protein L44	-0.26	-0.35
NCU05027	hypothetical protein	-0.27	-0.36
NCU02534	NADH:ubiquinone oxidoreductase 49kD subunit	-0.27	-0.36
NCU07465	mitochondrial phosphate carrier protein 2	-0.27	-0.36
NCU05623	mitochondrial inner membrane translocase subuni	-0.27	-0.36
NCU02705	F1F0 ATP synthase assembly protein Atp10	-0.28	-0.37
NCU06606	ubiquinol-cytochrome c reductase iron-sulfu	-0.29	-0.38
NCU08410	50S ribosomal protein L24	-0.29	-0.38
NCU03156	NUO	-0.29	-0.38
NCU03798	mitochondrial import inner membrane translocas	-0.3	-0.39
NCU02727	glycine cleavage system T protein	-0.3	-0.39
NCU08071	ribosomal protein S16	-0.3	-0.39
NCU06452	cysteine synthase	-0.3	-0.39
NCU09539	40S ribosomal protein S13	-0.3	-0.39
NCU01343	TPR repeat protein	-0.31	-0.40
NCU04806	hypothetical protein	-0.31	-0.40
NCU04481	mitochondrial ATPase	-0.31	-0.40
NCU01179	outer membrane translocase 40 kDa subunit	-0.32	-0.41
NCU05633	stomatin family protein	-0.33	-0.42
NCU03908	fmp-52	-0.33	-0.42
NCU05313	mitochondria fission 1 protein	-0.33	-0.42
NCU05390	mitochondrial phosphate carrier protein	-0.33	-0.42
NCU08728	mitochondrial ribosomal protein S19	-0.34	-0.43
NCU11348	NADH-ubiquinone oxidoreductase B18 subunit	-0.34	-0.43
NCU09223	protein disulfide-isomerase	-0.36	-0.45
NCU01657	cytochrome-c oxidase assembly protein	-0.36	-0.45
NCU04579	dihydroxy-acid dehydratase	-0.37	-0.47
NCU01689	mitochondrial DNA replication protein YHM2	-0.37	-0.47
NCU01454	mitochondrial hydrolase	-0.37	-0.47
NCU00103	hypothetical protein	-0.37	-0.47
NCU07493	hypothetical protein	-0.38	-0.48
NCU00660	glutamyl-tRNA amidotransferase	-0.38	-0.48
NCU03827	40S ribosomal protein S9	-0.39	-0.49
NCU00536	homoserine O-acetyltransferase	-0.4	-0.50
NCU00216	NADH-cytochrome b5 reductase 1	-0.4	-0.50
NCU04068	60S ribosomal protein L6	-0.41	-0.51
NCU01666	acetolactate synthase small subunit	-0.41	-0.51
NCU02804	mitochondrial 60S ribosomal protein L25	-0.41	-0.51

NCU09222	hypothetical protein	-0.41	-0.51
NCU03989	ADP,ATP carrier protein	-0.41	-0.51
NCU01241	mitochondrial carrier protein	-0.42	-0.52
NCU07263	carnitine/acyl carnitine carrier	-0.42	-0.52
NCU04412	hypothetical protein	-0.43	-0.53
NCU03739	protein disulfide-isomerase tigA	-0.43	-0.53
NCU02812	uridylate kinase	-0.44	-0.54
NCU03030	tyrosyl-tRNA synthetase	-0.44	-0.54
NCU03982	glucose-regulated protein	-0.44	-0.54
NCU03695	phosphatidylserine decarboxylase proenzyme 1	-0.45	-0.55
NCU06749	60S ribosomal protein L3	-0.46	-0.56
NCU05601	cytochrome c heme lyase	-0.46	-0.56
NCU01484	rho-type GTPase	-0.46	-0.56
NCU03093	NADH:ubiquinone oxidoreductase 12.3kD subunit	-0.46	-0.56
NCU08893	60S ribosomal protein L1	-0.47	-0.57
NCU03230	mitochondrial ribosomal protein subunit S18	-0.47	-0.57
NCU02419	mitochondrial 37S ribosomal protein S17	-0.49	-0.59
NCU05459	mitochondrial AAA ATPase	-0.5	-0.61
NCU10468	arginine biosynthesis argJ	-0.51	-0.62
NCU05593	mitochondrial outer membrane beta-barrel protei	-0.52	-0.63
NCU05299	NADH:ubiquinone oxidoreductase	-0.52	-0.63
NCU05689	cytochrome c oxidase polypeptide IV	-0.52	-0.63
NCU03711	GTP-binding protein ypt7	-0.52	-0.63
NCU02690	mitochondrial integral membrane protein	-0.52	-0.63
NCU03608	ketol-acid reductoisomerase	-0.54	-0.65
NCU04754	branched-chain-amino-acid aminotransferase	-0.55	-0.66
NCU07982	acetolactate synthase	-0.57	-0.68
NCU04768	electron transfer flavoprotein-ubiquinon	-0.57	-0.68
NCU09002	NADH:ubiquinone oxidoreductase 10.6kD subunit	-0.57	-0.68
NCU02123	mitochondrial GTPase	-0.57	-0.68
NCU02280	NADH:ubiquinone oxidoreductase 21.3kD subunit B	-0.58	-0.69
NCU03188	sugar 1,4-lactone oxidase	-0.59	-0.70
NCU03076	delta-1-pyrroline-5-carboxylate dehydrogenase	-0.59	-0.70
NCU09460	NADH:ubiquinone oxidoreductase 20.1kD subunit	-0.59	-0.70
NCU03394	ribosomal protein S15	-0.59	-0.70
NCU05890	hypothetical protein	-0.6	-0.71
NCU00385	ATP synthase subunit delta	-0.6	-0.71
NCU01821	alanine-glyoxylate aminotransferase	-0.6	-0.71
NCU06451	hypothetical protein	-0.6	-0.71
NCU07793	hypothetical protein	-0.61	-0.72
NCU02564	cysteine synthase 2	-0.61	-0.72

NCU01800	37S ribosomal protein S5	-0.62	-0.74
NCU03129	threonyl-tRNA synthetase	-0.63	-0.75
NCU07947	glycolipid transfer protein HET-C2	-0.63	-0.75
NCU06647	enoyl-CoA hydratase/isomerase	-0.64	-0.76
NCU00211	mitochondrial ribosomal protein subunit L31	-0.66	-0.78
NCU03653	hypothetical protein	-0.66	-0.78
NCU01894	hypothetical protein	-0.67	-0.79
NCU05221	NADH:ubiquinone oxidoreductase 21kD subunit	-0.68	-0.80
NCU01754	alcohol dehydrogenase I	-0.69	-0.81
NCU05410	acetylornithine aminotransferase	-0.69	-0.81
NCU09299	NADH:ubiquinone oxidoreductase 14kD subunit	-0.7	-0.82
NCU09025	glutamyl-tRNA	-0.72	-0.84
NCU02757	60S ribosomal protein L2	-0.72	-0.84
NCU06404	GTP-binding protein	-0.72	-0.84
NCU07988	ATPase family AAA domain-containing protein 1	-0.72	-0.84
NCU05717	mito ribosomal protein S6	-0.73	-0.85
NCU05457	cytochrome c oxidase subunit IV	-0.74	-0.86
NCU04245	outer mitochondrial membrane translocase	-0.74	-0.86
NCU02677	carbamoyl-phosphate synthase large subunit	-0.74	-0.86
NCU08146	hypothetical protein	-0.75	-0.88
NCU00605	ThiF domain-containing protein	-0.77	-0.90
NCU07732	carbamoyl-phosphate synthase small subunit	-0.77	-0.90
NCU00347	peroxin-26 Pex26-Penicillium chrysogenum	-0.77	-0.90
NCU08296	mito ribosomal protein S4	-0.78	-0.91
NCU00670	NADH:ubiquinone oxidoreductase 9.5kD subunit	-0.79	-0.92
NCU02451	mitochondrial hypoxia responsiv	-0.8	-0.93
NCU00114	30S ribosomal protein S10	-0.8	-0.93
NCU07112	hypothetical protein	-0.81	-0.94
NCU08930	NADH:ubiquinone oxidoreductase 21.3kD subunit A	-0.81	-0.94
NCU06741	cytochrome c oxidase subunit VIb	-0.82	-0.95
NCU04781	NADH:ubiquinone oxidoreductase 9.8 kDa subunit	-0.82	-0.95
NCU01401	mitochondrial outer membrane protein, variant	-0.84	-0.97
NCU08561	succinate/fumarate mitochondrial transporter	-0.84	-0.97
NCU03802	trimethyllysine dioxygenase	-0.85	-0.98
NCU08552	50S ribosomal protein L14	-0.85	-0.98
NCU01680	plasma membrane ATPase	-0.86	-0.99
NCU08272	cytochrome b2	-0.86	-0.99
NCU12023	mito ribosomal protein S2	-0.87	-1.01
NCU02269	mitochondrial carnitine/acylcarnitine carrie	-0.87	-1.01
NCU03966	mitochondrial Rho GTPase 1	-0.87	-1.01
NCU06495	mitochondrial inner membrane organizatio	-0.87	-1.01

NCU00958	5-azacytidine resistance protein azr1	-0.88	-1.02
NCU05029	iron-sulfur clusters transporter atm-1	-0.89	-1.03
NCU07724	mitochondrial division protein 1	-0.89	-1.03
NCU05989	hypothetical protein	-0.89	-1.03
NCU08940	ubiquinol-cytochrome c reductase comple	-0.9	-1.04
NCU06924	kynurenine 3-monooxygenase	-0.91	-1.05
NCU03561	mitochondrial carrier protein	-0.91	-1.05
NCU08661	pantoate-beta-alanine ligase	-0.91	-1.05
NCU05075	mitochondrial tricarboxylate transporter	-0.92	-1.06
NCU03558	hypothetical protein	-0.92	-1.06
NCU04837	mitochondrial 2-oxodicarboxylate carrier 1	-0.93	-1.07
NCU09816	cytochrome-26	-0.94	-1.08
NCU05714	50S ribosomal subunit protein L15	-0.94	-1.08
NCU08329	mitochondrial ribosomal protein subunit L23	-0.94	-1.08
NCU08947	ubiquinol-cytochrome-c reductase chain VIII	-0.94	-1.08
NCU05226	ABC transporter	-0.96	-1.10
NCU03953	mitochondrial NADH-ubiquinone oxidoreductase 2	-0.98	-1.12
NCU03343	37S ribosomal protein S25	-0.98	-1.12
NCU00436	GTPase FZO1	-1	-1.15
NCU11345	hypothetical protein	-1.01	-1.16
NCU00977	aconitate hydratase	-1.04	-1.19
NCU02544	ABC transporter	-1.04	-1.19
NCU04276	hypothetical protein	-1.05	-1.20
NCU00051	hypothetical protein	-1.05	-1.20
NCU06450	mitochondrial ribosomal protein	-1.05	-1.20
NCU08356	acetamidase	-1.06	-1.21
NCU10008	fumarate hydratase	-1.07	-1.22
NCU05009	NADH-quinone oxidoreductase chain I, variant	-1.09	-1.24
NCU09826	RNase III domain-containing protein	-1.1	-1.25
NCU02475	glycine dehydrogenase	-1.11	-1.26
NCU08299	60S ribosomal protein L3	-1.13	-1.29
NCU09345	thiamine biosynthesis protein NMT-1, variant 2	-1.13	-1.29
NCU00418	NADH:ubiquinone oxidoreductase 14.8kD subunit	-1.13	-1.29
NCU04502	hypothetical protein	-1.16	-1.32
NCU00564	mitochondrial 40S ribosomal protein MRP2	-1.24	-1.40
NCU06768	60S ribosomal protein L16	-1.25	-1.42
NCU09999	hypothetical protein	-1.27	-1.44
NCU00371	mitochondrial import inner membrane translocas	-1.3	-1.47
NCU04230	isocitrate lyase	-1.31	-1.48
NCU05338	hypothetical protein	-1.33	-1.50
NCU07057	hypothetical protein	-1.37	-1.55

NCU01633	hexose transporter HXT13	-1.37	-1.55
NCU11258	LYR family protein	-1.38	-1.56
NCU06110	thiazole biosynthetic enzyme	-1.39	-1.57
NCU04225	60S ribosomal protein L20	-1.45	-1.63
NCU00477	carboxypeptidase Y	-1.46	-1.64
NCU04946	hypothetical protein	-1.47	-1.65
NCU05552	hypothetical protein	-1.49	-1.67
NCU00411	hypothetical protein	-1.53	-1.72
NCU01142	NADH:ubiquinone oxidoreductase 13.4kD subunit	-1.59	-1.78
NCU00227	mitochondrial cation transporter	-1.59	-1.78
NCU03359	intermembrane space AAA protease IAP-1	-1.63	-1.83
NCU03926	37S ribosomal protein Rsm24	-1.64	-1.84
NCU02936	proline oxidase	-1.84	-2.05
NCU06189	5-aminolevulinate synthase	-1.86	-2.07
NCU00107	mitochondrial inner membrane protease ATP-23	-2.41	-2.67
NCU02504	DUF1640 domain-containing protein	-2.62	-2.90
NCU00565	lipoic acid synthetase	-2.82	-3.11
NCU08354	hypothetical protein	-2.84	-3.13
NCU01024	hypothetical protein	-2.9	-3.20
NCU09143	hypothetical protein	-3.93	-4.31
NCU04304	outer mitochondrial membrane protein porin	-4.96	-5.42

Table 6.4 Levels of predicted mitochondrial proteins in Δ Por-1 relative to 238Por.

Log2 differences that are statistically different are highlighted in blue.			
Log2 differences that are statistically different but may not be mitochondrial are highlighted in grey.			
Locus	Description	log2 Difference	Z-Score
NCU03558	hypothetical protein	5.11	6.04
NCU01092	3-oxoacyl-(acyl-carrier-protein) reductase	3.23	3.82
NCU05005	HHE domain-containing protein	2.96	3.50
NCU00565	lipoic acid synthetase	2.59	3.06
NCU05459	mitochondrial AAA ATPase	2.46	2.91
NCU00477	carboxypeptidase Y	2.22	2.62
NCU02097	short chain dehydrogenase	2.10	2.48
NCU04837	mitochondrial 2-oxodicarboxylate carrier 1	1.97	2.33
NCU03359	intermembrane space AAA protease IAP-1	1.91	2.26
NCU09599	hypothetical protein	1.82	2.15
NCU06778	OXA-2	1.74	2.05
NCU02906	NAD-dependent malic enzyme 1	1.73	2.04
NCU16968	cytochrome c mitochondrial import factor	1.60	1.89
NCU02705	F1F0 ATP synthase assembly protein Atp10	1.53	1.81
NCU02504	DUF1640 domain-containing protein	1.52	1.79
NCU08138	cytochrome C1 heme lyase	1.45	1.71
NCU02451	mitochondrial hypoxia responsiv	1.45	1.71
NCU00371	mitochondrial import inner membrane translocas	1.44	1.70
NCU08329	mitochondrial ribosomal protein subunit L23	1.43	1.69
NCU02948	non-anchored cell wall protein 4	1.42	1.68
NCU09826	RNase III domain-containing protein	1.41	1.66
NCU06740	hypothetical protein	1.41	1.66
NCU03926	37S ribosomal protein Rsm24	1.40	1.65
NCU01650	hypothetical protein	1.36	1.60
NCU05717	mito ribosomal protein S6	1.33	1.57
NCU09862	ubiquinone biosynthesis methyltransferase coq5	1.26	1.49
NCU00958	5-azacytidine resistance protein azr1	1.23	1.45
NCU07362	L-lactate ferricytochrome c oxidoreductase	1.20	1.42
NCU09025	glutamyl-tRNA	1.19	1.40
NCU02002	hypothetical protein	1.16	1.37
NCU00977	aconitate hydratase	1.14	1.34
NCU00831	extracellular serine carboxypeptidase, variant	1.13	1.33
NCU06403	hypothetical protein	1.10	1.30
NCU04334	chaperonin	1.09	1.29
NCU02128	D-arabinitol dehydrogenase	1.07	1.26
NCU08909	beta-1,3-glucanosyltransferase	1.06	1.25

NCU04502	hypothetical protein	1.04	1.23
NCU01102	mitochondrial export translocase Oxa1	1.03	1.21
NCU00183	DUF185 domain-containing protein	0.99	1.17
NCU05302	GTP-binding protein Obg	0.97	1.14
NCU04764	hypothetical protein	0.95	1.12
NCU06495	mitochondrial inner membrane organizatio	0.94	1.11
NCU00051	hypothetical protein	0.93	1.10
NCU04412	hypothetical protein	0.90	1.06
NCU03749	hydroxyacylglutathione hydrolase	0.90	1.06
NCU06749	60S ribosomal protein L3	0.89	1.05
NCU01657	cytochrome-c oxidase assembly protein	0.88	1.04
NCU08299	60S ribosomal protein L3	0.88	1.04
NCU07670	CYT-19 DEAD-box protein	0.87	1.02
NCU05248	hypothetical protein	0.86	1.01
NCU05552	hypothetical protein	0.86	1.01
NCU08893	60S ribosomal protein L1	0.86	1.01
NCU06450	mitochondrial ribosomal protein	0.85	1.00
NCU03637	CaaX prenyl protease Ste24	0.85	1.00
NCU09539	40S ribosomal protein S13	0.84	0.99
NCU04068	60S ribosomal protein L6	0.83	0.98
NCU06536	hypothetical protein	0.82	0.97
NCU03343	37S ribosomal protein S25	0.81	0.95
NCU03231	mitochondrial chaperone BCS1	0.80	0.94
NCU09754	mitochondrial chaperone Frataxin	0.80	0.94
NCU00103	hypothetical protein	0.79	0.93
NCU05029	iron-sulfur clusters transporter atm-1	0.77	0.91
NCU06246	ATP-dependent RNA helicase mrh-4	0.77	0.91
NCU02630	heat shock protein 78	0.76	0.89
NCU05220	ATP synthase subunit F	0.75	0.88
NCU02423	mitoferrin-1	0.75	0.88
NCU03229	mitochondrial inner membrane translocase subuni	0.73	0.86
NCU00673	serine protease p2	0.73	0.86
NCU08410	50S ribosomal protein L24	0.72	0.85
NCU04817	electron transfer protein 1	0.71	0.84
NCU06647	enoyl-CoA hydratase/isomerase	0.70	0.82
NCU02959	hypothetical protein	0.70	0.82
NCU01894	hypothetical protein	0.69	0.81
NCU05850	rubredoxin-NAD	0.68	0.80
NCU06307	multisynthetase complex auxiliary component p43	0.67	0.79
NCU05778	iron sulfur cluster assembly protein 1	0.66	0.78
NCU10226	mmf1	0.66	0.78

NCU03823	ABC1 protein	0.66	0.78
NCU02727	glycine cleavage system T protein	0.65	0.76
NCU03030	tyrosyl-tRNA synthetase	0.65	0.76
NCU06643	oleate-induced peroxisomal protein	0.64	0.75
NCU07682	acetylglutamate synthase	0.63	0.74
NCU05714	50S ribosomal subunit protein L15	0.63	0.74
NCU03310	prohibitin-2	0.63	0.74
NCU03296	F1 ATPase assembly protein 11	0.62	0.73
NCU01473	mitochondrial large ribosomal subunit YmL35	0.61	0.72
NCU00737	presequence translocated-associated moto	0.60	0.71
NCU04225	60S ribosomal protein L20	0.60	0.71
NCU02804	mitochondrial 60S ribosomal protein L25	0.60	0.71
NCU03908	fmp-52	0.60	0.71
NCU05633	stomatin family protein	0.59	0.69
NCU04803	2-nitropropane dioxygenase famil	0.59	0.69
NCU06371	mitochondrial ATP-dependent RNA helicase Suv3	0.59	0.69
NCU05515	mitochondrial import inner membrane translocas	0.59	0.69
NCU02273	vacuolar protease A	0.59	0.69
NCU09517	hypothetical protein	0.59	0.69
NCU08552	50S ribosomal protein L14	0.58	0.68
NCU07298	CAIB/BAIF family enzyme	0.58	0.68
NCU05890	hypothetical protein	0.57	0.67
NCU00114	30S ribosomal protein S10	0.56	0.66
NCU08946	hypothetical protein	0.56	0.66
NCU00660	glutamyl-tRNA amidotransferase	0.55	0.65
NCU03653	hypothetical protein	0.55	0.65
NCU04181	TOM7, variant 2	0.55	0.65
NCU08861	hypothetical protein	0.55	0.65
NCU00137	ssDNA binding protein	0.55	0.65
NCU03217	MRS7 family protein	0.54	0.63
NCU07465	mitochondrial phosphate carrier protein 2	0.54	0.63
NCU07263	carnitine/acyl carnitine carrier	0.52	0.61
NCU09331	HMF1	0.52	0.61
NCU00952	mitochondrial ribosomal protein L44	0.51	0.60
NCU12046	gamma-butyrobetaine dioxygenase	0.49	0.58
NCU00466	glutamyl-tRNA synthetase	0.48	0.56
NCU09560	superoxide dismutase	0.47	0.55
NCU05287	50S ribosomal protein L4	0.46	0.54
NCU06761	sphingosine-1-phosphate lyase	0.45	0.53
NCU07724	mitochondrial division protein 1	0.45	0.53
NCU08093	hypothetical protein	0.45	0.53

NCU06768	60S ribosomal protein L16	0.44	0.52
NCU04171	50S ribosomal protein L5	0.44	0.52
NCU09999	hypothetical protein	0.44	0.52
NCU02955	elongation factor G 1	0.43	0.50
NCU02544	ABC transporter	0.43	0.50
NCU03338	hypothetical protein	0.43	0.50
NCU03979	biotin synthase	0.42	0.49
NCU02887	voltage-gated potassium channel beta-2 subunit	0.42	0.49
NCU03199	ATP synthase subunit H	0.41	0.48
NCU01589	heat shock protein 60	0.40	0.47
NCU09058	enoyl-CoA hydratase	0.40	0.47
NCU00904	D-lactate dehydrogenase	0.40	0.47
NCU16385	glutaredoxin domain-containing protein	0.40	0.47
NCU07794	2Fe-2S iron-sulfur cluster bindin	0.39	0.46
NCU00360	NAD dependent epimerase/dehydratase	0.38	0.45
NCU00655	mitochondrial enoyl reductase	0.38	0.45
NCU02807	hypothetical protein	0.38	0.45
NCU05419	hydroxymethylglutaryl-CoA lyase	0.38	0.45
NCU04336	60S ribosomal protein L19	0.38	0.45
NCU01272	mitochondrial presequence protease	0.38	0.45
NCU03173	HAD superfamily hydrolase	0.37	0.43
NCU05196	mitochondrial DnaJ chaperone	0.37	0.43
NCU08146	hypothetical protein	0.37	0.43
NCU06546	hypothetical protein	0.36	0.42
NCU06881	succinyl-CoA:3-ketoacid-coenzyme A transferas	0.36	0.42
NCU08048	NAD dehydrogenase	0.36	0.42
NCU09327	protein phosphatase	0.35	0.41
NCU05623	mitochondrial inner membrane translocase subuni	0.35	0.41
NCU00599	mito ribosomal protein S22	0.35	0.41
NCU07793	hypothetical protein	0.34	0.40
NCU07852	ribosomal protein L13	0.34	0.40
NCU02701	dipeptidyl peptidase	0.34	0.40
NCU03957	COQ7	0.33	0.39
NCU04578	ATP-dependent Clp protease proteolytic subuni	0.33	0.39
NCU05593	mitochondrial outer membrane beta-barrel protei	0.32	0.37
NCU03155	hypothetical protein	0.32	0.37
NCU03777	mitochondrial 3-hydroxyisobutyryl-CoA hydrolase	0.31	0.36
NCU04013	aldehyde dehydrogenase	0.31	0.36
NCU08120	mitochondrial ribosomal protein DAP3	0.31	0.36
NCU05008	acp-1	0.30	0.35
NCU02064	hypothetical protein	0.30	0.35

NCU07560	50S ribosomal subunit L30	0.29	0.34
NCU07057	hypothetical protein	0.29	0.34
NCU08005	NADPH-adrenodoxin reductase Arh1	0.28	0.33
NCU03339	glutathione reductase	0.27	0.31
NCU01484	rho-type GTPase	0.27	0.31
NCU00395	mRNA processing protein	0.27	0.31
NCU05454	glycerol-3-phosphate dehydrogenase	0.26	0.30
NCU07756	succinate dehydrogenase cytochrome b560 subunit	0.26	0.30
NCU03297	cytochrome c peroxidase	0.26	0.30
NCU05517	mitochondrial genome maintenance protein MGM101	0.26	0.30
NCU00905	N-acylethanolamine amidohydrolase	0.25	0.29
NCU02157	COQ4	0.25	0.29
NCU12023	mito ribosomal protein S2	0.25	0.29
NCU08998	4-aminobutyrate aminotransferase	0.25	0.29
NCU06017	thiosulfate sulfurtransferase	0.25	0.29
NCU03020	IdgA domain-containing protein	0.25	0.29
NCU16742	hypothetical protein	0.25	0.29
NCU01479	matrix AAA protease MAP-1	0.24	0.28
NCU05601	cytochrome c heme lyase	0.24	0.28
NCU11258	LYR family protein	0.24	0.28
NCU09598	mitochondrial escape protein 2	0.23	0.27
NCU02287	acyl-CoA dehydrogenase	0.23	0.27
NCU02580	fumarate reductase Osm1	0.23	0.27
NCU03925	toxin biosynthesis protein	0.22	0.26
NCU01680	plasma membrane ATPase	0.22	0.26
NCU01485	hypothetical protein	0.22	0.26
NCU08980	alternative NADH-dehydrogenase	0.22	0.26
NCU01546	coproporphyrinogen III oxidase	0.22	0.26
NCU02269	mitochondrial carnitine/acylcarnitine carrier	0.22	0.26
NCU02545	hypothetical protein	0.22	0.26
NCU05772	TOM6	0.21	0.24
NCU08728	mitochondrial ribosomal protein S19	0.20	0.23
NCU01516	mitochondrial co-chaperone GrpE	0.20	0.23
NCU01006	complex I intermediate-associated protein CIA84	0.20	0.23
NCU08296	mito ribosomal protein S4	0.20	0.23
NCU03006	sterol 24-C-methyltransferase	0.20	0.23
NCU03008	hypothetical protein	0.19	0.22
NCU02305	decaprenyl-diphosphate synthase subunit 1	0.19	0.22
NCU02291	glutaryl-CoA dehydrogenase	0.19	0.22
NCU02943	mitochondrial import inner membrane translocas	0.18	0.21
NCU02954	homoisocitrate dehydrogenase	0.18	0.21

NCU01304	mitochondrial mRNA processing protein PET127	0.18	0.21
NCU04806	hypothetical protein	0.17	0.20
NCU00378	aldehyde dehydrogenase	0.17	0.20
NCU09266	methylmalonate-semialdehyde dehydrogenase	0.17	0.20
NCU03814	leucyl-tRNA synthetase	0.17	0.20
NCU03394	ribosomal protein S15	0.17	0.20
NCU01023	50S ribosomal protein L17	0.17	0.20
NCU00405	glycyl-tRNA synthetase 1	0.17	0.20
NCU06031	mitochondrial peroxiredoxin PRX1	0.17	0.20
NCU06189	5-aminolevulinate synthase	0.16	0.18
NCU09223	protein disulfide-isomerase	0.16	0.18
NCU08476	hypothetical protein	0.16	0.18
NCU07112	hypothetical protein	0.16	0.18
NCU03004	pyruvate dehydrogenase E1 component	0.15	0.17
NCU01975	complex I intermediate-associated protein CIA30	0.15	0.17
NCU04212	hypothetical protein	0.15	0.17
NCU01808	cytochrome c	0.14	0.16
NCU00122	aspartyl aminopeptidase	0.14	0.16
NCU07904	short chain dehydrogenase/reductase	0.14	0.16
NCU02267	mitochondrial protein Fmp25	0.13	0.15
NCU04594	4-carboxymuconolactone decarboxylase	0.13	0.15
NCU00726	peptidyl-prolyl cis-trans isomerase	0.13	0.15
NCU02514	mitochondrial ATP synthase alpha subunit	0.13	0.15
NCU01474	60S ribosomal protein L4, variant	0.13	0.15
NCU09477	ADP/ATP carrier protein, variant	0.12	0.14
NCU01667	ornithine carbamoyltransferase	0.12	0.14
NCU00775	isocitrate dehydrogenase subunit 1	0.12	0.14
NCU02419	mitochondrial 37S ribosomal protein S17	0.12	0.14
NCU02407	dihydrolipoyl dehydrogenase	0.11	0.13
NCU10008	fumarate hydratase	0.11	0.13
NCU07858	DUF498 domain-containing protein	0.10	0.11
NCU08693	hsp70-like protein	0.09	0.10
NCU01343	TPR repeat protein	0.09	0.10
NCU09403	NmrA family protein	0.09	0.10
NCU03230	mitochondrial ribosomal protein subunit S18	0.09	0.10
NCU00030	mitochondrial nuclease	0.09	0.10
NCU03177	sco1	0.08	0.09
NCU06556	thioredoxin II	0.08	0.09
NCU01255	mitochondrial dynamin GTPase	0.08	0.09
NCU02438	dihydrolipoamide succinyltransferase	0.08	0.09
NCU04899	malate dehydrogenase	0.07	0.08

NCU00676	F1-ATP synthase assembly protein	0.07	0.08
NCU04138	hypothetical protein	0.07	0.08
NCU06587	hypothetical protein	0.07	0.08
NCU01218	hypothetical protein	0.06	0.07
NCU06448	enoyl-CoA hydratase	0.06	0.07
NCU03112	NADH-cytochrome b5 reductase 2	0.05	0.05
NCU05225	mitochondrial NADH dehydrogenase	0.05	0.05
NCU00527	mitochondrial genome maintenance protein Mgr2	0.05	0.05
NCU00431	mitochondrial import receptor subunit Tom22	0.05	0.05
NCU01179	outer membrane translocase 40 kDa subunit	0.05	0.05
NCU01965	valyl-tRNA synthetase	0.04	0.04
NCU06441	D-lactate dehydrogenase 2	0.04	0.04
NCU00278	hypothetical protein	0.04	0.04
NCU11345	hypothetical protein	0.04	0.04
NCU06695	cytochrome c oxidase polypeptide VI, variant	0.03	0.03
NCU06211	malate dehydrogenase, variant	0.03	0.03
NCU06308	DNA-directed RNA polymerase	0.03	0.03
NCU01761	hypothetical protein	0.03	0.03
NCU03188	sugar 1,4-lactone oxidase	0.02	0.02
NCU08291	ferrochelatase	0.02	0.02
NCU01689	mitochondrial DNA replication protein YHM2	0.02	0.02
NCU04098	monothiol glutaredoxin-5	0.01	0.01
NCU04429	mitochondrial import protein mmp37	0.00	0.00
NCU05457	cytochrome c oxidase subunit IV	0.00	0.00
NCU06086	regulatory protein suaprga1	-0.01	-0.02
NCU06880	AhpC/TSA family protein	-0.02	-0.03
NCU09553	3-hydroxybutyryl CoA dehydrogenase	-0.02	-0.03
NCU04368	glutathione S-transferase Gst3	-0.02	-0.03
NCU05838	hypothetical protein	-0.02	-0.03
NCU08477	small GTP-binding protein	-0.03	-0.04
NCU05425	2-oxoglutarate dehydrogenase E1 component	-0.03	-0.04
NCU06482	pyruvate dehydrogenase E1 component alph	-0.03	-0.04
NCU00502	ATP synthase subunit 4	-0.03	-0.04
NCU00564	mitochondrial 40S ribosomal protein MRP2	-0.03	-0.04
NCU06309	hypothetical protein	-0.03	-0.04
NCU00894	hypothetical protein	-0.04	-0.05
NCU08272	cytochrome b2	-0.04	-0.05
NCU02366	aconitase	-0.04	-0.05
NCU09222	hypothetical protein	-0.04	-0.05
NCU00680	2-methylcitrate dehydratase	-0.04	-0.05
NCU04245	outer mitochondrial membrane translocase	-0.05	-0.06

NCU10468	arginine biosynthesis argJ	-0.05	-0.06
NCU00211	mitochondrial ribosomal protein subunit L31	-0.05	-0.06
NCU04280	aconitate hydratase	-0.05	-0.06
NCU07493	hypothetical protein	-0.05	-0.06
NCU08002	carnitine acetyl transferase	-0.05	-0.06
NCU09602	heat shock protein 70	-0.05	-0.06
NCU03031	succinate dehydrogenase cytochrome b smal	-0.06	-0.08
NCU08004	electron transfer flavoprotein alpha-subunit	-0.06	-0.08
NCU01169	NADH:ubiquinone oxidoreductase 24	-0.06	-0.08
NCU06452	cysteine synthase	-0.06	-0.08
NCU04202	nucleoside diphosphate kinase	-0.06	-0.08
NCU02734	citrate lyase beta subunit	-0.07	-0.09
NCU00264	hypothetical protein	-0.07	-0.09
NCU08936	clock-controlled gene-15, variant	-0.08	-0.10
NCU09732	acetyl-CoA acetyltransferase	-0.09	-0.11
NCU06270	mitochondrial-processing peptidase subuni	-0.09	-0.11
NCU01241	mitochondrial carrier protein	-0.09	-0.11
NCU04768	electron transfer flavoprotein-ubiquinon	-0.09	-0.11
NCU06451	hypothetical protein	-0.09	-0.11
NCU06924	kynurenine 3-monooxygenase	-0.09	-0.11
NCU01606	ATP synthase subunit 5	-0.10	-0.12
NCU01142	NADH:ubiquinone oxidoreductase 13.4kD subunit	-0.10	-0.12
NCU01550	adenylate kinase cytosolic	-0.11	-0.13
NCU04945	mitochondrial intermembrane space protein Mia40	-0.11	-0.13
NCU03739	protein disulfide-isomerase tigA	-0.11	-0.13
NCU00227	mitochondrial cation transporter	-0.11	-0.13
NCU07871	hypothetical protein	-0.11	-0.13
NCU06760	pyruvate dehydrogenase kinase	-0.11	-0.13
NCU04380	acyl-CoA synthetase	-0.12	-0.15
NCU00050	pyruvate dehydrogenase X component	-0.12	-0.15
NCU04074	NADH:ubiquinone oxidoreductase 30.4 kDa subunit	-0.12	-0.15
NCU01227	succinyl-CoA ligase alpha-chain	-0.12	-0.15
NCU00562	hypothetical protein	-0.12	-0.15
NCU05313	mitochondria fission 1 protein	-0.13	-0.16
NCU01140	NAD	-0.13	-0.16
NCU02481	mitochondrial 2-methylisocitrate lyase	-0.13	-0.16
NCU09255	acetate non-utilizing protein 9	-0.13	-0.16
NCU02623	mitochondrial hypoxia responsiv	-0.14	-0.17
NCU08356	acetamidase	-0.14	-0.17
NCU05075	mitochondrial tricarboxylate transporter	-0.14	-0.17
NCU08898	homoaconitase	-0.14	-0.17

NCU08336	succinate dehydrogenase flavoprotein subunit	-0.15	-0.18
NCU02549	ubiquinol-cytochrome-c reductase subunit beta	-0.15	-0.18
NCU00484	NADH:ubiquinone oxidoreductase 18.4kD subunit	-0.15	-0.18
NCU01800	37S ribosomal protein S5	-0.16	-0.19
NCU01454	mitochondrial hydrolase	-0.16	-0.19
NCU05261	ATP-dependent protease La	-0.17	-0.21
NCU03737	elongation factor Tu	-0.18	-0.22
NCU03893	short-chain dehydrogenase/reductase SDR	-0.18	-0.22
NCU03525	3-oxoacyl-[acyl-carrier-protein]-reductase	-0.18	-0.22
NCU09228	aminopeptidase 2	-0.19	-0.23
NCU06543	acyl-CoA dehydrogenase	-0.19	-0.23
NCU02044	GTP-binding protein	-0.19	-0.23
NCU03949	FMN-dependent 2-nitropropane dioxygenase	-0.19	-0.23
NCU01692	mitochondrial citrate synthase	-0.19	-0.23
NCU01666	acetolactate synthase small subunit	-0.20	-0.24
NCU07697	isocitrate dehydrogenase subunit 2	-0.20	-0.24
NCU01765	NADH:ubiquinone oxidoreductase 78	-0.20	-0.24
NCU04636	cysteine desulfurase	-0.21	-0.25
NCU08954	hypothetical protein	-0.21	-0.25
NCU00605	ThiF domain-containing protein	-0.22	-0.26
NCU07659	pyruvate dehydrogenase complex	-0.22	-0.26
NCU03156	NUO	-0.22	-0.26
NCU07982	acetolactate synthase	-0.22	-0.26
NCU00895	RAB GTPase Ypt5	-0.23	-0.28
NCU05430	ATP synthase beta subunit	-0.23	-0.28
NCU03556	peroxisomal membrane protein Pmp47	-0.23	-0.28
NCU04579	dihydroxy-acid dehydratase	-0.23	-0.28
NCU08471	succinyl-CoA ligase beta-chain	-0.23	-0.28
NCU09285	zinc-containing alcohol dehydrogenase	-0.23	-0.28
NCU06469	54S ribosomal protein L12	-0.24	-0.29
NCU02534	NADH:ubiquinone oxidoreductase 49kD subunit	-0.24	-0.29
NCU09002	NADH:ubiquinone oxidoreductase 10.6kD subunit	-0.24	-0.29
NCU07295	mitochondrial import inner membrane translocas	-0.24	-0.29
NCU02585	aspartyl-tRNA synthetase	-0.26	-0.31
NCU00959	succinate dehydrogenase iron-sulfur protein	-0.27	-0.32
NCU01528	glyceraldehyde 3-phosphate-dehydrogenase	-0.27	-0.32
NCU08541	hypothetical protein	-0.27	-0.32
NCU03094	hypothetical protein	-0.28	-0.34
NCU04754	branched-chain-amino-acid aminotransferase	-0.28	-0.34
NCU03559	ubiquinol-cytochrome c reductase complex cor	-0.28	-0.34
NCU05982	hexaprenyldihydroxybenzoate methyltransferase	-0.28	-0.34

NCU03857	tricarboxylic acid-5 protein, variant 2	-0.28	-0.34
NCU06103	Mito Translation initiation factor	-0.28	-0.34
NCU01564	calcium dependent mitochondrial carrier protein	-0.28	-0.34
NCU10732	mitochondrial dicarboxylate transporter	-0.28	-0.34
NCU08071	ribosomal protein S16	-0.29	-0.35
NCU04481	mitochondrial ATPase	-0.30	-0.36
NCU03516	mitochondrial ribosomal protein subunit L32	-0.31	-0.37
NCU05299	NADH:ubiquinone oxidoreductase	-0.32	-0.38
NCU02690	mitochondrial integral membrane protein	-0.33	-0.39
NCU06786	50S ribosomal protein L30	-0.34	-0.41
NCU09119	ATP synthase subunit gamma	-0.34	-0.41
NCU05495	CVNH domain-containing protein	-0.34	-0.41
NCU16657	tryptophanyl-tRNA synthetase	-0.35	-0.42
NCU07021	peptide chain release factor 3	-0.35	-0.42
NCU05971	xaa-Pro dipeptidase	-0.36	-0.43
NCU00936	succinate semialdehyde dehydrogenase	-0.36	-0.43
NCU03877	C-1-tetrahydrofolate synthase	-0.36	-0.43
NCU07608	ribose 5-phosphate isomerase A, variant	-0.36	-0.43
NCU05009	NADH-quinone oxidoreductase chain I, variant	-0.37	-0.44
NCU03076	delta-1-pyrroline-5-carboxylate dehydrogenase	-0.37	-0.44
NCU00567	Arg-6 protein, variant	-0.39	-0.47
NCU06958	mito ribosomal protein S21	-0.40	-0.48
NCU08877	glycine cleavage system H protein	-0.40	-0.48
NCU04230	isocitrate lyase	-0.40	-0.48
NCU03929	acyl-CoA synthetase	-0.42	-0.50
NCU01007	mito ribosomal protein S18	-0.42	-0.50
NCU08411	aspartate aminotransferase	-0.43	-0.51
NCU09770	acetyl-coa hydrolase	-0.43	-0.51
NCU02677	carbamoyl-phosphate synthase large subunit	-0.44	-0.53
NCU03759	methionine-tRNA synthetase	-0.44	-0.53
NCU05390	mitochondrial phosphate carrier protein	-0.46	-0.55
NCU03982	glucose-regulated protein	-0.46	-0.55
NCU02482	2-methylcitrate synthase, variant 2	-0.47	-0.56
NCU02757	60S ribosomal protein L2	-0.47	-0.56
NCU08924	acyl-CoA dehydrogenase	-0.48	-0.57
NCU01767	phosphatase 2C family protein	-0.48	-0.57
NCU01821	alanine-glyoxylate aminotransferase	-0.49	-0.58
NCU05027	hypothetical protein	-0.49	-0.58
NCU05221	NADH:ubiquinone oxidoreductase 21kD subunit	-0.50	-0.60
NCU03608	ketol-acid reductoisomerase	-0.51	-0.61
NCU05805	serine hydroxymethyltransferase	-0.52	-0.62

NCU06424	aminomethyl transferase	-0.52	-0.62
NCU05279	hypothetical protein	-0.53	-0.63
NCU04100	vacuolar sorting protein 1	-0.53	-0.63
NCU09594	seryl-tRNA synthetase	-0.53	-0.63
NCU09816	cytochrome-26	-0.53	-0.63
NCU05558	3-ketoacyl-CoA thiolase	-0.53	-0.63
NCU00418	NADH:ubiquinone oxidoreductase 14.8kD subunit	-0.54	-0.64
NCU03561	mitochondrial carrier protein	-0.54	-0.64
NCU02475	glycine dehydrogenase	-0.55	-0.66
NCU06632	outer mitochondrial membrane translocase 20	-0.56	-0.67
NCU02403	ubiquinone biosynthesis protein COQ9	-0.56	-0.67
NCU08707	iron sulfur assembly protein	-0.56	-0.67
NCU00644	ATP synthase subunit G	-0.56	-0.67
NCU02136	transaldolase	-0.56	-0.67
NCU00951	inorganic pyrophosphatase	-0.57	-0.68
NCU04044	NADH2 dehydrogenase flavoprotein 1	-0.58	-0.69
NCU06247	hypothetical protein	-0.59	-0.70
NCU03129	threonyl-tRNA synthetase	-0.59	-0.70
NCU01512	phenylalanyl-tRNA synthetase	-0.59	-0.70
NCU01467	NADH:ubiquinone oxidoreductase 10.4kD subunit	-0.59	-0.70
NCU00536	homoserine O-acetyltransferase	-0.59	-0.70
NCU03211	hypothetical protein	-0.59	-0.70
NCU03711	GTP-binding protein ypt7	-0.61	-0.73
NCU05288	rab GDP-dissociation inhibitor	-0.61	-0.73
NCU05410	acetylornithine aminotransferase	-0.62	-0.74
NCU03827	40S ribosomal protein S9	-0.62	-0.74
NCU09263	anchored cell wall protein 4	-0.63	-0.75
NCU07733	electron transfer flavoprotein beta-subunit	-0.64	-0.76
NCU05689	cytochrome c oxidase polypeptide IV	-0.65	-0.77
NCU01469	hypothetical protein	-0.65	-0.77
NCU08940	ubiquinol-cytochrome c reductase comple	-0.65	-0.77
NCU05813	mitochondrial large ribosomal subunit	-0.66	-0.79
NCU03695	phosphatidylserine decarboxylase proenzyme 1	-0.69	-0.82
NCU03347	kynurenine-oxoglutarate transaminase 1	-0.72	-0.86
NCU10042	enolase, variant	-0.72	-0.86
NCU02063	mitochondrial intermediate peptidase	-0.72	-0.86
NCU07550	triosephosphate isomerase	-0.73	-0.87
NCU07286	membrane-associated progesterone recepto	-0.73	-0.87
NCU01328	transketolase	-0.76	-0.90
NCU01962	encodes anonymous transcript-5 protein, variant	-0.76	-0.90
NCU05226	ABC transporter	-0.77	-0.92

NCU02193	pyruvate decarboxylase	-0.78	-0.93
NCU07386	Fe superoxide dismutase	-0.79	-0.94
NCU00584	hypothetical protein	-0.79	-0.94
NCU07732	carbamoyl-phosphate synthase small subunit	-0.81	-0.96
NCU03796	pyruvate dehydrogenase kinase	-0.82	-0.97
NCU00385	ATP synthase subunit delta	-0.84	-1.00
NCU08949	hypothetical protein	-0.84	-1.00
NCU05526	homocitrate synthase, variant 2	-0.85	-1.01
NCU09057	hypothetical protein	-0.86	-1.02
NCU09741	NADPH-cytochrome P450 reductase	-0.86	-1.02
NCU04605	hypothetical protein	-0.87	-1.03
NCU04276	hypothetical protein	-0.90	-1.07
NCU09886	hypothetical protein	-0.90	-1.07
NCU02812	uridylate kinase	-0.92	-1.09
NCU08947	ubiquinol-cytochrome-c reductase chain VIII	-0.92	-1.09
NCU01360	NADH:ubiquinone oxidoreductase 11.5kD subunit	-0.92	-1.09
NCU09143	hypothetical protein	-0.95	-1.13
NCU08195	arginyl-tRNA synthetase	-0.96	-1.14
NCU01859	NADH:ubiquinone oxidoreductase 20.9kD subunit	-1.02	-1.21
NCU02566	alanyl-tRNA synthetase	-1.04	-1.24
NCU05338	hypothetical protein	-1.05	-1.25
NCU03093	NADH:ubiquinone oxidoreductase 12.3kD subunit	-1.08	-1.28
NCU00075	mitochondrial import inner membrane translocas	-1.08	-1.28
NCU06606	ubiquinol-cytochrome c reductase iron-sulfu	-1.08	-1.28
NCU04588	hypothetical protein	-1.09	-1.29
NCU11348	NADH-ubiquinone oxidoreductase B18 subunit	-1.13	-1.34
NCU03953	mitochondrial NADH-ubiquinone oxidoreductase 2	-1.16	-1.38
NCU00670	NADH:ubiquinone oxidoreductase 9.5kD subunit	-1.18	-1.40
NCU01633	hexose transporter HXT13	-1.19	-1.41
NCU08930	NADH:ubiquinone oxidoreductase 21.3kD subunit A	-1.19	-1.41
NCU02013	hypothetical protein	-1.20	-1.42
NCU06741	cytochrome c oxidase subunit VIb	-1.21	-1.44
NCU08661	pantoate-beta-alanine ligase	-1.28	-1.52
NCU01401	mitochondrial outer membrane protein, variant	-1.32	-1.57
NCU03802	trimethyllysine dioxygenase	-1.36	-1.61
NCU06518	NADH-cytochrome b5 reductase 2	-1.37	-1.63
NCU02070	peroxisomal biogenesis factor 2	-1.38	-1.64
NCU04946	hypothetical protein	-1.42	-1.68
NCU09299	NADH:ubiquinone oxidoreductase 14kD subunit	-1.44	-1.71
NCU09810	succinyl-CoA synthetase subunit alpha	-1.45	-1.72
NCU02179	D-lactate dehydrogenase	-1.46	-1.73

NCU00969	NADH:ubiquinone oxidoreductase 17.8kD subunit	-1.54	-1.83
NCU02802	mitochondrial ornithine carrier protein	-1.55	-1.84
NCU02472	NADH:ubiquinone oxidoreductase 20.8kD subunit	-1.56	-1.85
NCU02280	NADH:ubiquinone oxidoreductase 21.3kD subunit B	-1.57	-1.86
NCU04287	hypothetical protein	-1.59	-1.89
NCU06687	glycogen synthase, variant 3	-1.59	-1.89
NCU06550	pyridoxine 1	-1.67	-1.98
NCU08561	succinate/fumarate mitochondrial transporter	-1.68	-1.99
NCU04736	plasma membrane calcium-transporting ATPase 3	-1.69	-2.00
NCU00153	pyridine nucleotide-disulfide oxidoreductase	-1.70	-2.02
NCU02095	hypothetical protein	-1.80	-2.13
NCU01916	mitochondrial carrier protein RIM2	-1.93	-2.29
NCU02951	40S ribosomal protein S8	-2.07	-2.45
NCU07253	1,3-beta-glucanosyltransferase gel1	-2.08	-2.47
NCU02564	cysteine synthase 2	-2.11	-2.50
NCU02373	NADH-ubiquinone oxidoreductase 40 kDa subunit	-2.17	-2.57
NCU10021	MFS monosaccharide transporter	-2.18	-2.58
NCU00436	GTPase FZO1	-2.27	-2.69
NCU04781	NADH:ubiquinone oxidoreductase 9.8 kDa subunit	-2.57	-3.05
NCU01024	hypothetical protein	-2.71	-3.21
NCU09345	thiamine biosynthesis protein NMT-1, variant 2	-3.10	-3.67
NCU06110	thiazole biosynthetic enzyme	-3.16	-3.74
NCU09460	NADH:ubiquinone oxidoreductase 20.1kD subunit	-4.43	-5.25

7. References

1. Uhlen, M., L. Fagerberg, B. M. Hallstrom, C. Lindskog, P. Oksvold, A. Mardinoglu, A. Sivertsson, C. Kampf, E. Sjostedt, A. Asplund, I. Olsson, K. Edlund, E. Lundberg, S. Navani, C. A. Szgyarto, J. Odeberg, D. Djureinovic, J. O. Takanen, S. Hober, T. Alm, P. H. Edqvist, H. Berling, H. Tegel, J. Mulder, J. Rockberg, P. Nilsson, J. M. Schwenk, M. Hamsten, K. von Feilitzen, M. Forsberg, L. Persson, F. Johansson, M. Zwahlen, G. von Heijne, J. Nielsen, and F. Ponten. 2015. Proteomics. Tissue-based map of the human proteome. *Science* 347(6220):1260419.
2. Moraes, I., G. Evans, J. Sanchez-Weatherby, S. Newstead, and P. D. Stewart. 2014. Membrane protein structure determination - the next generation. *Biochim Biophys Acta* 1838(1 Pt A):78-87.
3. Berman, H. M., Westbrook, J., Feng, Z., Gilliland, G., Bhat, T.N., Weissig, H., Shindyalov, I.N., Bourne, P.E. 2000. The Protein Data Bank. *Nucleic Acids Research* 28(1):235-241.
4. Singer, S. J., Nicolson, G.L. 1972. The Fluid Mosaic Model of the Structure of Cell Membranes. *Science* 175(4023):720-731.
5. Saier M.H. Jr, B., J.T., Goffeau A., Harley, K.T., Heijne, W.H.M., Huang, S., Jack, D.L., Jähn, P.S., Lew, K., Liu, J., Pao, S.S., Paulsen I.T., Tseng, T., Virk, P.S.,. 1999. The Major Facilitator Superfamily. *J. Mol. Microbiol. Biotechnol.* 1(2):257-279.
6. Grecco, H. E., M. Schmick, and P. I. Bastiaens. 2011. Signaling from the living plasma membrane. *Cell* 144(6):897-909.
7. Ng, D. P., B. E. Poulsen, and C. M. Deber. 2012. Membrane protein misassembly in disease. *Biochim Biophys Acta* 1818(4):1115-1122.
8. Shoshan-Barmatz, V., and D. Ben-Hail. 2012. VDAC, a multi-functional mitochondrial protein as a pharmacological target. *Mitochondrion* 12(1):24-34.
9. Molnar, J., G. Szakacs, and G. E. Tusnady. 2016. Characterization of Disease-Associated Mutations in Human Transmembrane Proteins. *PLoS One* 11(3):e0151760.
10. SPOLAR R.S., H. J., RECORD M.T. JR. 1989. Hydrophobic effect in protein folding and other noncovalent processes involving proteins. *Proc. Natl. Acad. Sci. USA* 86:8382-8385.

11. Muller, D. J., N. Wu, and K. Palczewski. 2008. Vertebrate membrane proteins: structure, function, and insights from biophysical approaches. *Pharmacol Rev* 60(1):43-78.
12. Koebnik, R., Locher, K.P., Gelder, P. 2000. Structure and function of bacterial outer membrane proteins: barrels in a nutshell. *Molecular Microbiology* 37(2):239-253.
13. White, S. H., and W. C. Wimley. 1999. MEMBRANE PROTEIN FOLDING AND STABILITY: Physical Principles. *Annual Review of Biophysics and Biomolecular Structure* 28(1):319-365.
14. Duquesne, K., and J. N. Sturgis. 2010. Membrane Protein Solubilization. *Heterologous Expression of Membrane Proteins: Methods and Protocols*. I. Mus-Veteau, editor. Humana Press, Totowa, NJ, pp. 205-217.
15. Seddon, A. M., P. Curnow, and P. J. Booth. 2004. Membrane proteins, lipids and detergents: not just a soap opera. *Biochim Biophys Acta* 1666(1-2):105-117.
16. Acin-Perez, R., P. Fernandez-Silva, M. L. Peleato, A. Perez-Martos, and J. A. Enriquez. 2008. Respiratory active mitochondrial supercomplexes. *Mol Cell* 32(4):529-539.
17. BASSI R., D. P. 1992. A supramolecular light-harvesting complex from chloroplast photosystem-II membranes. *Eur. J. Biochem.* 204:317-326.
18. Nooren I.M.A., T. J. M. 2003. Diversity of protein-protein interactions. *The EMBO Journal* 22(14):3486-3492.
19. Leavitt S., F. E. 2001. Direct measurement of protein binding energetics by isothermal titration calorimetry. *Current Opinion in Structural Biology* 11:560-566.
20. Scheuermann, T. H., S. B. Padrick, K. H. Gardner, and C. A. Brautigam. 2016. On the acquisition and analysis of microscale thermophoresis data. *Anal Biochem* 496:79-93.
21. Jerabek-Willemsen, M., C. J. Wienken, D. Braun, P. Baaske, and S. Duhr. 2011. Molecular interaction studies using microscale thermophoresis. *Assay Drug Dev Technol* 9(4):342-353.

22. Jerabek-Willemsen, M., T. André, R. Wanner, H. M. Roth, S. Duhr, P. Baaske, and D. Breitsprecher. 2014. MicroScale Thermophoresis: Interaction analysis and beyond. *Journal of Molecular Structure* 1077:101-113.
23. Ahmed, Z., Z. Timsah, K. M. Suen, N. P. Cook, G. R. t. Lee, C. C. Lin, M. Gagea, A. A. Marti, and J. E. Ladbury. 2015. Grb2 monomer-dimer equilibrium determines normal versus oncogenic function. *Nat Commun* 6:7354.
24. Lebowitz, J., M. S. Lewis, and P. Schuck. 2009. Modern analytical ultracentrifugation in protein science: A tutorial review. *Protein Science* 11(9):2067-2079.
25. Patel, T. R., D. J. Winzor, and D. J. Scott. 2016. Analytical ultracentrifugation: A versatile tool for the characterisation of macromolecular complexes in solution. *Methods* 95:55-61.
26. Schuck, P. 2000. Size-Distribution Analysis of Macromolecules by Sedimentation Velocity Ultracentrifugation and Lamm Equation Modeling. *Biophys J* 78:1606-1619.
27. Salvay, A. G., M. Santamaria, M. le Maire, and C. Ebel. 2007. Analytical ultracentrifugation sedimentation velocity for the characterization of detergent-solubilized membrane proteins Ca⁺⁺-ATPase and ExbB. *J Biol Phys* 33(5-6):399-419.
28. Brown, P. H., A. Balbo, H. Zhao, C. Ebel, and P. Schuck. 2011. Density contrast sedimentation velocity for the determination of protein partial-specific volumes. *PLoS One* 6(10):e26221.
29. Zhao, H., P. H. Brown, and P. Schuck. 2011. On the distribution of protein refractive index increments. *Biophys J* 100(9):2309-2317.
30. Cole, J. L., J. W. Lary, T. P. Moody, and T. M. Laue. 2008. Analytical Ultracentrifugation: Sedimentation Velocity and Sedimentation Equilibrium. In *Methods in Cell Biology. Biophysical Tools for Biologists, Volume One: In Vitro Techniques*, pp. 143-179.
31. Slotboom, D. J., R. H. Duurkens, K. Olieman, and G. B. Erkens. 2008. Static light scattering to characterize membrane proteins in detergent solution. *Methods* 46(2):73-82.
32. Some, D. 2013. Light-scattering-based analysis of biomolecular interactions. *Biophys Rev* 5(2):147-158.

33. Brown, P. H., and P. Schuck. 2006. Macromolecular size-and-shape distributions by sedimentation velocity analytical ultracentrifugation. *Biophys J* 90(12):4651-4661.
34. Grant, T. D., J. R. Luft, J. R. Wolfley, H. Tsuruta, A. Martel, G. T. Montelione, and E. H. Snell. 2011. Small angle X-ray scattering as a complementary tool for high-throughput structural studies. *Biopolymers* 95(8):517-530.
35. Franke, D., M. V. Petoukhov, P. V. Konarev, A. Panjkovich, A. Tuukkanen, H. D. T. Mertens, A. G. Kikhney, N. R. Hajizadeh, J. M. Franklin, C. M. Jeffries, and D. I. Svergun. 2017. ATSAS 2.8: a comprehensive data analysis suite for small-angle scattering from macromolecular solutions. *J Appl Crystallogr* 50(Pt 4):1212-1225.
36. Perez, J., and A. Koutsioubas. 2015. Memprot: a program to model the detergent corona around a membrane protein based on SEC-SAXS data. *Acta Crystallogr D Biol Crystallogr* 71(Pt 1):86-93.
37. Russo Krauss, I., A. Merlino, A. Vergara, and F. Sica. 2013. An overview of biological macromolecule crystallization. *Int J Mol Sci* 14(6):11643-11691.
38. Midgett, C. R., and D. R. Madden. 2007. Breaking the bottleneck: eukaryotic membrane protein expression for high-resolution structural studies. *J Struct Biol* 160(3):265-274.
39. Graewert, M. A., D. Franke, C. M. Jeffries, C. E. Blanchet, D. Ruskule, K. Kuhle, A. Fliieger, B. Schafer, B. Tartsch, R. Meijers, and D. I. Svergun. 2015. Automated pipeline for purification, biophysical and x-ray analysis of biomacromolecular solutions. *Sci Rep* 5:10734.
40. Hajizadeh, N. R., D. Franke, and D. I. Svergun. 2018. Integrated beamline control and data acquisition for small-angle X-ray scattering at the P12 BioSAXS beamline at PETRAIII storage ring DESY. *J Synchrotron Radiat* 25(Pt 3):906-914.
41. Jeffries, C. M., M. A. Graewert, C. E. Blanchet, D. B. Langley, A. E. Whitten, and D. I. Svergun. 2016. Preparing monodisperse macromolecular samples for successful biological small-angle X-ray and neutron-scattering experiments. *Nat Protoc* 11(11):2122-2153.
42. Gabel, F., M. F. Lensink, B. Clantin, F. Jacob-Dubuisson, V. Villeret, and C. Ebel. 2014. Probing the conformation of FhaC with small-angle neutron scattering and molecular modeling. *Biophys J* 107(1):185-196.

43. Breyton, C., F. Gabel, M. Lethier, A. Flayhan, G. Durand, J. M. Jault, C. Juillan-Binard, L. Imbert, M. Moulin, S. Ravaud, M. Hartlein, and C. Ebel. 2013. Small angle neutron scattering for the study of solubilised membrane proteins. *Eur Phys J E Soft Matter* 36(7):71.
44. Bu Z., E. D. M. 1999. A Method for Determining Transmembrane Helix Association and Orientation in Detergent Micelles Using Small Angle X-Ray Scattering. *Biophysical Journal* 77:1064–1073.
45. Lipfert, J., L. Columbus, V. B. Chu, S. A. Lesley, and D. S. 2007. Size and shape of detergent micelles determined by small-angle X-ray scattering. *J Phys Chem B* 111:12427-12438.
46. Koutsioubas, A., A. Berthaud, S. Mangenot, and J. Perez. 2013. Ab initio and all-atom modeling of detergent organization around Aquaporin-0 based on SAXS data. *J Phys Chem B* 117(43):13588-13594.
47. Grant, T. D. 2018. Ab initio electron density determination directly from solution scattering data. *Nat Methods* 15(3):191-193.
48. Petoukhov, M. V., D. Franke, A. V. Shkumatov, G. Tria, A. G. Kikhney, M. Gajda, C. Gorba, H. D. Mertens, P. V. Konarev, and D. I. Svergun. 2012. New developments in the ATSAS program package for small-angle scattering data analysis. *J Appl Crystallogr* 45(Pt 2):342-350.
49. Summers, W. A., and D. A. Court. 2010. Origami in outer membrane mimetics: correlating the first detailed images of refolded VDAC with over 20 years of biochemical data. *Biochem Cell Biol* 88(3):425-438.
50. Young, M. J., D. C. Bay, G. Hausner, and D. A. Court. 2007. The evolutionary history of mitochondrial porins. *BMC Evol. Biol.* 7:31.
51. Bay, D. C., M. Hafez, M. J. Young, and D. A. Court. 2012. Phylogenetic and coevolutionary analysis of the beta-barrel protein family comprised of mitochondrial porin (VDAC) and Tom40. *Biochim Biophys Acta* 1818(6):1502-1519.
52. Cesar Mde, C., and J. E. Wilson. 2004. All three isoforms of the voltage-dependent anion channel (VDAC1, VDAC2, and VDAC3) are present in mitochondria from bovine, rabbit, and rat brain. *Arch Biochem Biophys* 422(2):191-196.

53. Weeber, E. J., M. Levy, M. J. Sampson, K. Anflous, D. L. Armstrong, S. E. Brown, J. D. Sweatt, and W. J. Craigen. 2002. The role of mitochondrial porins and the permeability transition pore in learning and synaptic plasticity. *J Biol Chem* 277(21):18891-18897.
54. Cheng, E. H., T. V. Sheiko, J. K. Fisher, W. J. Craigen, and S. J. Korsmeyer. 2003. VDAC2 inhibits BAK activation and mitochondrial apoptosis. *Science* 301(5632):513-517.
55. Sampson, M. J., W. K. Decker, A. L. Beaudet, W. Ruitenbeek, D. Armstrong, M. J. Hicks, and W. J. Craigen. 2001. Immotile sperm and infertility in mice lacking mitochondrial voltage-dependent anion channel type 3. *J Biol Chem* 276(42):39206-39212.
56. Summers, W. A., J. A. Wilkins, R. C. Dwivedi, P. Ezzati, and D. A. Court. 2012. Mitochondrial dysfunction resulting from the absence of mitochondrial porin in *Neurospora crassa*. *Mitochondrion* 12(2):220-229.
57. Ujwal, R., D. Cascio, J. P. Colletier, S. Faham, J. Zhang, L. Toro, P. Ping, and J. Abramson. 2008. The crystal structure of mouse VDAC1 at 2.3 Å resolution reveals mechanistic insights into metabolite gating. *Proc Natl Acad Sci U S A* 105(46):17742-17747.
58. Hiller, S., R. G. Garces, T. J. Malia, V. Y. Orekhov, M. Colombini, and G. Wagner. 2008. Solution structure of the integral human membrane protein VDAC-1 in detergent micelles. *Science* 321(5893):1206-1210.
59. Villinger, S., K. Giller, M. Bayrhuber, A. Lange, C. Griesinger, S. Becker, and M. Zweckstetter. 2014. Nucleotide interactions of the human voltage-dependent anion channel. *J Biol Chem* 289(19):13397-13406.
60. Clemençon, B., M. Fine, and M. A. Hediger. 2016. Conservation of the oligomeric state of native VDAC1 in detergent micelles. *Biochimie* 127:163-172.
61. Shoshan-Barmatz, V., N. Keinan, S. Abu-Hamad, D. Tyomkin, and L. Aram. 2010. Apoptosis is regulated by the VDAC1 N-terminal region and by VDAC oligomerization: release of cytochrome c, AIF and Smac/Diablo. *Biochim Biophys Acta* 1797(6-7):1281-1291.
62. Bryan, N., and K. P. Raisch. 2015. Identification of a mitochondrial-binding site on the N-terminal end of hexokinase II. *Biosci Rep* 35(3).

63. Arzoine, L., N. Zilberberg, R. Ben-Romano, and V. Shoshan-Barmatz. 2009. Voltage-dependent anion channel 1-based peptides interact with hexokinase to prevent its anti-apoptotic activity. *J Biol Chem* 284(6):3946-3955.
64. Abu-Hamad, S., H. Zaid, A. Israelson, E. Nahon, and V. Shoshan-Barmatz. 2008. Hexokinase-I protection against apoptotic cell death is mediated via interaction with the voltage-dependent anion channel-1: mapping the site of binding. *J Biol Chem* 283(19):13482-13490.
65. Lauterwasser, J., F. Todt, R. M. Zerbes, T. N. Nguyen, W. Craigen, M. Lazarou, M. van der Laan, and F. Edlich. 2016. The porin VDAC2 is the mitochondrial platform for Bax retrotranslocation. *Sci Rep* 6:32994.
66. Shoshan-Barmatz, V., Y. Krelin, A. Shteinifer-Kuzmine, and T. Arif. 2017. Voltage-Dependent Anion Channel 1 As an Emerging Drug Target for Novel Anti-Cancer Therapeutics. *Front Oncol* 7:154.
67. Simamura, E., H. Shimada, T. Hatta, and K. Hirai. 2008. Mitochondrial voltage-dependent anion channels (VDACs) as novel pharmacological targets for anti-cancer agents. *J Bioenerg Biomembr* 40(3):213-217.
68. Schredelseker, J., A. Paz, C. J. Lopez, C. Altenbach, C. S. Leung, M. K. Drexler, J. N. Chen, W. L. Hubbell, and J. Abramson. 2014. High resolution structure and double electron-electron resonance of the zebrafish voltage-dependent anion channel 2 reveal an oligomeric population. *J Biol Chem* 289(18):12566-12577.
69. Ujwal, R., D. Cascio, V. Chaptal, P. Ping, and J. Abramson. 2009. Crystal packing analysis of murine VDAC1 crystals in a lipidic environment reveals novel insights on oligomerization and orientation. *Channels (Austin)* 3(3):167-170.
70. Bayrhuber, M., T. Meins, M. Habeck, S. Becker, K. Giller, S. Villinger, C. Vonrhei, C. Griesinger, M. Zweckstetter, and K. Zeth. 2008. Structure of the human voltage-dependent anion channel. *Proceedings of the National Academy of Sciences* 105(40):15370-15375.
71. Bergdoll, L. A., M. T. Lerch, J. W. Patrick, K. Belardo, C. Altenbach, P. Bisignano, A. Laganowsky, M. Grabe, W. L. Hubbell, and J. Abramson. 2018. Protonation state of glutamate 73 regulates the formation of a specific dimeric association of mVDAC1. *Proc Natl Acad Sci U S A* 115(2):E172-E179.

72. Goncalves, R. P., N. Buzhynskyy, V. Prima, J. N. Sturgis, and S. Scheuring. 2007. Supramolecular assembly of VDAC in native mitochondrial outer membranes. *J Mol Biol* 369(2):413-418.
73. Ferens, F. G., V. Spicer, O. V. Krokhin, A. Motnenko, W. A. Summers, and D. A. Court. 2017. A deletion variant partially complements a porin-less strain of *Neurospora crassa*. *Biochem Cell Biol* 95(2):318-327.
74. Miroux, B., and W. J. E. 1996. Over-production of Proteins in *Escherichia coli* Mutant Hosts that Allow Synthesis of some Membrane Proteins and Globular Proteins at High Levels. *J Mol Biol* 260:289-298.
75. DAVIS, R. H., and F. J. DE SERRES. 1970. Genetic and Microbiological Research Techniques for *Neurospora crassa*. *Microbiological Techniques*:79-143.
76. Summers, W. A. T. 2010. An in vivo Approach to Elucidating the Function of Mitochondrial Porin by the Characterization of *Neurospora crassa* Strains Deficient in Porin. In Department of Microbiology. University of Manitoba, Winnipeg, Manitoba. 296.
77. Bay, D. C., J. D. O'Neil, and D. A. Court. 2008. Two-step folding of recombinant mitochondrial porin in detergent. *Biophys J* 94(2):457-468.
78. Abdul-Gader, A., A. J. Miles, and B. A. Wallace. 2011. A reference dataset for the analyses of membrane protein secondary structures and transmembrane residues using circular dichroism spectroscopy. *Bioinformatics* 27(12):1630-1636.
79. Whitmore, L., and B. A. Wallace. 2004. DICHROWEB, an online server for protein secondary structure analyses from circular dichroism spectroscopic data. *Nucleic Acids Res* 32(Web Server issue):W668-673.
80. Whitmore, L., and B. A. Wallace. 2008. Protein secondary structure analyses from circular dichroism spectroscopy: methods and reference databases. *Biopolymers* 89(5):392-400.
81. Zimmer, J., D. A. Doyle, and J. G. Grossmann. 2006. Structural characterization and pH-induced conformational transition of full-length KcsA. *Biophys J* 90(5):1752-1766.

82. Brown P.H., B. A., Schuck P. 2007. Using prior knowledge in the determination of macromolecular size distributions by analytical ultracentrifugation. *Biomacromolecules* 8(6):2011-2024.
83. Kopetzki, E., and K. D. Entian. 1982. Purification of Yeast Hexokinase Isoenzymes Using Affinity Chromatography and Chromatofocusing. *Analytical Biochemistry* 121:181-185.
84. Freitag, H., W. Neupert, and R. Benz. 1982. Purification and Characterisation of a Pore Protein of the Outer Mitochondrial Membrane from *Neurospora*. *European Journal of Biochemistry* 123:629-636.
85. De Pinto, V., Benz, R. and Palmert, F. 1989. Interaction of non-classical detergents with the mitochondrial porin: A new purification procedure and characterization of the pore-forming unit. *Eur. J. Biochem.* 183:179-187.
86. Thompson, A. A., J. J. Liu, E. Chun, D. Wacker, H. Wu, V. Cherezov, and R. C. Stevens. 2011. GPCR stabilization using the bicelle-like architecture of mixed sterol-detergent micelles. *Methods* 55(4):310-317.
87. Hennessey, J. P., Jr., and W. C. Johnson, Jr. 1982. Experimental errors and their effect on analyzing circular dichroism spectra of proteins. *Anal Biochem* 125(1):177-188.
88. Sreerama, N. a. W., R.W. 2004. Computation and Analysis of Protein Circular Dichroism Spectra. *Methods in Enzymology* 383:318-351.
89. Runke, G., E. Maier, W. A. Summers, D. C. Bay, R. Benz, and D. A. Court. 2006. Deletion variants of *Neurospora* mitochondrial porin: electrophysiological and spectroscopic analysis. *Biophys J* 90(9):3155-3164.
90. Roman, I., J. Figys, G. Steurs, and M. Zizi. 2006. Hunting interactomes of a membrane protein: obtaining the largest set of voltage-dependent anion channel-interacting protein epitopes. *Mol Cell Proteomics* 5(9):1667-1680.
91. Betaneli, V., E. P. Petrov, and P. Schwill. 2012. The role of lipids in VDAC oligomerization. *Biophys J* 102(3):523-531.
92. Gimpl, K., J. Klement, and S. Keller. 2016. Characterising protein/detergent complexes by triple-detection size-exclusion chromatography. *Biol Proced Online* 18:4.

93. Garcia-Ruiz C., M. M., Colell A., Morales A., Caballero F., Montero J., Terrones O., Basañez G. and Fernández-Checa J.C. 2009. Mitochondrial cholesterol in health and disease. *Histol. Histopathol.* 24:117-132.
94. Lucken-Ardjomande, S., S. Montessuit, and J. C. Martinou. 2008. Bax activation and stress-induced apoptosis delayed by the accumulation of cholesterol in mitochondrial membranes. *Cell Death Differ* 15(3):484-493.
95. Wei B H.M., G. R. 2002. Purification and characterization of the human adenosine A2a receptor functionally expressed in *Escherichia coli*. *Eur. J. Biochem.* 269:82-92.
96. Prasanna, X., A. Chattopadhyay, and D. Sengupta. 2014. Cholesterol modulates the dimer interface of the beta(2)-adrenergic receptor via cholesterol occupancy sites. *Biophys J* 106(6):1290-1300.
97. Pluhackova, K., S. Gahbauer, F. Kranz, T. A. Wassenaar, and R. A. Bockmann. 2016. Dynamic Cholesterol-Conditioned Dimerization of the G Protein Coupled Chemokine Receptor Type 4. *PLoS Comput Biol* 12(11):e1005169.
98. Chiara, F., D. Castellaro, O. Marin, V. Petronilli, W. S. Brusilow, M. Juhaszova, S. J. Sollott, M. Forte, P. Bernardi, and A. Rasola. 2008. Hexokinase II detachment from mitochondria triggers apoptosis through the permeability transition pore independent of voltage-dependent anion channels. *PLoS One* 3(3):e1852.
99. Chong, Y. T., J. L. Koh, H. Friesen, S. K. Duffy, M. J. Cox, A. Moses, J. Moffat, C. Boone, and B. J. Andrews. 2015. Yeast Proteome Dynamics from Single Cell Imaging and Automated Analysis. *Cell* 161(6):1413-1424.
100. Roberts, G. G., and A. P. Hudson. 2006. Transcriptome profiling of *Saccharomyces cerevisiae* during a transition from fermentative to glycerol-based respiratory growth reveals extensive metabolic and structural remodeling. *Mol Genet Genomics* 276(2):170-186.
101. Hiller, S., J. Abramson, C. Mannella, G. Wagner, and K. Zeth. 2010. The 3D structures of VDAC represent a native conformation. *Trends Biochem. Sci.* 35(9):514-521.
102. Bayrhuber, M., T. Meins, M. Habeck, S. Becker, K. Giller, S. Villinger, C. Vornhein, C. Griesinger, M. Zweckstetter, and K. Zeth. 2008. Structure of the human voltage-dependent anion channel. *Proc. Natl. Acad. Sci. (U.S.A.)* 105(40):15370-15375.

103. Gattin, Z., R. Schneider, Y. Laukat, K. Giller, E. Maier, M. Zweckstetter, C. Griesinger, R. Benz, S. Becker, and A. Lange. 2015. Solid-state NMR, electrophysiology and molecular dynamics characterization of human VDAC2. *J Biomol NMR* 61(3-4):311-320.
104. Summers, W. A., and D. A. Court. 2010. Origami in outer membrane mimetics: correlating the first detailed images of refolded VDAC with over 20 years of biochemical data. *Biochem. Cell Biol.* 88(3):425-438.
105. Benz, R. 1994. Permeation of hydrophilic solutes through mitochondrial outer membranes: review on mitochondrial porins. *Biochim. Biophys. Acta* 1197(2):167-196.
106. Homble, F., E. M. Krammer, and M. Prevost. 2012. Plant VDAC: facts and speculations. *Biochim Biophys Acta* 1818(6):1486-1501.
107. Roman, I., J. Figys, G. Steurs, and M. Zizi. 2005. In vitro interactions between the two mitochondrial membrane proteins VDAC and cytochrome c oxidase. *Biochemistry* 44(39):13192-13201.
108. Shoshan-Barmatz, V., and D. Mizrahi. 2012. VDAC1: from structure to cancer therapy. *Front Oncol* 2:164.
109. Colombini, M. 2009. The published 3D structure of the VDAC channel: native or not? *Trends Biochem Sci* 34(8):382-389.
110. Summers, W. A. T., J. A. Wilkins, R. C. Dwivedi, P. Ezzati, and D. A. Court. 2012. Mitochondrial dysfunction resulting from the absence of mitochondrial porin in *Neurospora crassa*. *Mitochondrion* 12(2):220-229.
111. Runke, G., E. Maier, W. A. T. Summers, D. C. Bay, R. Benz, and D. A. Court. 2006. Deletion variants of *Neurospora* mitochondrial porin: Electrophysiological and spectroscopic analysis. *Biophys. J.* 90:3155-3164.
112. Kelley, L. A., and M. J. Sternberg. 2009. Protein structure prediction on the Web: a case study using the Phyre server. *Nat Protoc* 4(3):363-371.
113. McCluskey, K., A. Wiest, and M. Plamann. 2010. The Fungal Genetics Stock Center: a repository for 50 years of fungal genetics research. *J. Biosci.* 35(1):119-126.

114. Colot, H. V., G. Park, G. E. Turner, C. Ringelberg, C. M. Crew, L. Litvinkova, R. L. Weiss, K. A. Borkovich, and J. C. Dunlap. 2006. A high-throughput gene knockout procedure for *Neurospora* reveals functions for multiple transcription factors. *Proc Natl Acad Sci U S A* 103(27):10352-10357.
115. Staben, C., B. Jensen, M. Singer, J. Pollock, M. Schechtman, J. Kinsey, and E. U. Selker. 1989. Use of a bacterial Hygromycin B resistance gene as a dominant selectable marker in *Neurospora crassa* transformation. *Fungal Genet. Newsl.* 36:79-81.
116. Davis, R. H., and F. J. De Serres. 1970. Genetic and microbiological research techniques for *Neurospora crassa*. *Methods Enzymol.* 17:79-143.
117. Harkness, T. A., R. L. Metzenberg, H. Schneider, R. Lill, W. Neupert, and F. E. Nargang. 1994. Inactivation of the *Neurospora crassa* gene encoding the mitochondrial protein import receptor MOM19 by the technique of "sheltered RIP". *Genetics* 136(1):107-118.
118. Sherman, E. L., N. E. Go, and F. E. Nargang. 2005. Functions of the small proteins in the TOM complex of *Neurospora crassa*. *Mol Biol Cell* 16(9):4172-4182.
119. Drab, T., J. Kracmerova, I. Ticha, E. Hanzlikova, M. Ticha, and J. Liberda. 2011. Native polyacrylamide electrophoresis in the presence of Ponceau Red to study oligomeric states of protein complexes. *J Sep Sci* 34(14):1692-1695.
120. Calvaruso, M. A., J. Smeitink, and L. Nijtmans. 2008. Electrophoresis techniques to investigate defects in oxidative phosphorylation. *Methods* 46(4):281-287.
121. Rifkin, M. R., and D. J. Luck. 1971. Defective production of mitochondrial ribosomes in the *poky* mutant of *Neurospora crassa*. *Proc Natl Acad Sci U S A* 68(2):287-290.
122. Wideman, J. G., N. E. Go, A. Klein, E. Redmond, S. W. Lackey, T. Tao, H. Kalbacher, D. Rapaport, W. Neupert, and F. E. Nargang. 2010. Roles of the Mdm10, Tom7, Mdm12, and Mmm1 proteins in the assembly of mitochondrial outer membrane proteins in *Neurospora crassa*. *Mol Biol Cell* 21(10):1725-1736.
123. Gungormusler-Yilmaz, M., D. Shamshurin, M. Grigoryan, M. Taillefer, V. Spicer, O. V. Krokhn, R. Sparling, and D. B. Levin. 2014. Reduced catabolic protein expression in *Clostridium butyricum* DSM 10702 correlate with reduced 1,3-propanediol synthesis at high glycerol loading. *AMB Express* 4:63.

124. Schmitt, S., H. Prokisch, T. Schlunck, D. G. Camp, 2nd, U. Ahting, T. Waizenegger, C. Scharfe, T. Meitinger, A. Imhof, W. Neupert, P. J. Oefner, and D. Rapaport. 2006. Proteome analysis of mitochondrial outer membrane from *Neurospora crassa*. *Proteomics* 6(1):72-80.
125. Emanuelsson, O., H. Nielsen, S. Brunak, and G. von Heijne. 2000. Predicting subcellular localization of proteins based on their N-terminal amino acid sequence. *J Mol Biol* 300(4):1005-1016.
126. Court, D. A., R. Kleene, W. Neupert, and R. Lill. 1996. Role of the N- and C-termini of porin in import into the outer membrane of *Neurospora* mitochondria. *FEBS Lett.* 390(1):73-77.
127. Descheneau, A. T., I. A. Cleary, and F. E. Nargang. 2005. Genetic evidence for a regulatory pathway controlling alternative oxidase production in *Neurospora crassa*. *Genetics* 169(1):123-135.
128. Lambowitz, A. M., and C. W. Slayman. 1971. Cyanide-resistant respiration in *Neurospora crassa*. *J Bacteriol* 108(3):1087-1096.
129. Shuvo, S. R., U. Kovaltchouk, A. Zubaer, A. Kumar, W. A. T. Summers, L. J. Donald, G. Hausner, and D. A. Court. 2017. Functional characterization of an N-terminally-truncated mitochondrial porin expressed in *Neurospora crassa*. *Canadian journal of microbiology* 63(8):730-738.
130. Keeping, A., D. Deabreu, M. Dibernardo, and R. A. Collins. 2011. Gel-based mass spectrometric and computational approaches to the mitochondrial proteome of *Neurospora*. *Fungal Genet Biol* 48(5):526-536.
131. Popov-Celeketic, J., T. Waizenegger, and D. Rapaport. 2008. Mim1 functions in an oligomeric form to facilitate the integration of Tom20 into the mitochondrial outer membrane. *J Mol Biol* 376(3):671-680.
132. Marques, I., M. Duarte, and A. Videira. 2003. The 9.8 kDa subunit of complex I, related to bacterial Na(+)-translocating NADH dehydrogenases, is required for enzyme assembly and function in *Neurospora crassa*. *J Mol Biol* 329(2):283-290.
133. Carneiro, P., M. Duarte, and A. Videira. 2004. The main external alternative NAD(P)H dehydrogenase of *Neurospora crassa* mitochondria. *Biochim Biophys Acta* 1608(1):45-52.

134. Duarte, M., M. Peters, U. Schulte, and A. Videira. 2003. The internal alternative NADH dehydrogenase of *Neurospora crassa* mitochondria. *Biochem J* 371(Pt 3):1005-1011.
135. Carneiro, P., M. Duarte, and A. Videira. 2007. The external alternative NAD(P)H dehydrogenase NDE3 is localized both in the mitochondria and in the cytoplasm of *Neurospora crassa*. *J Mol Biol* 368(4):1114-1121.
136. Gameiro, P. A., L. A. Laviolette, J. K. Kelleher, O. Iliopoulos, and G. Stephanopoulos. 2013. Cofactor balance by nicotinamide nucleotide transhydrogenase (NNT) coordinates reductive carboxylation and glucose catabolism in the tricarboxylic acid (TCA) cycle. *J Biol Chem* 288(18):12967-12977.
137. Carneiro, P., M. Duarte, and A. Videira. 2012. Characterization of apoptosis-related oxidoreductases from *Neurospora crassa*. *PLoS One* 7(3):e34270.
138. Lemaire, C., F. Guibet-Grandmougin, D. Angles, G. Dujardin, and N. Bonnefoy. 2004. A yeast mitochondrial membrane methyltransferase-like protein can compensate for oxal mutations. *J Biol Chem* 279(46):47464-47472.
139. Funes, S., F. E. Nargang, W. Neupert, and J. M. Herrmann. 2004. The Oxa2 protein of *Neurospora crassa* plays a critical role in the biogenesis of cytochrome oxidase and defines a ubiquitous subbranch of the Oxa1/YidC/Alb3 protein family. *Mol Biol Cell* 15(4):1853-1861.
140. Tanton, L. L., C. E. Nargang, K. E. Kessler, Q. Li, and F. E. Nargang. 2003. Alternative oxidase expression in *Neurospora crassa*. *Fungal Genet Biol* 39(2):176-190.
141. Tetaud, E., F. Godard, M. F. Giraud, S. H. Ackerman, and J. P. di Rago. 2014. The depletion of F(1) subunit epsilon in yeast leads to an uncoupled respiratory phenotype that is rescued by mutations in the proton-translocating subunits of F(0). *Mol Biol Cell* 25(6):791-799.
142. Zeng, X., R. Kucharczyk, J. P. di Rago, and A. Tzagoloff. 2007. The leader peptide of yeast Atp6p is required for efficient interaction with the Atp9p ring of the mitochondrial ATPase. *J Biol Chem* 282(50):36167-36176.
143. Maxwell, D. P., Y. Wang, and L. McIntosh. 1999. The alternative oxidase lowers mitochondrial reactive oxygen production in plant cells. *Proc Natl Acad Sci U S A* 96(14):8271-8276.

144. Seo, M. S., S. W. Kang, K. Kim, I. C. Baines, T. H. Lee, and S. G. Rhee. 2000. Identification of a new type of mammalian peroxiredoxin that forms an intramolecular disulfide as a reaction intermediate. *J Biol Chem* 275(27):20346-20354.
145. Goncalves, R. L., D. E. Rothschild, C. L. Quinlan, G. K. Scott, C. C. Benz, and M. D. Brand. 2014. Sources of superoxide/H₂O₂ during mitochondrial proline oxidation. *Redox biology* 2:901-909.
146. Chatterjee, A., N. D. Abeydeera, S. Bale, P. J. Pai, P. C. Dorrestein, D. H. Russell, S. E. Ealick, and T. P. Begley. 2011. *Saccharomyces cerevisiae* THI4p is a suicide thiamine thiazole synthase. *Nature* 478(7370):542-546.
147. Franken, J., S. Kroppenstedt, J. H. Swiegers, and F. F. Bauer. 2008. Carnitine and carnitine acetyltransferases in the yeast *Saccharomyces cerevisiae*: a role for carnitine in stress protection. *Curr Genet* 53(6):347-360.
148. Petersen Shay, K., R. F. Moreau, E. J. Smith, and T. M. Hagen. 2008. Is alpha-lipoic acid a scavenger of reactive oxygen species in vivo? Evidence for its initiation of stress signaling pathways that promote endogenous antioxidant capacity. *IUBMB Life* 60(6):362-367.
149. Hamon, M. P., A. L. Bulteau, and B. Friguet. 2015. Mitochondrial proteases and protein quality control in ageing and longevity. *Ageing research reviews* 23(Pt A):56-66.
150. Malki, A., T. Caldas, J. Abdallah, R. Kern, V. Eckey, S. J. Kim, S. S. Cha, H. Mori, and G. Richarme. 2005. Peptidase activity of the *Escherichia coli* Hsp31 chaperone. *J Biol Chem* 280(15):14420-14426.
151. Lee, H. C., and L. Zhang. 2009. A unique mechanism of chaperone action: heme regulation of Hsp1 activity involves separate control of repression and activation. *Protein and peptide letters* 16(6):642-649.
152. Scranton, M. A., A. Yee, S. Y. Park, and L. L. Walling. 2012. Plant leucine aminopeptidases moonlight as molecular chaperones to alleviate stress-induced damage. *J Biol Chem* 287(22):18408-18417.
153. Klanner, C., H. Prokisch, and T. Langer. 2001. MAP-1 and IAP-1, two novel AAA proteases with catalytic sites on opposite membrane surfaces in mitochondrial inner membrane of *Neurospora crassa*. *Mol Biol Cell* 12(9):2858-2869.

154. Morikawa, T., R. Yasuno, and H. Wada. 2001. Do mammalian cells synthesize lipoic acid? Identification of a mouse cDNA encoding a lipoic acid synthase located in mitochondria. *FEBS Lett* 498(1):16-21.
155. Zhang, S., M. W. Hulver, R. P. McMillan, M. A. Cline, and E. R. Gilbert. 2014. The pivotal role of pyruvate dehydrogenase kinases in metabolic flexibility. *Nutrition & metabolism* 11(1):10.
156. Strijbis, K., C. W. van Roermund, W. F. Visser, E. C. Mol, J. van den Burg, D. M. MacCallum, F. C. Odds, E. Paramonova, B. P. Krom, and B. Distel. 2008. Carnitine-dependent transport of acetyl coenzyme A in *Candida albicans* is essential for growth on nonfermentable carbon sources and contributes to biofilm formation. *Eukaryot Cell* 7(4):610-618.
157. Fernandez, M., E. Fernandez, and R. Rodicio. 1994. ACR1, a gene encoding a protein related to mitochondrial carriers, is essential for acetyl-CoA synthetase activity in *Saccharomyces cerevisiae*. *Mol Gen Genet* 242(6):727-735.
158. Hunter, G. A., and G. C. Ferreira. 2011. Molecular enzymology of 5-aminolevulinic synthase, the gatekeeper of heme biosynthesis. *Biochim Biophys Acta* 1814(11):1467-1473.
159. Schonauer, M. S., A. J. Kastaniotis, V. A. Kursu, J. K. Hiltunen, and C. L. Dieckmann. 2009. Lipoic acid synthesis and attachment in yeast mitochondria. *J Biol Chem* 284(35):23234-23242.
160. Dukanovic, J., and D. Rapaport. 2011. Multiple pathways in the integration of proteins into the mitochondrial outer membrane. *Biochim Biophys Acta* 1808(3):971-980.
161. Messerschmitt, M., S. Jakobs, F. Vogel, S. Fritz, K. S. Dimmer, W. Neupert, and B. Westermann. 2003. The inner membrane protein Mdm33 controls mitochondrial morphology in yeast. *J Cell Biol* 160(4):553-564.
162. Kurashima, K., M. Chae, H. Inoue, S. Hatakeyama, and S. Tanaka. 2013. A *uvs-5* strain is deficient for a mitofusin gene homologue, *fzo1*, involved in maintenance of long life span in *Neurospora crassa*. *Eukaryot Cell* 12(2):233-243.
163. Wagner, K., P. Rehling, L. K. Sanjuan Szklarz, R. D. Taylor, N. Pfanner, and M. van der Laan. 2009. Mitochondrial F1Fo-ATP synthase: the small subunits e and g associate with monomeric complexes to trigger dimerization. *J Mol Biol* 392(4):855-861.

164. Davies, K. M., C. Anselmi, I. Wittig, J. D. Faraldo-Gomez, and W. Kuhlbrandt. 2012. Structure of the yeast F1Fo-ATP synthase dimer and its role in shaping the mitochondrial cristae. *Proc Natl Acad Sci U S A* 109(34):13602-13607.
165. Hoppins, S., S. R. Collins, A. Cassidy-Stone, E. Hummel, R. M. Devay, L. L. Lackner, B. Westermann, M. Schuldiner, J. S. Weissman, and J. Nunnari. 2011. A mitochondrial-focused genetic interaction map reveals a scaffold-like complex required for inner membrane organization in mitochondria. *J Cell Biol* 195(2):323-340.